

Heat transport of cuprate-based low-dimensional quantum magnets with strong exchange coupling

Christian Hess^{a,b}

^a*IFW Dresden, 01069 Dresden, Germany*

^b*Center for Transport and Devices, TU Dresden, 01069 Dresden, Germany*

Abstract

Transport properties provide important access to a solid's quasiparticles, such as quasiparticle density, mobility, and scattering. The transport of heat can be particularly revealing because, in principle, all types of excitations in a solid may contribute. Heat transport is well understood for phonons and electrons, but relatively little is known about heat transported by magnetic excitations. However, during the last about two decades, the magnetic heat transport attracted increasing attention after the discovery of large and unusual signatures of it in low-dimensional quantum magnetic cuprate materials. Today it constitutes an important probe to otherwise often elusive, topological quasiparticles in a broader class of quantum magnets. This review summarizes the experimental foundation of this research, i.e. the state of the art for the magnetic heat transport in the mentioned cuprate materials which host prototypical low-dimensional antiferromagnetic $S = 1/2$ Heisenberg models. These comprise, in particular, the two-dimensional square lattice, and one-dimensional spin chain and two-leg ladder spin models. It is shown, how studying the heat transport provides direct access to the thermal occupation and the scattering of the already quite exotic quasiparticles of these models which range from spin-1 spin wave and triplon excitations to fractionalized spin-1/2 spinons. Remarkable transport properties of these quasiparticles have been revealed: the spin-heat transport often is highly efficient and in some cases even ballistic, in agreement with theoretical predictions.

Keywords: heat transport, quantum magnetism, low-dimensionality, experiment, cuprates

Contents

1	Introduction	2
1.1	Spin models	3
1.2	Materials	3
1.3	Experimental signatures of magnetic heat transport	4
1.4	Modeling	5
2	Spin planes	6
2.1	Qualitative proof of magnon heat transport	6
2.2	Extraction of the magnetic heat conductivity	10
2.3	Analysis of the magnetic heat conductivity	10
3	Two-leg spin ladders	14
3.1	Materials aspects	14
3.2	Qualitative proof of magnon heat transport in the spin ladders	17
3.3	Extraction of the magnetic heat conductivity	18

3.4	Analysis of the magnon heat conductivity	19
3.5	Time-dependent measurements	25
4	Spin chains	26
4.1	Theoretical preliminaries	26
4.2	Spinon heat transport in 'dirty' spin chains	28
4.3	'Ballistic' spinon heat transport in 'clean' spin chains	30
4.4	Spin chains with doping induced disorder	38
5	Conclusion	40

1. Introduction

The heat transport properties of a solid provide important information about the generation, mobility, scattering, and dissipation of various kinds of excitations, such as electrons, phonons and magnons. Deep fundamental knowledge in this regard exists about the heat transport by phonons and electrons [1], yet very little is known about heat transport by magnetic excitations.

After the original prediction of magnetic heat transport in 1936 by Fröhlich and Heitler [2], it took almost 30 years until the first convincing experimental evidence for heat transport by classical spin waves was found in ferrimagnetic yttrium-iron-garnet (YIG) [3–6]. Analogous to the case of phononic and electronic heat conduction, the analysis of this magnon heat conductivity is intriguing because it should in principle yield valuable information about the excitation and scattering of magnetic excitations (e.g. off defects, phonons, and electrons). However, most of the pioneering experiments on YIG and following experiments on other materials [7–9] focused on the mere identification of the new heat transport phenomenon. Furthermore, these early experiments typically were restricted to spin waves emerging from magnetically ordered phases at very low temperature ($T < 10$ K). The first signature of magnetic heat transport at higher temperatures ($T > 50$ K) was observed for the one-dimensional quantum antiferromagnet KCuF_3 [10], remarkably *above* its Néel temperature of $T_N \approx 38$ K [11]. These very intriguing first results for the heat transport of a low-dimensional *quantum magnet* remained for quite some time largely unnoticed. However, the rigorous theoretical prediction of dissipationless (so-called *ballistic*) heat conduction in one-dimensional antiferromagnetic spin-1/2 chains [12] and the discovery of huge magnetic contributions in quantum two-leg spin-1/2 ladder compounds [13–15] triggered intense research on the heat transport of low-dimensional quantum spin systems both experimentally [13–42] and theoretically [43–64].

On the experimental side, more and more evidence for *unconventional* heat conduction in low-dimensional quantum magnets has been observed over the years in various materials. Today, the clearest and often surprising experimental findings are known for spin systems realized in copper oxides (cuprates). In these compounds, a substantial magnetic heat conduction is often observed, despite a pronounced quantum nature of their spin systems with inherent absence of long-range magnetic order or even short range spin-spin correlations. Their actual magnetic heat conductivity can be unambiguously detected, because if present, it is usually large even at room temperature and above, often dwarfing the phononic heat conductivity of the system and thereby sometimes reaches values which are comparable to the heat conductivity of a metal.

The content of the review at hand is as follows: In the following paragraphs of this introductory Section 1, the essential basics of the spin models and the cuprate materials under scrutiny will be presented. Furthermore, the salient experimental signatures of magnetic heat conductivity in such systems will be presented, and the basics of analyzing the data will be introduced. This Section 1, i.e. the whole introductory part is based on [33]. Section 2 and Section 3.2 summarize the state of the art for the heat conductivity of the $S = 1/2$ two-dimensional Heisenberg antiferromagnet on a square lattice (2D-HAF) and of $S = 1/2$ two-leg spin ladders, respectively. Finally, Section 4 addresses the heat transport and related results on the spin dynamics of $S = 1/2$ Heisenberg spin chains.

1.1. Spin models

We are considering $S = 1/2$ models with Heisenberg interaction

$$\mathcal{H} = J_{i,j} \sum_{\langle i,j \rangle} \mathbf{S}_i \cdot \mathbf{S}_j, \quad (1)$$

where the sum runs over all nearest neighbors in the system. Here we are investigating three different spin models: the 2D-HAF, the two-leg spin ladder, and spin chains. For the 2D-HAF and the spin chain $J_{i,j} = J$ and for the spin ladder $J_{i,j} = J_{\parallel}$ along the legs and $J_{i,j} = J_{\perp}$ along the rungs of the ladder.

The corresponding low-dimensional quantum spin models are characterized by very peculiar ground states which are quantum disordered in the one-dimensional chain and ladder models. The elementary excitations which emerge from these ground states bear therefore a quite exotic character. For instance, the spin-spin correlations of $S = 1/2$ Heisenberg spin chains, decay algebraically with distance between the spins [65]. The elementary excitations are nevertheless well defined. They are fractionalized, i.e. $\Delta S = 1$ spin-flip excitations of the system decay into so-called spinons which are gapless and carry a spin $S = 1/2$ [66]. On the other hand, the ground state of a two-leg ladder possesses more short-range spin-spin correlations which decay exponentially as a function of distance [67, 68]. The elementary excitations are $S = 1$ particles (usually called magnons or triplons) and are separated from the ground state by a spin gap Δ ($\Delta/k_B \approx 400$ K in the case of the systems discussed here) [68]. Finally, the ground state of the 2D-HAF is a rather classical long-range ordered Néel state. However, also here due to incipient quantum disorder it only exists at temperature $T = 0$ and possesses a strongly reduced sublattice magnetization [69]. In this case the elementary excitations are well described using a spin wave framework where one should keep in mind that alternative descriptions have been discussed, too [70–72].

In the case of hole doping, all these model systems yield interesting and exotic properties. A Luttinger liquid forms in hole-doped spin chains. Here the electronic excitations decay into collective excitations of holes (holons) and spins (spinons). This phenomenon is often referred to as spin-charge separation. Quite different properties have been predicted for two-leg spin ladders: superconductivity competing with a charge ordered ground state is expected in this case [67, 73]. Finally, hole doping has great importance in the case of the 2D-HAF, because the interaction of the doped hole with the antiferromagnetic background forms a new quasiparticle, the spin polaron, which can be understood as a hole dressed with characteristic spin fluctuations [74]. The spin polaron is thought of playing a crucial role for the emergence of exotic ground states upon doping, including high-temperature superconductivity, which is observed in such systems [75, 76]. Note that the observation of spin-charge separation signatures upon controlled hole doping of $S = 1/2$ Heisenberg chain materials has not yet been achieved experimentally, Nevertheless, signatures of it have been derived e.g. from angular resolved photo emission experiments on undoped chain compounds [77]. On the other hand, charge ordering and superconductivity are prominent experimental features of hole-doped spin ladder and 2D-HAF materials [76, 78].

1.2. Materials

The materials at focus of this review are cuprate compounds which indeed host spin arrangements in the geometrical form of chains, two-leg ladders, and square lattices with a strong antiferromagnetic Heisenberg exchange ($J/k_B \approx 1500 - 2000$ K) between nearest neighbor spins. Sketches of such spin arrangements are shown in Fig. 1a-c. These low-dimensional arrangements of interacting spins arise from similarly low-dimensional structures composed of Cu-O-Cu bonds, within which a dominant antiferromagnetic exchange is present if these bonds are straight, i.e. a bonding angle of 180° is realized as depicted in Fig. 1d. In all the considered cuprate systems the spins have $S = 1/2$, resulting from the $3d^9$ configuration of Cu^{2+} -ions and therefore possess generally a strong quantum nature.

Good realizations of $S = 1/2$ Heisenberg chains as depicted in Fig. 1a are found in the compounds CaCu_2O_3 , SrCu_2O_2 , and SrCuO_2 , where chains of straight Cu-O-Cu bonds and hence a strong antiferromagnetic exchange exists along one particular crystallographic direction only; the magnetic exchange perpendicular to this direction is much weaker [79, 80]. Two-leg spin ladders are realized (cf. Fig. 1b) in the $(\text{Sr}, \text{Ca}, \text{La})_{14}\text{Cu}_{24}\text{O}_{41}$ family of compounds, where parallel pairs of such Cu-O-Cu chains (the ladder

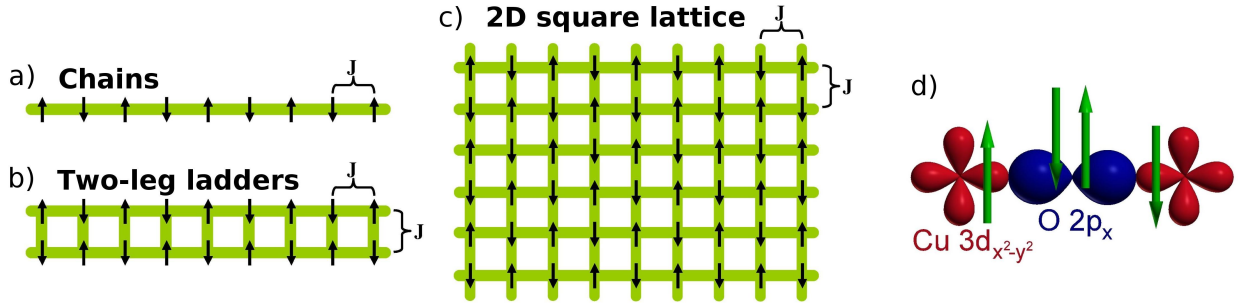


Figure 1: Illustration of low-dimensional spin structures: (a) a spin chain, (b) a two-leg spin ladder, and (c) a two-dimensional square lattice. Arrows represent localized electrons with spin $S = 1/2$ spin and shaded bars symbolize strong antiferromagnetic exchange between them. (d) Schematic illustration of the underlying chemical building block giving rise to the localized spins and their interaction. Only the relevant Cu- $3d_{x^2-y^2}$ and O- $2p_x$ orbitals are indicated. Arrows represent the spins of the electrons involved. Figure reproduced from [33].

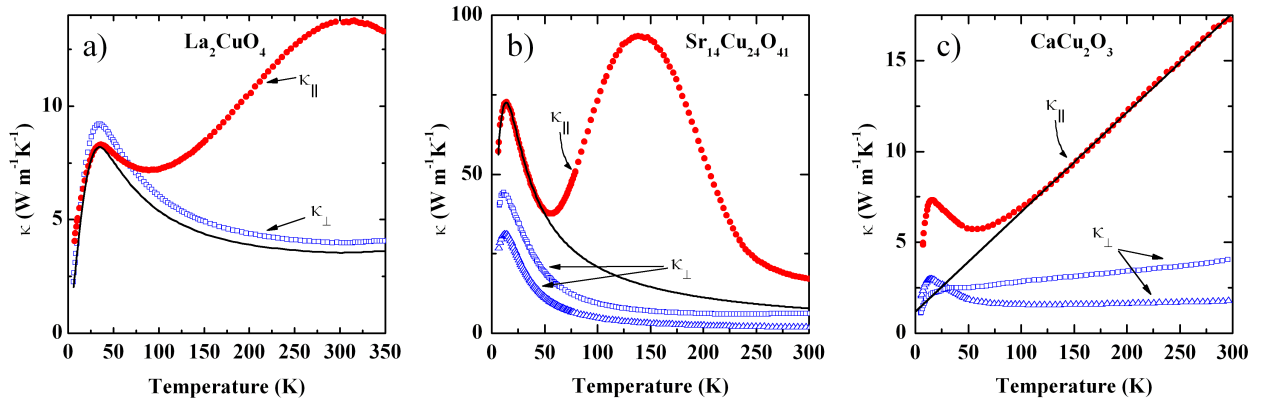


Figure 2: Anisotropic thermal conductivity of various low-dimensional spin materials as a function of temperature: a) the 2D-HAF as realized in La_2CuO_4 , b) the two-leg spin ladder material $\text{Sr}_{14}\text{Cu}_{24}\text{O}_{41}$, and c) the spin chain compound CaCu_2O_3 . Filled and open symbols represent κ_{\parallel} and κ_{\perp} of the materials. The solid line in a) represents a linear fit to the data in the range $T > 100$ K. The axis intercept of its extrapolation towards $T = 0$ is an approximation of κ_{ph} in the fit range. Solid lines in b) and c) represent estimations for the phonon background. Figure adapted from [15, 18, 38].

legs) are coupled to each other via bridging O-ions, producing in straight Cu-O-Cu bonds perpendicular to the chains direction (the ladder rungs), where the interchain coupling (or rung coupling) perpendicular to the chain direction J_{\perp} is of a similar magnitude to the intrachain coupling (or leg coupling), i.e. $J_{\perp} \approx J$ [68]. Ladder structures with more legs can in principle be created by coupling more chains to the structure; eventually, this would lead to a 2D-HAF in the infinite limit. A good realization of a 2D-HAF with $S = 1/2$ is given by La_2CuO_4 and other related antiferromagnetic parent compounds of high-temperature superconductors.

1.3. Experimental signatures of magnetic heat transport

The typical experimental signature of low-dimensional magnetic heat transport in a given material is a very anisotropic heat conductivity tensor of the material which reflects the dimensionality of the spin system. The origin of the anisotropy is the magnetic heat conduction of the low-dimensional magnetic structures which add to the always present phononic heat conduction. In principle, electronic heat conduction could occur as well. However, for all materials discussed here, such a contribution is irrelevant because the electrical conductivity is very low.

The experimental method which has been employed for obtaining the here discussed data is, in the largest portion of cases, the so-called standard steady-state method [1] which is proven to be very reliable

for obtaining the different components of the heat conductivity tensor. An exception concerns additional results on the two-leg spin ladder materials, where fluctuations in the magnetic signal provided the motivation for dynamic heat transport studies (Section 3.2).

Fig. 2 shows selected corresponding examples for experimental results of the heat conductivity κ of La_2CuO_4 , $\text{Sr}_{14}\text{Cu}_{24}\text{O}_{41}$ and CaCu_2O_3 , which are good representatives of the 2D-HAF, the two-leg spin ladder, and the isotropic antiferromagnetic Heisenberg chain [15, 18, 33, 38]. The data of the heat conductivity perpendicular to the low-dimensional magnetic structures (κ_{\perp}), i.e. along the directions with negligible magnetic exchange interaction, the temperature dependence of κ is characteristic of conventional *phononic* heat conduction κ_{ph} [1]. More specifically, $\kappa(T)$ has a low-temperature peak centered at temperature $T \approx 20 \dots 30$ K, with a continuously decaying high-temperature edge. An exception is found for CaCu_2O_3 , where one component of κ_{\perp} increases monotonically. Such an increase is well known for systems with a strongly suppressed κ_{ph} due to disorder [38, 81].

Completely different characteristics are found if κ is measured parallel to the low-dimensional structures, i.e. along the directions with a large J (κ_{\parallel}). Also in these cases, signatures of a phononic low-temperature peak are present. However, upon increasing the temperature further, κ_{\parallel} is very different from κ_{\perp} . In all three cases, κ_{\parallel} strongly increases for $T \gtrsim 60$ K ($T \gtrsim 90$ K in the case of La_2CuO_4) with increasing temperature, and in the case of La_2CuO_4 and $\text{Sr}_{14}\text{Cu}_{24}\text{O}_{41}$, a high-temperature peak at 310 K and 140 K, respectively, is formed, while for CaCu_2O_3 the increase continues up to room temperature. This remarkably clear anisotropy of κ is the clear qualitative evidence for large magnetic contributions to κ_{\parallel} of these three materials, i.e. a large κ_{mag} of the low-dimensional spin structures.

Generally, in the shown examples, κ_{mag} can be well extracted from the measured data for κ_{\parallel} by subtracting the phononic contribution κ_{ph} , which turns out to be reasonably approximated by the experimentally obtained κ_{\perp} . This is the essential basis for analyzing κ_{mag} in order to yield information on the thermal generation and the scattering of the magnetic quasiparticles.

1.4. Modeling

In theoretical works, the attention often is focused on the possibility of ballistic magnetic heat transport in 1D-systems: in integrable models like the XXZ Heisenberg spin chain the Hamiltonian and the thermal current operator commute, i.e. once a thermal current is established in such a system, it will never decay [12]. In other words, the thermal resistance vanishes and the magnetic thermal conductivity κ_{mag} diverges. While such surprising properties are well established for integrable spin models [12], ballistic heat transport in non-integrable quasi 1D-systems (e.g. two-leg spin ladders) has been a subject of intense discussion [46, 47, 54, 62, 63]. However, in real materials scattering processes involving defects and other quasiparticles such as phonons and charge carriers must play an important role and render κ_{mag} finite in all cases [51]. The analysis of κ_{mag} should hence provide further insight into the nature of these scattering processes and the dissipation of magnetic heat currents.

Kinetic model

We set up a kinetic model which should be able to capture the most important features of the magnetic heat conductivity [33]. Apparently, the qualitative temperature dependence of κ_{mag} often is a simple peak structure (La_2CuO_4 and $\text{Sr}_{14}\text{Cu}_{24}\text{O}_{41}$) or a monotonic increase (CaCu_2O_3) in the studied range $T = 100 \dots 350$ K, where the latter may be regarded as the low temperature edge of a peak. A peak structure is very common for the temperature dependence of the thermal conductivity κ of any kind of heat carrying particle, such as phonons or electrons [1]. In principle, one can expect that the same kinetic considerations which successfully describe the physics for phononic and electronic heat transport, can be applied to magnetic excitations as well.

The basic physics which determines the T -dependence of κ can be inferred from the kinetic estimate [82]

$$\kappa = \frac{1}{d} \frac{1}{(2\pi)^d} \int c_{\mathbf{k}} v_{\mathbf{k}} l_{\mathbf{k}} d\mathbf{k}, \quad (2)$$

with d the dimensionality of the considered system, $c_{\mathbf{k}} = \frac{d}{dT} \epsilon_{\mathbf{k}} n_{\mathbf{k}}$ the specific heat, $v_{\mathbf{k}}$ the velocity and $l_{\mathbf{k}}$ the mean free path of a mode with wave vector \mathbf{k} . $\epsilon_{\mathbf{k}}$ and $n_{\mathbf{k}}$ are the energy and the statistical occupation function of the mode \mathbf{k} .

Here, we are interested in magnetic excitations, i.e., a crucial parameter which determines the thermal occupation is the thermal energy $k_B T$ in relation to the magnetic exchange energy J . For all systems discussed here $J/k_B \approx 1500 \dots 2000$ K, whereas the experimental data only extend over temperatures $T < 350$ K. Thus, all considerations discussed in this review concern, from the viewpoint of the magnetic system, the situation of low temperature $k_B T \ll J$. The momentum of these particles naturally is confined to a small vicinity of the minima of the dispersion function. One can therefore safely ignore the momentum dependence of the mean free path, i.e., $l \approx l_{\mathbf{k}}$. Furthermore, at such low T , only a few magnetic modes are excited and contribute to the heat transport. If the temperature is also well below other relevant energy scales of the solid, such as the Debye temperature, scattering processes different from defect and boundary scattering which change the crystal momentum are rare.

In this situation, the low- T increase of κ is (a) characteristic of the excitation of the heat carrying particle (reflecting the T -dependence of the specific heat if $v_{\mathbf{k}}$ is momentum independent) and (b) proportional to the mean free path $l \approx l_{\mathbf{k}}$. At higher T , the momentum-dependent scattering becomes increasingly important and eventually leads to a decrease of the mean free path and hence to a decrease of κ . This decrease is characteristic of the relevant scattering mechanisms and allows an advanced analysis which potentially provides crucial information about these mechanisms.

The application of Eq. 2 for the case of 1D and 2D magnetic systems considered here leads to the general result

$$\kappa_{\text{mag}}(T) \propto l_{\text{mag}} f(T), \quad (3)$$

where $l_{\text{mag}}(T)$ is a general magnetic mean free path based on the approximation $l_{\text{mag}} \equiv l_{\mathbf{k}}$. As mentioned afore, for $k_B T \ll J$ this assumption is justified for the large- J systems considered here because the heat carrying excitations exist in significant numbers only in the vicinity of the band minima, i.e. a very small fraction of the Brillouin zone. The function $f(T)$ depends on temperature in a manner which is characteristic of the considered spin system. Details will be discussed in the respective sections.

2. Spin planes

2.1. Qualitative proof of magnon heat transport

As already indicated in section 1.3, the prominent signature of the magnetic heat conductivity in the 2D-HAF is a pronounced high-temperature peak in the in-plane thermal conductivity κ_{ab} , whereas the out-of-plane thermal conductivity κ_c is of purely phononic character (see Fig. 2). This strikingly anomalous heat conductivity was first observed in insulating parent compounds of cuprate high-temperature superconductors, in particular, La_2CuO_4 [83, 84] as well as in $\text{YBa}_2\text{Cu}_3\text{O}_{7-\delta}$ and $\text{PrBa}_2\text{Cu}_3\text{O}_{7-\delta}$ with $\delta \approx 1$ [85]. After these pioneering experimental findings, the origin of the high-temperature anomaly in κ_{ab} remained elusive for several years. Nakamura et al. were the first to speculate that the high-temperature maximum could be related to heat carried by magnetic excitations [84]. However, several attempts to explain this peak by anomalous phononic heat transport involving scattering processes of acoustic phonons with soft optical phonons [85] or magnons [83] have been made. Eventually, inspired by the observation of an exceptionally large one-dimensional κ_{mag} in two-leg spin ladder materials [14, 15] (see section 3.2), several groups reinvestigated the heat conductivity of La_2CuO_4 and related compounds [18, 27, 33, 81, 86–91]. Qualitatively, all these studies came to the conclusion that a conventional explanation for the high-temperature peak in κ_{ab} in the sense of electronic, phononic and even radiative heat transport can be excluded. Sizable electronic heat transport was readily ruled out due to the electronically insulating or only weakly conducting properties of La_2CuO_4 [18, 27] (and all other materials discussed below). The same holds for radiative heat transport [18] since the optical properties of La_2CuO_4 are almost isotropic in the relevant energy-range below $h\nu \lesssim 0.1$ eV [92]. The possibility of anomalous phononic heat transport, however, deserves further attention here because it is difficult to exclude it based on the heat conductivity data on La_2CuO_4 without further information and accordingly has been specifically addressed in several of the mentioned studies.

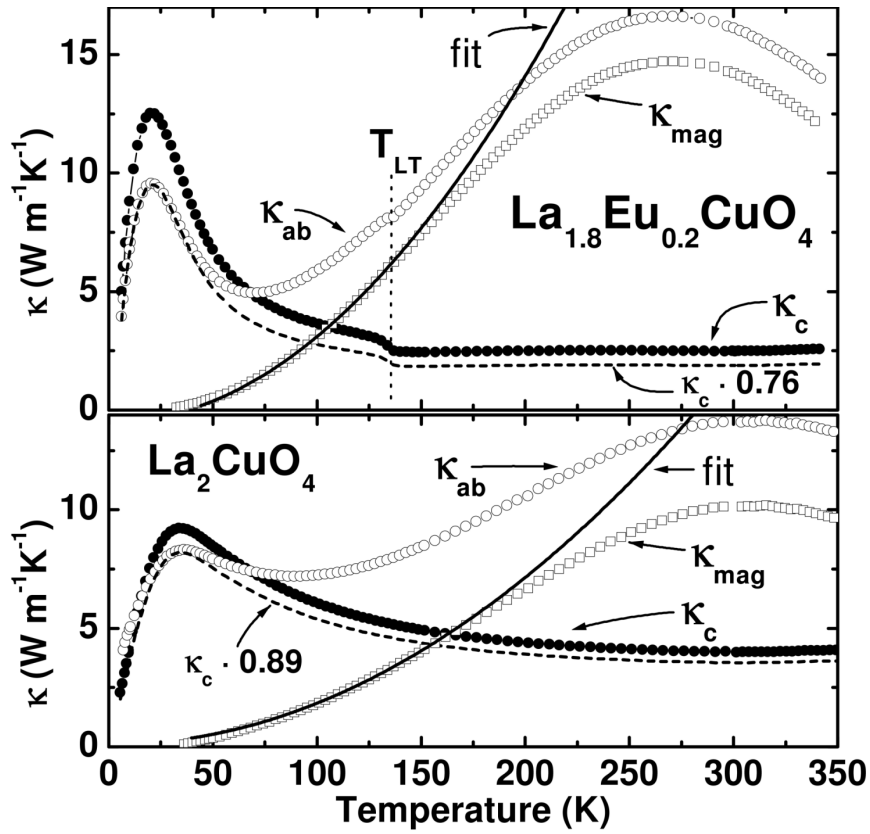


Figure 3: Thermal conductivity of La_2CuO_4 (bottom) and $\text{La}_{1.8}\text{Eu}_{0.2}\text{CuO}_4$ (top). Full circles: κ_c . Open circles: κ_{ab} . Open squares: κ_{mag} . Solid line: fit according to Eq. 7. Dashed line: $\kappa_{ab,\text{ph}}$. Reproduced from [18]. For similar measured data see also [84, 87, 91].

Anomalous phonon scattering versus magnetic heat transport

One thinkable hypothesis is that the heat conductivity of the 2D materials should be regarded as purely phononic, and thus the high-temperature anomaly in κ_{ab} should be regarded as not originating from an additional contribution but rather being the result of an unusual phonon damping by either magnetic excitations [83] or soft phonon modes [85]. Such phonon damping is known to be caused by *resonant* scattering of the heat-carrying phonons off such excitations. In such a case, a double-peak structure in $\kappa(T)$ results from a strong *reduction* of the heat conductivity in the temperature regime where the scattering is strongest. Well known examples where such a double peak is caused by local magnetic excitations and soft phonon modes are the heat conductivities of $\text{SrCu}_2(\text{BO}_3)_2$ [93], SrTiO_3 [94, 95], respectively. For La_2CuO_4 , one might consider such a scenario as being quite unlikely due to the complete absence of a double-peak in the heat conductivity perpendicular to the planes, κ_c . However, one could argue that both the magnetism and the crystal structure of the material are very anisotropic, and therefore an anisotropic phonon damping was thinkable. Hofmann et al. pointed out that in the 2D square-lattice cuprates, such as La_2CuO_4 , the dispersion of magnetic excitations which ranges from ~ 0 to $2J/k_B \sim 2000$ K (J is the in-plane exchange constant) is too stiff to cause phonon scattering on magnetic excitations being most pronounced in a narrow temperature interval around 100 K [27].

Damping of acoustic phonons due to soft optical phonon modes does, however, play an important role in the phonon heat conductivity of La_2CuO_4 , indeed. More specifically, soft optical phonon modes associated with the tilting of the CuO_6 octahedra which are present in the entire so-called low-temperature orthorhombic (LTO) phase, i.e. at $T \leq T_{\text{HT}} \approx 500$ K [96–98], have been shown to cause a significant suppression in the phononic heat conductivity of La_2CuO_4 [89]. Thus, in order to unambiguously rule out soft-phonon scattering as the origin of the anomalous κ_{ab} , the investigation of materials where the such soft phonons are not present is an obvious route.

Hess et al. therefore studied the heat conductivity of $\text{La}_{1.8}\text{Eu}_{0.2}\text{CuO}_4$ [18]. In this material the presence of Eu on the La-site has only little influence on the magnetism of the CuO_2 -planes [87] but has a strong impact on the structure, because it induces a new structural phase at low temperature, the so-called low-temperature tetragonal (LTT) phase, at $T \leq T_{\text{LT}} \approx 135$ K [99, 100]. Fig. 3 (top panel) shows $\kappa_{ab}(T)$ and $\kappa_c(T)$ of a $\text{La}_{1.8}\text{Eu}_{0.2}\text{CuO}_4$ single crystal. Both curves strongly resemble the findings for La_2CuO_4 (lower panel), yet exhibiting obvious differences: the low-temperature peaks of κ_{ab} and κ_c are slightly larger and more sharply shaped than in the case of La_2CuO_4 . Furthermore, a step-like anomaly is present at $T_{\text{LT}} \approx 135$ K. Above T_{LT} , κ_c remains almost constant and stays below the value for the undoped case, while κ_{ab} also exhibits a high-temperature maximum at $T \approx 270$ K which is even larger than that of La_2CuO_4 .

The difference between κ_c of Eu-doped and of pure La_2CuO_4 can be attributed to a difference in phononic heat conduction: Upon doping La_2CuO_4 with Eu, enhanced scattering of phonons reduces κ_c for $T > T_{\text{LT}}$, where both compounds have the same structure (LTO). The anomaly at T_{LT} ($\text{La}_{1.8}\text{Eu}_{0.2}\text{CuO}_4$) signals the transition to a new structural phase for $T < T_{\text{LT}}$ where κ_{ph} is enhanced. Indeed, soft phonon branches do exist in the LTO-phase of Rare Earth-doped La_2CuO_4 [101], which naturally explains a suppression of κ_{ph} of $\text{La}_{1.8}\text{Eu}_{0.2}\text{CuO}_4$. The change of κ_{ph} at T_{LT} then follows from the discontinuous hardening of the soft phonon branch in the LTT-phase [101, 102] and an associated reduced scattering rate of acoustic phonons.¹ The more striking observation is, however, that the high-temperature peak in κ_{ab} of $\text{La}_{1.8}\text{Eu}_{0.2}\text{CuO}_4$ is not affected by the transition. This unambiguously rules out that the double-peak structure in $\text{La}_{1.8}\text{Eu}_{0.2}\text{CuO}_4$ (and thus also in La_2CuO_4) is caused by soft-phonon scattering. Instead, the high-temperature peak has to be interpreted as stemming from another heat transport channel different from acoustic phonons which adds to the lattice thermal conductivity κ_{ph} .

This latter conclusion is corroborated by investigations on $\text{Sr}_2\text{CuO}_2\text{Cl}_2$ [27] and on R_2CuO_4 ($\text{R} = \text{Pr}, \text{Nd}, \text{Sm}, \text{Eu}, \text{Gd}$) [88, 105], where the soft-phonon scattering as is present in La_2CuO_4 is rigorously excluded due to different structural phases, yet practically preserving the magnetism of the CuO_2 -planes. On the one hand,

¹One should note that Sera et al. explain the change of κ_{ph} at T_{LT} by an observed change of the velocity of sound v_s at T_{LT} [103]. The actual changes of v_s are, however, far too small ($\sim 1\%$) [104] to account for the much larger changes of κ_{ph} . These changes of v_s at T_{LT} should thus be regarded as a further accompanying phenomenon of the structural phase transition.

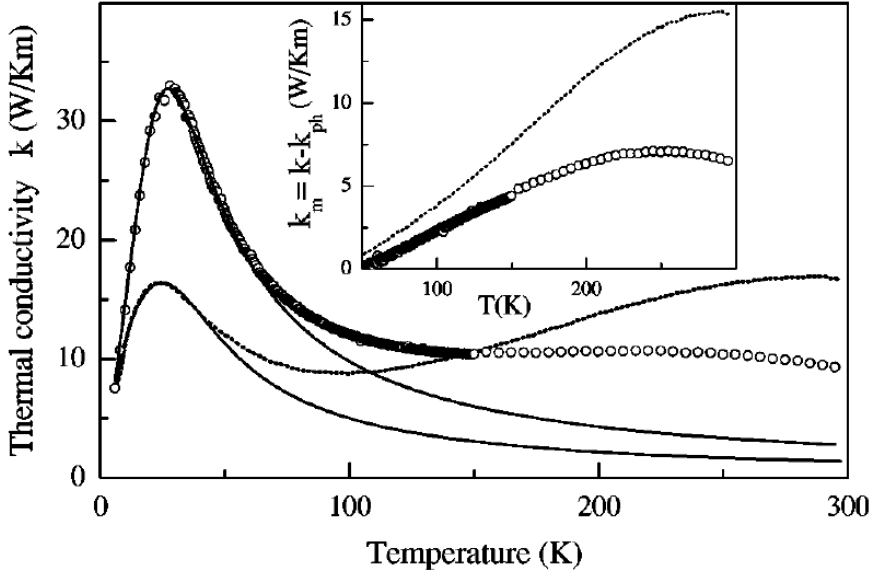


Figure 4: In-plane thermal conductivity (here labeled $k(T)$) of $\text{Sr}_2\text{CuO}_2\text{Cl}_2$ (circles) and La_2CuO_4 (dotted line; data from [84]). Solid lines: fits to the phonon thermal conductivity using the Callaway model [108]. Inset: The magnetic heat conductivity for $\text{Sr}_2\text{CuO}_2\text{Cl}_2$ (circles) and La_2CuO_4 (dotted line) (see text). Image taken from [27].

$\text{Sr}_2\text{CuO}_2\text{Cl}_2$ is practically isostructural to La_2CuO_4 with the small difference that (apart from having Sr^{2+} -ions on the La^{2+} -sites) Cl^{1-} -ions occupy the positions of the apical O^{2-} -ions of the CuO_6 octahedra which in La_2CuO_4 form the two-dimensional spin-1/2 planes. Unlike La_2CuO_4 , however, $\text{Sr}_2\text{CuO}_2\text{Cl}_2$ remains in the so-called high-temperature tetragonal (HTT) phase down to lowest temperature and thus does not exhibit any lattice instability which could give rise to soft-phonon scattering as in La_2CuO_4 [27]. On the other hand, the compounds R_2CuO_4 ($\text{R} = \text{Pr}, \text{Nd}, \text{Sm}, \text{Eu}, \text{Gd}$) crystallize in a structure quite different from that of La_2CuO_4 , viz. in the so-called tetragonal T' -phase without any apical oxygen but with very similar CuO_2 -planes as those in La_2CuO_4 . For $\text{R} = \text{Pr}, \text{Nd}, \text{Sm}$ the T' -phase is stable down to lowest temperature, whereas for $\text{R} = \text{Eu}, \text{Gd}$ the structure undergoes a phase transition towards an orthorhombic phase at 170 K and 685 K, respectively [88, 106, 107]. All three heat conductivity studies [27, 88, 105] reveal clearly a high-temperature hump in the in-plane thermal conductivity with a similar, albeit with a somewhat smaller magnitude than that of La_2CuO_4 , is also present in these layered cuprates despite having very different structural properties (see Fig. 4 for κ_{ab} of $\text{Sr}_2\text{CuO}_2\text{Cl}_2$ in comparison of that of La_2CuO_4 [27, 84]). Thus the high-temperature peak turns out as a common feature in the layered cuprates which unambiguously is to be interpreted as a two-dimensional excess thermal conductivity within the magnetic CuO_2 -planes. Note that the high-temperature peaks in the thermal conductivity of $\text{YBa}_2\text{Cu}_3\text{O}_{7-\delta}$, $\text{PrBa}_2\text{Cu}_3\text{O}_{7-\delta}$ with $\delta \approx 1$ [85] should be interpreted in a similar way.

Thus, the bottom line of this section is that the high-temperature anomaly in the thermal conductivity of La_2CuO_4 and related layered insulating cuprates originates from a substantial two-dimensional excess thermal conduction which adds to the typical phononic thermal conductivity κ_{ph} . In lack of other candidates it is straightforward to conclude that magnetic excitations (i.e. magnons) of the two-dimensional antiferromagnetic planes cause this unusual heat conduction.² Hence, the thermal conductivity measured parallel to the CuO_2 -planes (κ_{\parallel}) can be considered as the sum of a conventional phonon heat conductivity κ_{ph} and a magnetic contribution, i.e.,

$$\kappa_{\parallel} = \kappa_{\text{ph}} + \kappa_{\text{mag}}. \quad (4)$$

²Note that dispersing optical phonons can be ruled out to play an important role because their contribution to the thermal conductivity have been estimated to be about one order of magnitude smaller ($\sim 1 \text{ Wm}^{-1}\text{K}^{-1}$) than that what is observed [81].

2.2. Extraction of the magnetic heat conductivity

Having qualitatively established that a sizable magnon contribution κ_{mag} is present in the in-plane thermal conductivity of La_2CuO_4 , it is interesting to move one step further and to extract the temperature dependence of κ_{mag} . In order to estimate this temperature dependence, it is of paramount importance to determine its phononic part as accurately as possible. The first step in this estimation is to exploit that κ_{mag} is expected to roughly follow $\kappa_{\text{mag}} \propto T^2$ (see below) at low temperature and therefore to become negligible in the temperature range of the phononic low-temperature peak. Thus one can estimate $\kappa_{\parallel} \approx \kappa_{\text{ph}}$ at $T \lesssim 40$ K and extrapolate $\kappa_{\text{ph}}(T)$ towards higher temperature. One possible approach for this extrapolation is to use the Callaway model [108] for fitting the low-temperature ($T \lesssim 40$ K) thermal conductivity and to use the thereby obtained fit parameters for the high-temperature extrapolation. This procedure has been applied to $\text{Sr}_2\text{CuO}_2\text{Cl}_2$ and R_2CuO_4 ($\text{R} = \text{La, Pr, Nd, Sm, Gd}$) [27, 88], see Fig. 4 and Fig. 5 for the fits and the resulting κ_{mag} .

For La_2CuO_4 the application of the Callaway model for extrapolating κ_{ph} is bound to be error-prone due to the dominant importance of soft-phonon scattering which is difficult to incorporate into the model. The step-like change of κ_c of $\text{La}_{1.8}\text{Eu}_{0.2}\text{CuO}_4$ at T_{LT} (Fig. 3) tellingly demonstrates this complication. One possibility to overcome this problem is to use a phenomenological approach the *measured* purely phononic κ_{\perp} perpendicular to the CuO_2 planes and to exploit the negligibly small κ_{mag} in the temperature range of the phononic low-temperature peak. Thus one can estimate $\kappa_{\parallel} \approx \kappa_{\text{ph}}$ at $T \lesssim 40$ K and extrapolate $\kappa_{\text{ph}} = A \cdot \kappa_{\perp}$ for higher temperatures, where A is a suitable scaling factor. Fig. 3 shows examples of in this way estimated κ_{ph} for the in-plane heat conductivity κ_{\parallel} of La_2CuO_4 and $\text{La}_{1.8}\text{Eu}_{0.2}\text{CuO}_4$ and the resulting κ_{mag} [18].

As we shall see further below, the magnetic heat conductivity is well detectable also in polycrystalline samples. However, due to the polycrystalline nature of such samples, anisotropic information on κ is averaged over. None of the above described approaches for estimating κ_{ph} (and thus κ_{mag}) can be applied to such data in a simple way because on the one hand the application of the Callaway model to polycrystalline data requires further, non-clarified assumptions, and, on the other hand, for a polycrystal κ_{\perp} can obviously not be obtained independently. Hess et al. therefore estimated the phonon contributions $\kappa_{\text{ph}}^{\text{poly}}$ by fitting κ at the high-temperature edge of its maximum (see Fig. 6) by $\kappa_{\text{ph}} = \alpha/T + \beta$ and by extrapolating this fit towards high temperature [18]. In turn, $\kappa_{\text{mag}}^{\text{poly}}$ on the polycrystals is obtained by $\kappa_{\text{mag}}^{\text{poly}} = \kappa - \kappa_{\text{ph}}$. Note, that the measured $\kappa_{\text{mag}}^{\text{poly}}$ is smaller than the intrinsic κ_{mag} of these compounds by the factor of 2/3 due to averaging over all three components of the κ tensor [18].

2.3. Analysis of the magnetic heat conductivity

Kinetic model

The application [18, 33] of the kinetic model (Eq. 2) to the 2D thermal conductivity of a single magnon dispersion branch (labeled by i) yields

$$\tilde{\kappa}^i = \frac{1}{2} \frac{1}{(2\pi)^2} \int v_{\mathbf{k}} l_{\mathbf{k}} \frac{d}{dT} n_{\mathbf{k}} \epsilon_{\mathbf{k}} d\mathbf{k}, \quad (5)$$

with $v_{\mathbf{k}}$, $l_{\mathbf{k}}$, $n_{\mathbf{k}}$ and $\epsilon_{\mathbf{k}}$ the velocity, mean free path, Bose-function and energy of a magnon, respectively. Note that κ_{mag}^i of a three-dimensional ensemble of planes, as realized in La_2CuO_4 , results from the multiplication of $\tilde{\kappa}^i$ with the number of planes per unit length, i.e., $\kappa_{\text{mag}}^i = \frac{2}{c} \tilde{\kappa}^i$, where $c = 13.2 \text{ \AA}$ is the lattice constant of La_2CuO_4 perpendicular to the planes. Then the total κ_{mag} is given by summing up κ_{mag}^i of each magnon branch.

In order to calculate κ_{mag}^i one can approximate the magnon dispersion relation $\epsilon_{\mathbf{k}}$ of the two branches $i = 1, 2$ with the 2D-isotropic expression

$$\epsilon_{\mathbf{k}} = \epsilon_k = \sqrt{\Delta_i^2 + (\hbar v_0 k)^2}, \quad (6)$$

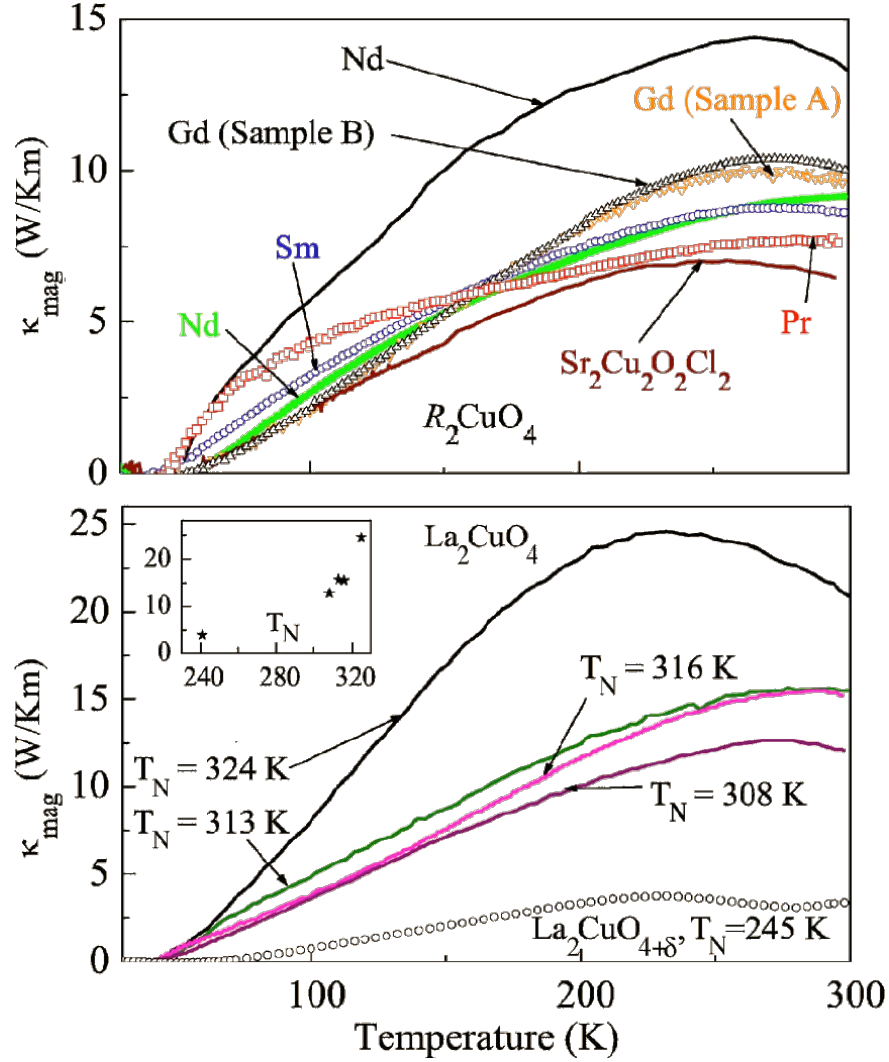


Figure 5: Magnetic contributions to the in-plane thermal conductivity, calculated via $\kappa_{\text{mag}} = \kappa_{\parallel} - \kappa_{\text{ph}}$, where κ_{ph} is determined by a Callaway fit of the low-temperature maximum. Upper panel: Values calculated from measurements of κ_{\parallel} of $R_2\text{CuO}_4$ [88, 105]. Lower panel: The same analysis for various data of $\text{La}_2\text{CuO}_{4+\delta}$ [84, 86, 88, 91]. Inset: The maximum of the calculated κ_{mag} vs. the Néel temperature of $\text{La}_2\text{CuO}_{4+\delta}$. It is worth to note, that for high excess oxygen contents a spatial phase separation into hole-rich and hole-poor regions occurs in $\text{La}_2\text{CuO}_{4+\delta}$ at $T \lesssim 290$ K [109, 110]. This explains the very small κ_{mag} and the dip at ~ 275 K for the sample with $T_N = 245$ K shown in Fig. 5 [88]. Image adapted from [88].

which describes the dispersion observed experimentally [70, 101] for small values of k . Here, v_0 is the spin wave velocity while Δ_1 and Δ_2 denote the spin gaps of each magnon branch. Assuming a momentum independent mean free path, i.e., $l_{\mathbf{k}} \equiv l_{\text{mag}}$ one finds for each magnon branch [18, 33],

$$\kappa_{\text{mag}}^i = \frac{k_B^3 T^2 l_{\text{mag}}}{2\pi \hbar^2 v_0 c} \int_{\frac{\Delta_i}{k_B T}}^{\infty} x^2 \sqrt{x^2 - x_{0,i}^2} \frac{e^x}{(e^x - 1)^2} dx, \quad (7)$$

with the spin wave velocity $v_0 \approx 1.287 \cdot 10^5$ m/s [111]. The integral is temperature dependent via its lower boundary $x_{0,i} = \Delta_i/(k_B T)$, where $\Delta_1/k_B \approx 26$ K and $\Delta_2/k_B \approx 58$ K [101]. However, the temperature dependence is weak in the T -range where the experimental data are discussed and thus one roughly has $\kappa_{\text{mag}} \propto T^2$, if one presumes l_{mag} to be temperature independent.

Low-temperature characteristics

Eq. 7 has been used to fit the κ_{mag} data of La_2CuO_4 and $\text{La}_{1.8}\text{Eu}_{0.2}\text{CuO}_4$ shown in Fig. 3 assuming a *temperature-independent* magnon mean free path l_{mag} [18]. In this procedure, an additive shift of the κ_{mag} -curve was allowed for which yields a further free parameter apart from l_{mag} and accounts for the aforementioned uncertainties in the magnitude of κ_{mag} . As can be seen in the figure, for both compounds satisfactory fits (solid lines) were obtained at intermediate temperature ranges (70-158 K for La_2CuO_4 and 54-131 K for $\text{La}_{1.8}\text{Eu}_{0.2}\text{CuO}_4$, [18]). While the slight deviations between the fitted and experimental data towards low T are due to the uncertainties in $\kappa_{\perp,\text{ph}}$ in this range, the deviations at high temperature can be understood in terms of l_{mag} becoming temperature-dependent due to enhanced magnon scattering off magnons or phonons.

Notably, the data are consistent with a temperature-independent l_{mag} for T both, within the fit interval and below, indicating that in this range the mentioned temperature-dependent scattering processes (magnon-magnon scattering, magnon-phonon scattering, or effects of a finite spin-correlation length at $T > T_N$) are frozen out and thus may be discarded. Therefore, relevant processes seem to be sample-boundary scattering or scattering off defects within the CuO_2 -planes. The analysis yields $l_{\text{mag}} \approx 1160$ Å and $l_{\text{mag}} \approx 560$ Å for $\text{La}_{1.8}\text{Eu}_{0.2}\text{CuO}_4$ and La_2CuO_4 , respectively. Since these values are far too small to correspond to the crystal dimensions, which are of the order of millimeters, these values naturally can be interpreted as the size of two-dimensional defect-free grains. Thus, magnon-defect scattering is the most likely scattering process which dominates the low-temperature magnon transport. This conclusion is consistent with the fact that κ_{mag} and l_{mag} are quantitatively different for $\text{La}_{1.8}\text{Eu}_{0.2}\text{CuO}_4$ and La_2CuO_4 : since the magnetic properties of both compounds are expected to be identical in essence (i.e., the same spin wave velocity v_0), unequal κ_{mag} can arise only due to a difference in densities of the magnetic defects that restrict l_{mag} .

Magnon-defect scattering

There is no clear alternative way to measure the defect density of a given crystal directly, in order to allow a quantitative comparison of the magnon mean free path l_{mag} with the defect density (or the defect distance). Hess et al. have therefore performed measurements of κ on samples with a well-defined density of magnetic defects. Such defects can be induced in La_2CuO_4 , e.g., by substituting a small amount of non-magnetic Zn^{2+} -ions for the magnetic Cu^{2+} -ions. Representative results obtained for such samples of $\text{La}_2\text{Cu}_{1-z}\text{Zn}_z\text{O}_4$ are shown in Fig. 6. The Zn-impurities represent both structural and magnetic impurities and therefore should affect the phononic as well as the magnetic peak in the heat conductivity. In fact, as can be inferred from the figure, the Zn-doping leads indeed to a gradual suppression of both, the phonon as well as the magnon contribution to κ . The analysis of the data for $\text{La}_2\text{Cu}_{1-z}\text{Zn}_z\text{O}_4$ using Eq. 7 in an analogous way as in the undoped case³ yields the interesting result for the low-temperature magnon mean free path that it scales linearly with the reciprocal Zn content [18]: $l_{\text{mag}} \approx 0.74 \cdot a/z$ (with the lattice constant a). Hence, these result suggests that l_{mag} is about equal to the unidirectional distance between the Zn-ions within the CuO_2 planes, i.e., κ_{mag} can be directly used to measure these distances.

³It is worth mentioning that a slight reduction of the spin wave velocity [112] and changes of the spin gaps induced by the Zn-ions can be safely ignored. These effects lead to corrections smaller than the experimental error.

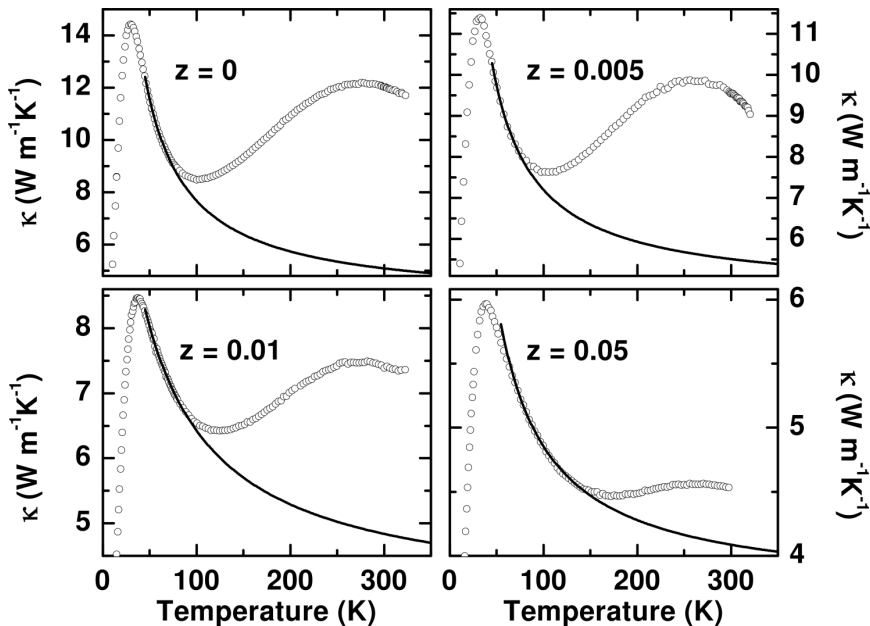


Figure 6: Open circles: Thermal conductivity κ of $\text{La}_2\text{Cu}_{1-z}\text{Zn}_z\text{O}_4$ polycrystals ($z = 0, 0.005, 0.01, 0.05$) as a function of T . Solid lines: extrapolated phonon heat conduction κ_{ph} assuming $\kappa_{\text{ph}} = \alpha/T + \beta$. Similar thermal conductivity data have been obtained on single crystalline $\text{La}_2\text{Cu}_{1-z}\text{Zn}_z\text{O}_4$ by Sun et al. [86] in qualitative agreement with the shown data. Image reproduced from [18].

It is important to note that the nature of the doped defects plays a decisive role in the effective strength of the magnon-defect scattering. In particular, *mobile* defects can be induced in La_2CuO_4 by hole-carrier doping. Such doping can be achieved either by substituting Sr for La or by enhancing the oxygen content of La_2CuO_4 , which at doping levels beyond about 5% leads to high-temperature superconductivity. Interestingly, in the case of Sr-doping, one observes a severe suppression of κ_{mag} already at $\sim 1\%$ doping level [86, 90], i.e. at much lower doping levels as compared to the afore-discussed Zn-doping. The different effect of these two doping schemes is consistent with the different impact of the defects on the antiferromagnetic correlations in the 2D-HAF. The doped charge strongly couples to the spin excitations resulting in a dressed quasiparticle (the spin polaron) which moves through the antiferromagnetic background. This motion of the spin polaron very effectively destroys the antiferromagnetic correlation of the spins in the plane (see Fig. 7 for an illustration) [74, 75], whereas static non-magnetic defects (which can be viewed as immobile holes, see Fig. 7a) only dilute the antiferromagnet and lead to a very moderate reduction of the spin correlation [112–114]. The strong suppression of κ_{mag} already at $\sim 1\%$ hole concentration suggests that the magnon mean free path amounts only a few lattice spacings, i.e. the effective ‘size’ of disturbed antiferromagnetic correlation due to the movement of a single hole is very large.

Berggold et al. pointed out that the magnitude of the peak in κ_{mag} of La_2CuO_4 significantly varies throughout the literature (see Fig. 5, bottom panel) and suggested that the difference arises due to different levels of excess oxygen in the material [88]. More specifically, they pointed out that the reported maximum κ_{mag} depends monotonically on the Néel temperature T_N (inset of Fig. 5). This relation is plausible since at small hole doping levels T_N is known to sensitively depend on the hole content not only for the case of Sr doping [114] but also for excess oxygen [115]. However, one bears in mind that, as has been shown for the case of $\text{La}_2\text{Cu}_{1-z}\text{Zn}_z\text{O}_4$, a reduced κ_{mag} can also be caused by chemical impurities through limiting the mean free path, yet having little effect on T_N , in particular, in very clean crystals. Furthermore, it is natural to expect that structural defects apart from chemical impurities play a crucial role, i.e. the degree of crystal perfection should have an impact on the size of the two-dimensional grains, which limit the mean free path, as well. This notion is confirmed by recent data for the heat conductivity of ultrapure La_2CuO_4

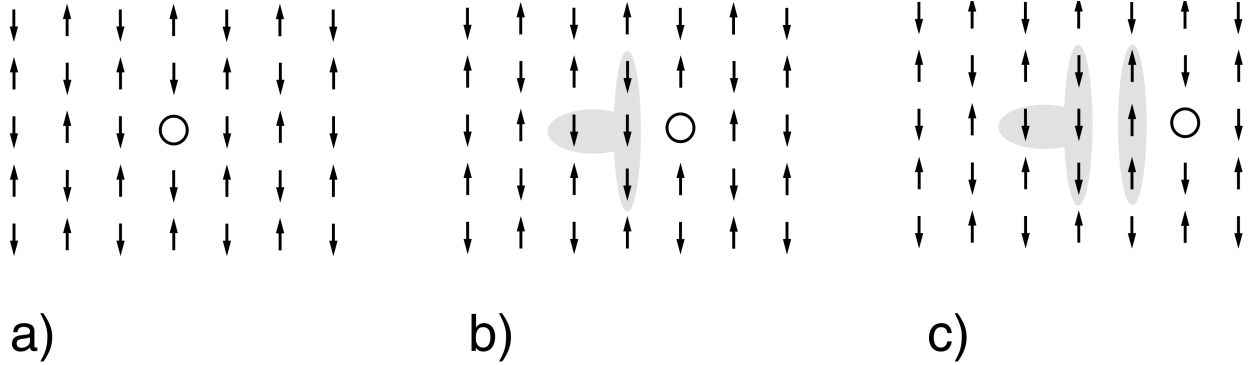


Figure 7: Sketch of a hole moving in an 2D-antiferromagnet. a) A hole in an antiferromagnet. b) Antiferromagnet after hopping of the hole to a neighboring site. c) Antiferromagnet after two hopping processes. The gray shaded areas highlight the regions of destroyed antiferromagnetic correlation.

with $T_N = 325$ K and κ_{mag} up to ~ 40 $\text{Wm}^{-1}\text{K}^{-1}$ [116], i.e., a much higher value than those collected in Fig. 5.

3. Two-leg spin ladders

3.1. Materials aspects

Magnetic thermal transport in a cuprate-based two-leg spin ladder system up to present primarily has been observed in the material $(\text{Sr, Ca, La})_{14}\text{Cu}_{24}\text{O}_{41}$. The crystal structure (see Fig. 8) and also the connected physical properties of this material are significantly more complex as compared to all materials discussed in this review and thus deserve a special attention. $(\text{Sr, Ca, La})_{14}\text{Cu}_{24}\text{O}_{41}$ is composed of two main structural elements which define the physical properties. These are, on the one hand, Cu_2O_3 planes which realize $S = 1/2$ two-leg spin ladders of the type as described in Section 1.2. Each of these planes is formed by a parallel network of individual two-leg ladders in the ac -plane (see right panel of Fig. 9). Each Cu spin (with $S = 1/2$) interacts strongly antiferromagnetically via 180° Cu-O-Cu bonds with its two neighboring Cu spins along the ladder legs (leg interaction J_{\parallel} , parallel to the c -axis) and also antiferromagnetically with its one neighboring Cu spin on the same rung within one two-leg ladder (rung interaction J_{\perp} , parallel to the a -axis). These interactions result in an effective $S = 1/2$ two-leg ladder model as described by Eq. 1 with $J_{i,j} = J_{\parallel}$ along the legs and $J_{i,j} = J_{\perp}$ along the rungs for each of the individual ladders. The interaction of the spins of one ladder to its neighboring ones is strongly frustrated and thus causes an effective decoupling of the individual ladders from each other [117]. The frustration arises since each Cu spin of one ladder interacts relatively weakly ferromagnetically via 90° Cu-O-Cu bonds with two strongly antiferromagnetically coupled Cu-spins (interaction J_{\parallel}) of the neighboring ladder.

On the other hand, the structure contains planes (again in the ac -direction) of CuO_2 chains of edge-shared CuO_4 plaquettes with the main exchange path of two neighboring Cu spins within one chain via the approximately 90° Cu-O-Cu bonds, running along the c -axis (see left panel of Fig. 9). The resulting magnetic interaction is about one order of magnitude smaller than those of the ladder and have been shown not to directly contribute to the magnetic heat transport [15].

The total crystal structure is composed of an alternating stacking of the ladder and chain planes along the b -axis where adjacent planes are separated by layers (Sr, Ca, La) ions (see Fig. 8 and central panel of Fig. 9). The chains and the ladders possess along the c -axis different translational periods and thus form two incommensurate sublattices. Together with the (Sr, Ca, La) ions, the ladders constitute a sublattice unit cell with $a \approx 11.3 \dots 11.5$ Å, $b \approx 12.5 \dots 13.4$ Å, and $c_L \approx 3.9$ Å. The sublattice unit cell of the chains has the same a and b lattice constants but is somewhat shorter along the chain direction with $c_C \approx 2.75$ Å. The almost commensurable average common unit cell is $c = 7 \times c_L \approx 10 \times c_C$. It should be noted, that the exact

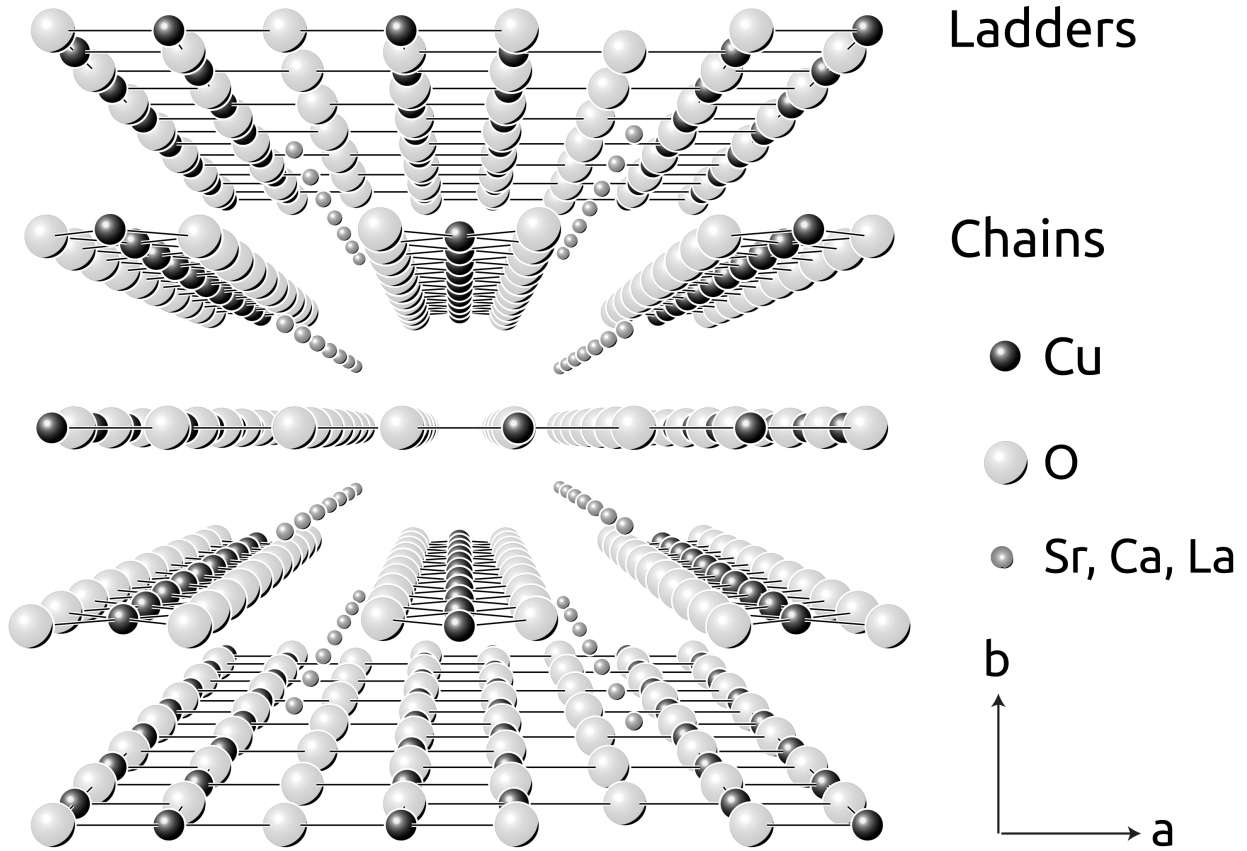


Figure 8: Three-dimensional representation of the crystal structure of $(\text{Sr}, \text{Ca}, \text{La})_{14}\text{Cu}_{24}\text{O}_{41}$ with a view in the direction of the CuO_3 -ladders and CuO_2 -chains (c -axis). From [118].

values of the lattice constants depend significantly on the relative ratio of the Sr, Ca, and La constituents [118].

Interestingly, the formal valencies of the stoichiometric compound are $(\text{Sr}^{2+})_{14}(\text{Cu}^{2.25+})_{24}(\text{O}^{2-})_{41}$. This means, the magnetically active ladder and chain structures are intrinsically hole-doped. These holes are not equally distributed among both structures. On the one hand, about one hole per formula unit is located in the ladders [119, 120], whereas the amount in the chains is estimated to about 6 holes per formula unit. The intrinsically doped holes have been shown to undergo a charge ordered state in both the chains and in the ladders. In the former, the ordered holes are found to yield a state of non-interacting spin dimer singlets with an excitation gap of about 130 K [121–125], whereas the holes in the ladders form a long-range ordered hole crystal [126, 127]. We shall see further below that this charge ordering has profound impact on the magnetic heat transport properties.

The isovalent substitution of Ca for Sr in $\text{Sr}_{14}\text{Cu}_{24}\text{O}_{41}$ has strong consequences for the physical properties. The charge transport properties gradually develop from a semiconductor-like temperature dependence for $\text{Sr}_{14-x}\text{Ca}_x\text{Cu}_{24}\text{O}_{41}$ at $x = 0$ to an increasingly metallic characteristics at maximal $x \approx 12$ [19, 78]. Remarkably, at $x \gtrsim 5$ the charge ordered state collapses [121, 122, 128] and at very high Ca doping levels, superconductivity occurs at high pressure [129, 130]. The increasing metallic nature upon Ca doping commonly is interpreted as a result of a doping induced transfer of holes from the chains into the ladder substructures [68, 119, 120].

Alternatively, the divalent Sr and Ca ions can be substituted by trivalent La, which causes a drastic

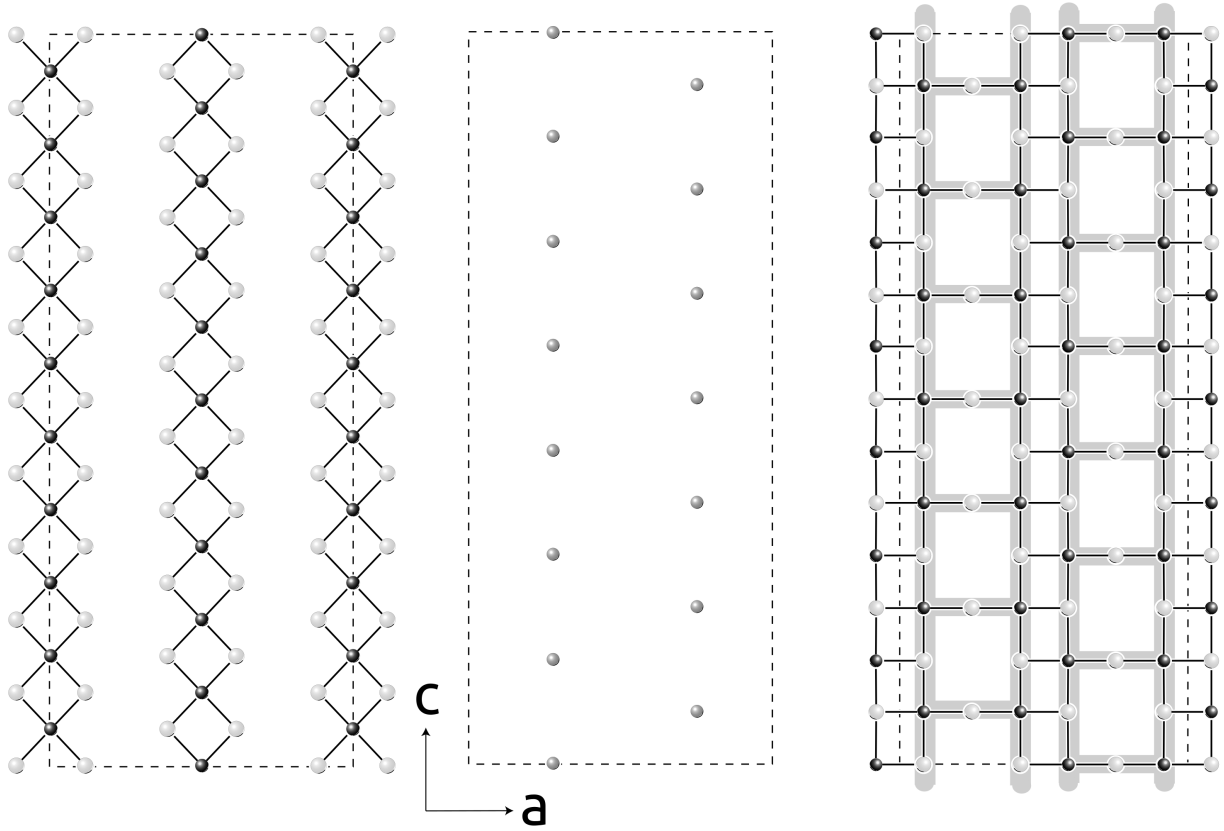


Figure 9: Structural elements of $(\text{Sr, Ca, La})_{14}\text{Cu}_{24}\text{O}_{41}$. Left: Plane of CuO_2 spin chains. Center: layer of (Sr, Ca, La). Right: Plane of Cu_2O_3 spin ladders with the structure of two separate two-leg ladders indicated in grey. The dashed line indicates the size of the in-plane average unit cell. Dark and light grey bullets represent the Cu and O sites, respectively. From [118].

reduction of the total hole content in $(\text{Sr, Ca})_{14-y}\text{La}_y\text{Cu}_{24}\text{O}_{41}$ with increasing y . Thus, at nominally $y = 6$ the system reaches the realization of 'hole-free' ladder and chain subsystems. It should be noted, however, that the highest La content at which phase pure single crystals can be achieved is $y \approx 5.2$ [118, 131]. Quite importantly, already a moderate La-content of $y \approx 2$ yields practically 'hole-free' spin ladders [120]. A further consequence of the La-doping is a rapid destruction of the dimer ground state in the chains and the formation of an antiferromagnetic ground state of the chains at $y \gtrsim 4$ [118, 132–136].

The hole-free ladders in $(\text{Sr, Ca})_{14-y}\text{La}_y\text{Cu}_{24}\text{O}_{41}$ at finite y exhibit the theoretically expected properties of an $S = 1/2$ two-leg quantum spin ladder in a remarkable way. Inelastic neutron scattering (INS) and optical spectroscopy experiments yield a large $J_{\parallel}/k_B \approx 1300 \dots 2200$ K and $J_{\perp}/k_B \approx 1300 \dots 1440$ K with a gapped ground state and a large triplet excitation gap $\Delta \approx 310 \dots 410$ K [134, 137, 138]. For $\text{Sr}_{14}\text{Cu}_{24}\text{O}_{41}$, despite the finite amount of doped holes, the magnetism is barely different [139, 140], whereas for $\text{Sr}_{14-x}\text{Ca}_x\text{Cu}_{24}\text{O}_{41}$ controversial reports exist concerning the spin gap Δ . INS results indicate that Δ remains practically unchanged up to the highest Ca-content [140], whereas findings from nuclear magnetic resonance (NMR) experiments suggest a gradual decrease of Δ [141–144]. It should be mentioned that the NMR findings suggest a somewhat larger Δ/k_B for $x = 0$ (up to ~ 650 K) than those from INS.

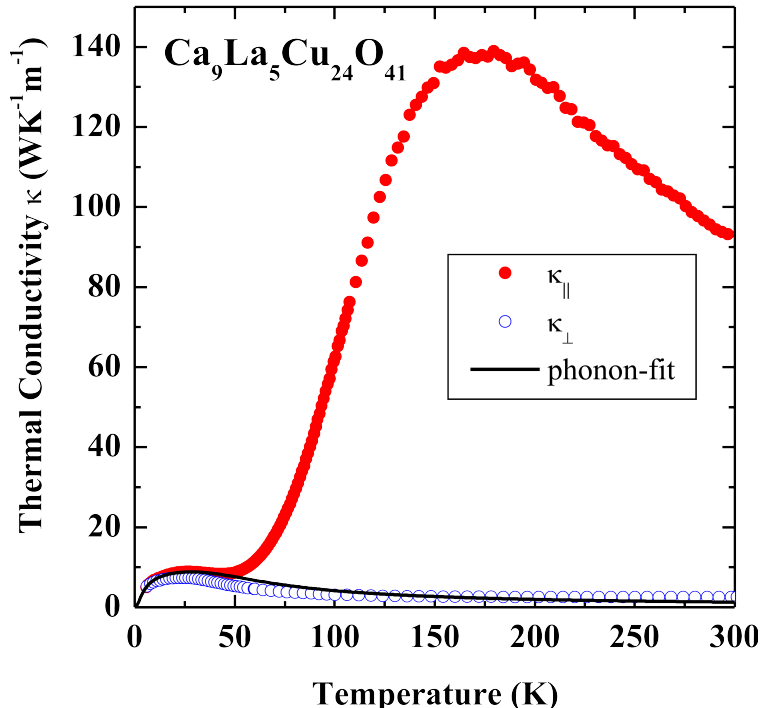


Figure 10: Thermal conductivity of $\text{Ca}_9\text{La}_5\text{Cu}_{24}\text{O}_{41}$ as a function of temperature measured along the a and c axes, κ_{\perp} and κ_{\parallel} , respectively. The solid line represents an estimate of the phonon contribution to κ_c based on the Callaway model. Figure adapted from [15].

3.2. Qualitative proof of magnon heat transport in the spin ladders

Kudo et al. were the first to report about unconventional magnon heat transport of the spin ladders in the material $\text{Sr}_{14-x}\text{Ca}_x\text{Cu}_{24}\text{O}_{41}$ with the Ca content ranging from $x = 0$ to $x = 9$ [13]. The data presented in their pioneering study are qualitatively compatible with the data shown in Figures 2, 10, and 15 and also with data by Sologubenko et al. [14]. In the following, instead of addressing these early works on first-generation single crystals of this material in detail, we focus on more recent work which allows better to carve out the relevant physics.

The data shown in Fig. 2 for the pristine material $\text{Sr}_{14}\text{Cu}_{24}\text{O}_{41}$ are qualitatively similar to the afore-discussed case of La_2CuO_4 with the remarkable difference that the high-temperature anomaly in κ_{\parallel} , which is measured parallel to the spin ladders along the c -axis, is purely one-dimensional, since it is absent in both directions perpendicular to the ladders [15]. The magnetic nature of the anomaly in κ_{\parallel} is thus evident, the more so as no structural instabilities as is the case for the two-dimensional layered cuprates are known to be present in this material. However, for the sake of meticulous correctness, one should exclude other thinkable one-dimensional contributions to the heat transport parallel to the ladder structures in the material. In particular, one could imagine unusual optical phonon modes related to the quasi-one-dimensional structural elements present in the materials as well magnetic heat transport by the also present CuO_2 -chain structure in $(\text{Sr}, \text{Ca}, \text{La})_{14}\text{Cu}_{24}\text{O}_{41}$.

Fig. 10 shows the thermal conductivity parallel (κ_{\parallel}) and perpendicular (κ_{\perp}) to the spin ladder structures in the compound $\text{Ca}_9\text{La}_5\text{Cu}_{24}\text{O}_{41}$ [15]. In this material, the Sr^{2+} site of the pristine compound $\text{Sr}_{14}\text{Cu}_{24}\text{O}_{41}$ is substituted by two different ions, namely Ca^{2+} and La^{3+} . The resulting structural disorder leads to a strong defect-scattering of the phonons in the system and, correspondingly, to a drastic suppression of its phonon heat conductivity κ_{ph} , which is evident from a direct comparison of κ_{\perp} of $\text{Ca}_9\text{La}_5\text{Cu}_{24}\text{O}_{41}$ and $\text{Sr}_{14}\text{Cu}_{24}\text{O}_{41}$ in Fig. 10 and Fig. 2, respectively. Interestingly, the high-temperature peak in κ_{\parallel} is not affected by this suppression. In contrast, in the direct comparison, this peak is even enhanced in $\text{Ca}_9\text{La}_5\text{Cu}_{24}\text{O}_{41}$.

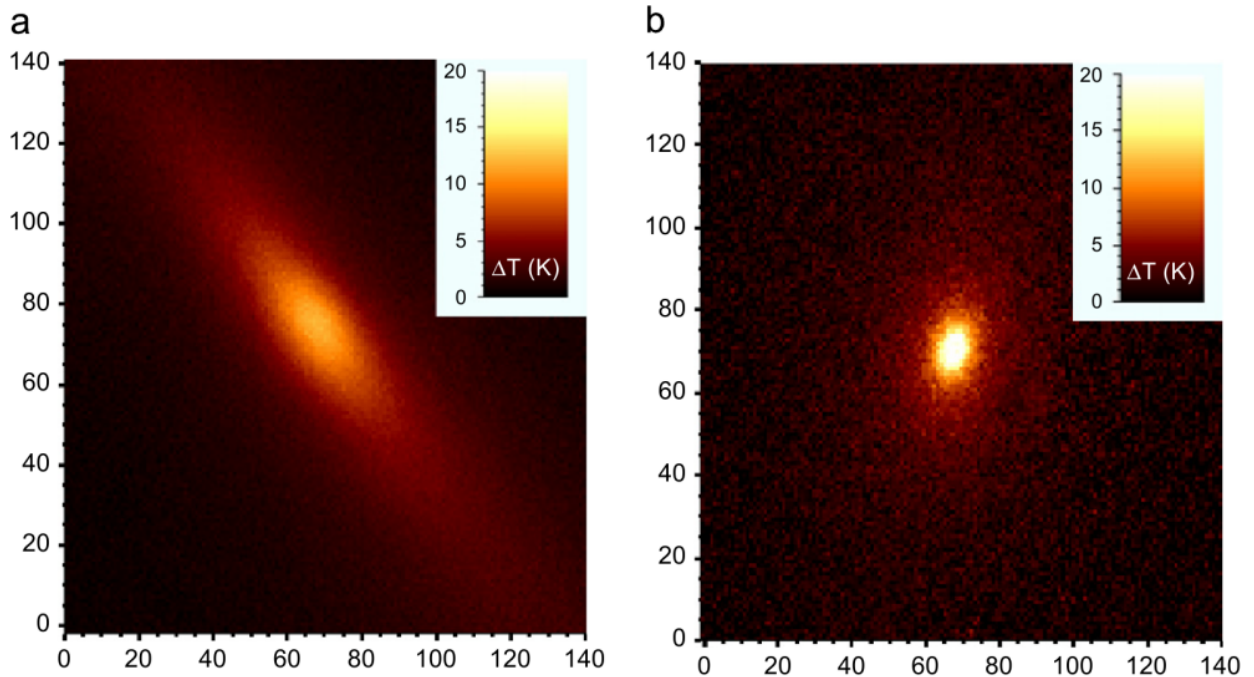


Figure 11: a) Fluorescent microthermal image of the ac -plane of $\text{Ca}_9\text{La}_5\text{Cu}_{24}\text{O}_{41}$ generated by a localized heat pulse in the center of the image. It shows a highly anisotropic pattern due to the high thermal conductivity in the (diagonal) c -direction (κ_{\parallel}). b) Fluorescent microthermal image of the ab -plane of $\text{Ca}_9\text{La}_5\text{Cu}_{24}\text{O}_{41}$ generated by a localized heat pulse in the center of the image shows an isotropic pattern. The distances on both x - and y -axis are in mm. Figure adapted from [145].

We shall see further below that this enhancement can be attributed to the vanishing hole content in the ladders of $\text{Ca}_9\text{La}_5\text{Cu}_{24}\text{O}_{41}$.

This observation clearly rules out that the high-temperature peak stems from unconventional phononic modes since the suppressed κ_{ph} demonstrates clearly that these modes are heavily disturbed by the disorder in the material. Furthermore, also thinkable magnetic heat transport of the CuO_2 chains can now safely be excluded because the magnetic state of these chains is fundamentally changed upon the substitution of La and Ca, for Sr [124, 125, 133, 136]. Thus, the high-temperature peak observed in κ_{\parallel} of $(\text{Sr}, \text{Ca}, \text{La})_{14}\text{Cu}_{24}\text{O}_{41}$ unambiguously represents the magnon heat conductivity κ_{mag} in the material. Furthermore, and remarkably, one finds the unusual materials property that $\kappa_{\text{ph}} \ll \kappa_{\text{mag}}$ at $T \gtrsim 40$ K which is most evident for $\text{Ca}_9\text{La}_5\text{Cu}_{24}\text{O}_{41}$. This remarkable anisotropy of the heat conductivity tensor has recently been visualized by fluorescent microthermal imaging at room temperature, see Fig. 11 [145].

3.3. Extraction of the magnetic heat conductivity

Due to the presence of a sizable spin gap in $(\text{Sr}, \text{Ca}, \text{La})_{14}\text{Cu}_{24}\text{O}_{41}$ of the order of $\Delta/k_B \sim 300 \dots 500$ K [134, 138, 139, 141, 143] one can safely assume that for low temperatures the magnon heat conductivity falls off as $\kappa_{\text{mag}} \propto \exp[-\Delta/(k_B T)]$ and becomes negligible at $T \lesssim 40$ K in comparison to the phonon heat conductivity κ_{ph} . Thus, one can safely fit κ_{ph} using the Callaway model [108] in this temperature range and extrapolate this fit towards higher temperature in order to estimate the phononic contribution to κ_{\parallel} [14, 15]. The solid lines in Fig. 2 and Fig. 10 represent corresponding results for $\text{Sr}_{14}\text{Cu}_{24}\text{O}_{41}$ and $\text{Ca}_9\text{La}_5\text{Cu}_{24}\text{O}_{41}$, respectively. Note, that the extreme suppression of κ_{ph} in $\text{Ca}_9\text{La}_5\text{Cu}_{24}\text{O}_{41}$ renders the possible errors in the estimation of κ_{ph} (and thus κ_{mag}) very small, which is particularly important at low temperature where κ_{mag} is still small. Assuming again $\kappa_{\parallel} = \kappa_{\text{ph}} + \kappa_{\text{mag}}$, the magnon heat conductivity data can now be computed from the measured data. The resulting temperature dependence of κ_{mag} for $\text{Sr}_{14}\text{Cu}_{24}\text{O}_{41}$ and $\text{Ca}_9\text{La}_5\text{Cu}_{24}\text{O}_{41}$ is depicted in Fig. 12 [15].

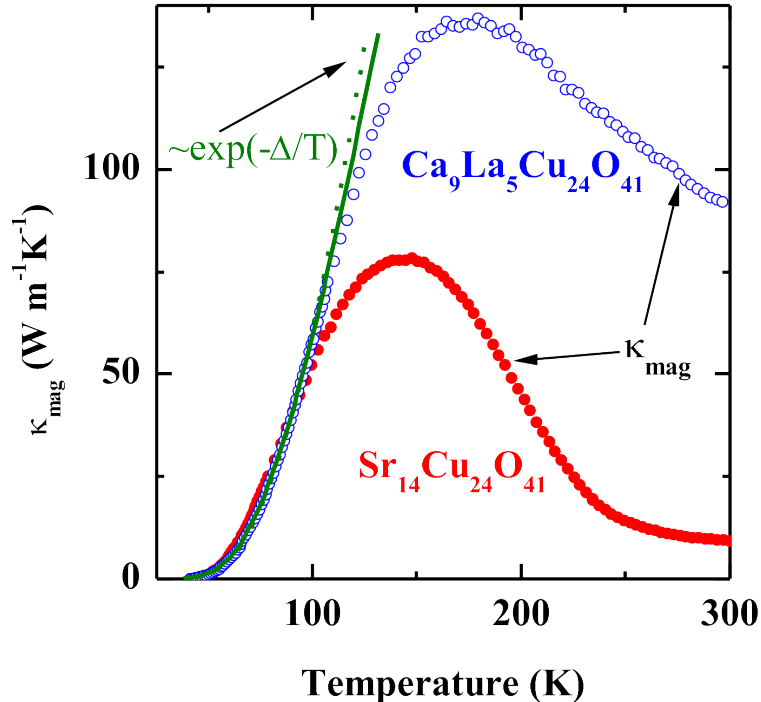


Figure 12: Temperature dependence of κ_{mag} of the ladder compounds $\text{Sr}_{14}\text{Cu}_{24}\text{O}_{41}$ and $\text{Ca}_9\text{La}_5\text{Cu}_{24}\text{O}_{41}$. The solid line represent a fit to the low-temperature data of κ_{mag} of $\text{Ca}_9\text{La}_5\text{Cu}_{24}\text{O}_{41}$ on basis of the kinetic model (Eq. 10). Figure adapted from [15]. Similar data for κ_{mag} of $\text{Sr}_{14}\text{Cu}_{24}\text{O}_{41}$ have been found by Sologubenko et al. [14].

3.4. Analysis of the magnon heat conductivity

The temperature dependence of the shown data is for both compounds very similar in the region of the low-temperature increase of κ_{mag} . Differences become apparent only at $T \gtrsim 100$ K: The increase of κ_{mag} of $\text{Sr}_{14}\text{Cu}_{24}\text{O}_{41}$ weakens and after reaching a maximum ($\sim 80 \text{ Wm}^{-1}\text{K}^{-1}$) at ~ 140 K, κ_{mag} decreases strongly and saturates at $\sim 10 \text{ Wm}^{-1}\text{K}^{-1}$ for $T \gtrsim 240$ K. In contrast, κ_{mag} of $\text{Ca}_9\text{La}_5\text{Cu}_{24}\text{O}_{41}$ increases much stronger at $T \gtrsim 100$ K. Also here a maximum value is reached ($\sim 140 \text{ Wm}^{-1}\text{K}^{-1}$), but at clearly higher temperature $T \approx 180$ K, after which κ_{mag} decreases only moderately and stays large at $\sim 90 \text{ Wm}^{-1}\text{K}^{-1}$ even at room temperature, i.e. it attains a value which is comparable to the heat conductivity of a metal.

Kinetic model

In the one-dimensional case, the kinetic model (Eq. 2) for the thermal conductivity of a single ladder yields [14, 15, 22]

$$\tilde{\kappa} = \frac{1}{2\pi} \int v_k l_k \frac{d}{dT} n_k \epsilon_k dk, \quad (8)$$

again with v_k , l_k , and ϵ_k the velocity, mean free path, and energy of a magnon⁴. The mathematical form of the occupation function n_k is, however, unclear for the case of a two-leg spin ladder. Based on the fact that the elementary excitations of a two-leg ladder are triplet excitations, i.e. bosons, Sologubenko et

⁴It should be noted that the term 'magnon' refers to the specific $\Delta S = 1$ triplet excitations of the $S = 1/2$ two-leg quantum spin ladder, which sometimes are also dubbed as 'triplon' excitations. They are not be confused with the spin-wave type magnon excitations of the 2D-HAF.

al. approximated it by the Bose-function [14]. However, Hess et al. argued that the Bose function leads to unphysically large triplet densities at higher temperatures and suggested an occupation function of the form

$$n_k = \frac{3}{e^{\frac{\epsilon_k}{k_B T}} + 3} \quad (9)$$

to account, on average, for the hard-core constraint of no on-site double occupancy for the triplet excitations [15]. The use of it and assuming $l_{\text{mag}} \equiv l_{\mathbf{k}}$ leads then to the expression [15, 33]

$$\kappa_{\text{mag}} = \frac{3n_s k_B^2}{\pi \hbar} l_{\text{mag}} T \int_{\frac{\Delta}{k_B T}}^{\frac{\epsilon_{\text{max}}}{k_B T}} x^2 \frac{e^x}{(e^x + 3)^2} dx, \quad (10)$$

where n_s is now the number of ladders per unit area. Note, that Eq. 10) differs from the expression used by Sologubenko *et al.* [14] for the heat-conductivity of one-dimensional bosons not only by the distribution function (9) but also by an overall factor of three accounting for the triplet degeneracy. Thus, the following considerations and the discussion of analyzing the κ_{mag} data for the two-leg ladder compounds will be based on Eq.10. Note further, that this result for a one-dimensional system does not depend on the specific form of the dispersion function ϵ_k and the velocity v_k [15]. The dispersion enters only through its band minimum, i.e., the spin gap Δ and its maximum ϵ_{max} . Experimentally, one finds a lower bound $\epsilon_{\text{max}} \sim 200$ meV in $(\text{Sr, Ca, La})_{14}\text{Cu}_{24}\text{O}_{41}$ [134, 138, 139]. At $T \lesssim 300$ K, the integral in Eq. 10 therefore does only depend weakly on ϵ_{max} . Its exact value thus does not play an important role and one might even set $\epsilon_{\text{max}} = \infty$ at very low temperature [33]. In any case, due the presence of a spin gap κ_{mag} is expected to be exponentially suppressed at low temperature $k_B T \ll \Delta < J$ and one might approximate $\kappa_{\text{mag}} \propto \exp[-\Delta/(k_B T)]$ presuming a temperature independent l_{mag} .

Low-temperature increase – thermal occupation of magnons

Apparently, for both materials κ_{mag} follows such an exponential increase at low temperature (see dotted line in Fig. 12. An even more accurate description of the data is obtained if the data is described by Eq. 10 [15]. The solid line in the figure shows a corresponding fit to the data of $\text{Ca}_9\text{La}_5\text{Cu}_{24}\text{O}_{41}$ with a temperature independent l_{mag} and the spin gap Δ as free parameters in the temperature range 54-102 K. The data for $\text{Sr}_{14}\text{Cu}_{24}\text{O}_{41}$ can be fitted similarly well but in the somewhat reduced temperature interval 61-91 K (see [15], for the details). In both cases, this analysis yields very similar values for the magnon mean free path l_{mag} and the spin gap. For the latter one finds $\Delta/k_B = 418 \pm 15$ K and $\Delta/k_B = 396 \pm 10$ K for $\text{Ca}_9\text{La}_5\text{Cu}_{24}\text{O}_{41}$ and $\text{Sr}_{14}\text{Cu}_{24}\text{O}_{41}$, respectively, which is in the same order of magnitude than results reported from neutron scattering and NMR measurements (see Section 3.1) [134, 138, 139, 141, 143]. The results for the low-temperature mean free path l_0 are almost identical, specifically $l_0 = 2980 \pm 110$ Å and $l_0 = 2890 \pm 230$ Å for $\text{Ca}_9\text{La}_5\text{Cu}_{24}\text{O}_{41}$ and $\text{Sr}_{14}\text{Cu}_{24}\text{O}_{41}$, respectively.⁵ This corresponds to about 750 lattice spacings along the ladder, which is surprisingly large in view of the rather complicated crystal structure of $(\text{Sr, Ca, La})_{14}\text{Cu}_{24}\text{O}_{41}$ [117], and, even more intriguing, in view of the spin-spin correlation length in a two-leg spin ladder which exponentially vanishes already after about 3-4 lattice spacings [67, 68]. This means, the mean free path becomes orders of magnitude larger than the size of antiferromagnetically correlated spin configurations. This underpins the fundamentally different quantum nature of the magnons in the two-leg spin ladders as compared to antiferromagnetic spin wave type magnons which emerge from an antiferromagnetic ground state with infinite spin-spin correlation length, as is the case for the 2D-HAF.

⁵Note, that l_0 specifically denotes the low-temperature value of l_{mag} used for fitting the low-temperature increase of κ_{mag} . As we shall see later, l_{mag} becomes temperature dependent at higher temperature. Note further, that the slightly smaller values of l_0 and Δ for $\text{Ca}_9\text{La}_5\text{Cu}_{24}\text{O}_{41}$ as compared to the values reported in the original paper by [15], are a consequence of the usage of more accurate lattice parameters and an optimized fit-interval. It is stressed that these small corrections have no further consequences on the conclusions drawn in the original paper.

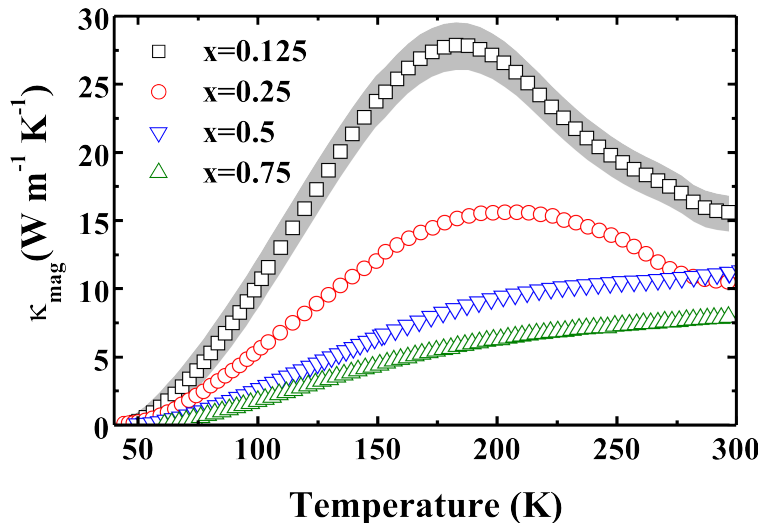


Figure 13: κ_{mag} of $\text{Sr}_{14}\text{Cu}_{24-x}\text{Zn}_x\text{O}_{41}$ at $x = 0.125, 0.25, 0.5, 0.75$. The gray shaded areas display the experimental uncertainty of κ_{mag} resulting from the uncertainties of κ_{ph} for the representative case $x = 0.125$. Figure adapted from [34].

Ballistic heat transport?

The report of a large magnon thermal conductivity in $\text{Sr}_{14}\text{Cu}_{24}\text{O}_{41}$ and $\text{Ca}_9\text{La}_5\text{Cu}_{24}\text{O}_{41}$ [14, 15] and pertinent large mean free paths soon after triggered a number of controversial theoretical works which addressed the conjecture that the heat transport of a two-leg spin ladder similar to that of a Heisenberg chain was *ballistic*, despite the non-integrability of the model (see also Section 4 for further elaboration on the connection between the integrability of the spin model and the thermal Drude weight) [46–48, 54, 61–63]. One particular aspect of this context has been addressed by Alvarez and Gros, who claimed that the heat transport of a two-leg ladder indeed was ballistic [46]. More specifically, based on exact diagonalization results they found a finite thermal Drude weight and evaluated a much shorter magnon mean free path as compared to the above findings through using the kinetic model. Theoretically, these findings have been challenged by several groups: Possible problems due to finite size effects of the exact diagonalization results have been pointed out [47]. Furthermore, high-temperature approximations yielded a vanishing Drude weight [54]. It has been argued, however, that the two-leg ladder model despite being non-integrable is still close enough to integrability to yield finite but large transport coefficients [61, 62].

Experimentally, the magnitude of the mean free paths extracted by means of the kinetic model have been verified by a specific doping experiment. Similarly as in the 2D-case of La_2CuO_4 the heat conductivity of Zn-doped $\text{Sr}_{14}\text{Cu}_{24}\text{O}_{41}$ has been studied, in order to render the determination of the mean free path model-independent [34]. The non-magnetic Zn-ions act as scatterers for the magnons and cause a gradual suppression of κ_{mag} as can be inferred from Fig. 13 which reproduces the obtained data for $\text{Sr}_{14}\text{Cu}_{24-z}\text{Zn}_z\text{O}_{41}$. Since the mean distance of Zn-ions within a ladder, $d_{\text{Zn-Zn}}$, can be computed from the Zn content z , it is instructive to compare this distance with the magnon mean free path which has been extracted from the κ_{mag} data in Fig. 13 using the kinetic model (Eq. 10). The resulting l_{mag} vs. $d_{\text{Zn-Zn}}$ is shown in Fig. 14. As is evident from the figure, l_{mag} roughly scales with $d_{\text{Zn-Zn}}$, and a linear fit to the data points yields a slope of 1.17 ± 0.25 , which is close to unity. This confirms unambiguously that the values for l_{mag} obtained from the kinetic model are in fair agreement with real scattering lengths in the material [34].

The above findings allow to stress several important points: Despite the strong quantum nature of the two-leg spin ladder (which manifests itself in a large spin gap and a short-range spin correlation) the experimentally observed magnetic heat conductivity can be successfully described by the simple Boltzmann-type kinetic model (Eq. 10). The model is non-integrable and thus ballistic heat transport is not expected from fundamental conservation laws [12, 146], yet the heat conductivity seems anomalously large because the experimental mean free paths are up to several orders of magnitude larger than the spin correlation

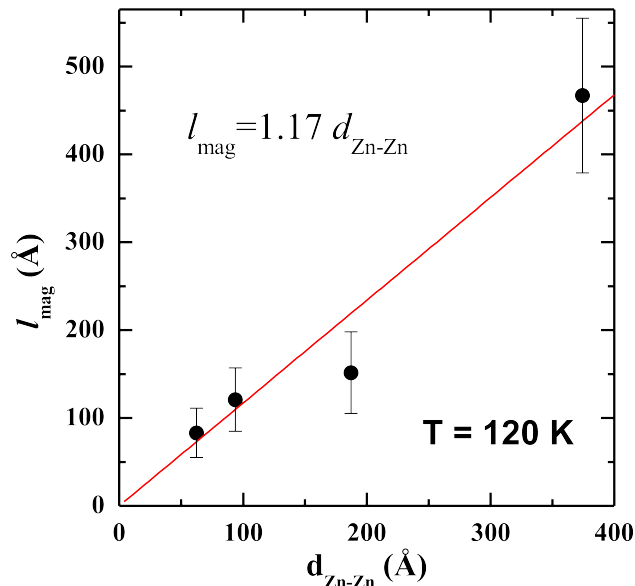


Figure 14: l_{mag} as a function of $d_{\text{Zn-Zn}}$. Solid line: linear fit line through the origin. The error bars arise due to uncertainties in determining κ_{ph} . Figure reproduced from [34].

lengths in the system.

Temperature dependent scattering processes

We will now briefly address the characteristics of κ_{mag} of the spin ladders at higher temperatures, in order to study the influence of temperature-dependent scattering processes on the magnon heat transport, i.e. scattering of magnons off other excitations in a solid such as phonons, charge carriers, and also other magnons. The spin ladder material $(\text{Sr, Ca, La})_{14}\text{Cu}_{24}\text{O}_{41}$ is an ideal 'playground' in this regard because it can be doped in very different ways. Definitely, the possibility of doping the spin ladders with charge carriers is intriguing and unique among one-dimensional cuprate quantum magnets.

Magnon-hole scattering

In the previous discussion of the low-temperature increase at $T \lesssim 100$ K the fact that the hole content in the ladders of $\text{Sr}_{14}\text{Cu}_{24}\text{O}_{41}$ and $\text{Ca}_9\text{La}_5\text{Cu}_{24}\text{O}_{41}$ is very different did not play an important role. Apparently, at this low temperatures the presence of the hole in the ladders of $\text{Sr}_{14}\text{Cu}_{24}\text{O}_{41}$ is unimportant for the magnetic heat transport, as is reflected by the very similar values for κ_{mag} (see Fig. 12) and thus the mean free path and the spin gap of both compounds. New light is shed on the relevance of the holes in the ladders from the direct comparison of the magnon heat conductivity κ_{mag} of $\text{Ca}_9\text{La}_5\text{Cu}_{24}\text{O}_{41}$ with that of $\text{Sr}_{14}\text{Cu}_{24}\text{O}_{41}$ in Fig. 12 at $T \gtrsim 100$ K. The impact of the higher hole content in the ladders of $\text{Sr}_{14}\text{Cu}_{24}\text{O}_{41}$ can directly be read off the figure: while κ_{mag} is practically identical for both compounds at $T \lesssim 100$ K, one observes the already described differences at higher temperature. It is straightforward to explain the comparatively stronger high-temperature suppression of κ_{mag} of $\text{Sr}_{14}\text{Cu}_{24}\text{O}_{41}$ by a significant magnon-hole scattering because the presence of holes in the ladders is the essential difference to the undoped ladders in $\text{Ca}_9\text{La}_5\text{Cu}_{24}\text{O}_{41}$. The equality of both κ_{mag} data below the characteristic temperature $T_0 \approx 100$ K implies in addition that this scattering process, on the one hand, is completely unimportant at low temperature $T \lesssim T_0$, but on the other hand unfurls its full strength above another characteristic temperature $T^* \approx 240$ K where κ_{mag} saturates [14, 15, 17, 19].

This surprising temperature dependence of the magnon-hole scattering strength has been investigated towards its robustness against changes of the hole concentration [14, 19]. κ_{mag} was studied in a series of $\text{Sr}_{14-x}\text{Ca}_x\text{Cu}_{24}\text{O}_{41}$ single crystals. Results for κ_{mag} at low doping levels $x \leq 5$ [19] are shown in Fig. 15.

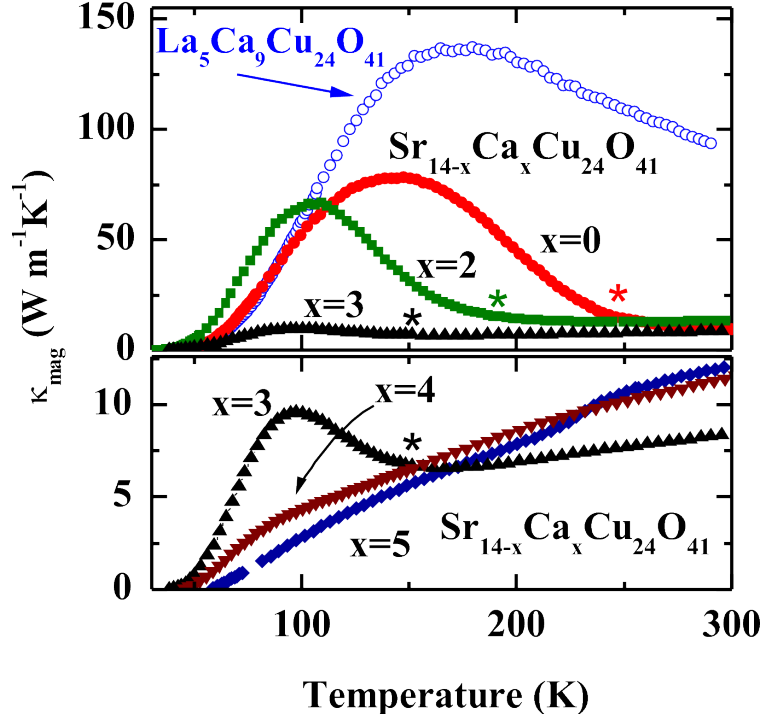


Figure 15: $\kappa_{\text{mag}}(T)$ of $\text{Sr}_{14-x}\text{Ca}_x\text{Cu}_{24}\text{O}_{41}$ ($x = 0, 2, 3, 4, 5$). Top panel: Data for ($x = 0, 2, 3$) in comparison with κ_{mag} of $\text{Ca}_9\text{La}_5\text{Cu}_{24}\text{O}_{41}$. Lower panel: enlarged representation for $x = 3, 4, 5$. Stars indicate the approximative T^* for $x \leq 3$. Similar results for $x = 0, 2$ have been reported by [14]. Figure adapted from [19, 33].

One can infer quite clearly that T^* is gradually shifted towards lower temperature with increasing x , i.e., the temperature interval in which κ_{mag} is suppressed due to magnon-hole scattering is extended to lower temperatures. At $x = 4, 5$ the magnon-hole scattering is apparently so dominant, that even the low-temperature peak is suppressed.

The observed doping dependence of the magnon-hole scattering can clearly be related to the charge-ordered state [126, 127] of the holes in the ladder below T^* [14, 15, 17, 19]. More specifically, the charge order is accompanied by a drastic enhancement of the magnon mean free path l_{mag} of the magnons where the scattering probability turns out to be practically one (inferred from comparing the l_{mag} with the estimated distance of holes in the ladders, see below) in the case of completely mobile holes ($T > T^*$), and vanishes in the long-range ordered state ($T < T_0$) [14, 19]. Note, that charge order is also present at $x = 4, 5$ [147, 148]. However, its onset temperature T^* is already so low that κ_{mag} is significantly suppressed. Note that the magnon heat conductivity in these samples is still well detectable, despite the substantial suppression, see Fig. 15. Sologubenko et al. have shown that a large κ_{mag} exists even at a very high doping level $x = 12$ [14], where no charge order is present [127, 147, 148].

The above qualitative analysis of the magnon-hole scattering in $\text{Sr}_{14-x}\text{Ca}_x\text{Cu}_{24}\text{O}_{41}$ demonstrates, that κ_{mag} of a quantum magnet beyond being intriguing in itself can also be used as a *probe* for the charge dynamics and order in the material. A very interesting quantitative result which can be inferred from the above discussion for the undoped $\text{Sr}_{14}\text{Cu}_{24}\text{O}_{41}$ is that through the determination of the low-temperature value of the mean free path l_0 , i.e. the mean free path deep in the charge ordered phase, the correlation length of the charge order ξ can be estimated. Since $l_0 \sim 3000 \text{ \AA}$ is much larger than the mean hole distance in the ladders and l_0 is practically identical for the hole-free $\text{Ca}_9\text{La}_5\text{Cu}_{24}\text{O}_{41}$, the charge order should be perfect at least on this length scale, i.e. $\xi \gtrsim 3000 \text{ \AA}$ [19].

It should be noted, that the magnon-hole scattering and the impact of the charge order on it can be well analyzed by studying the temperature dependence of the magnon mean free path $l_{\text{mag}}(T)$ which can

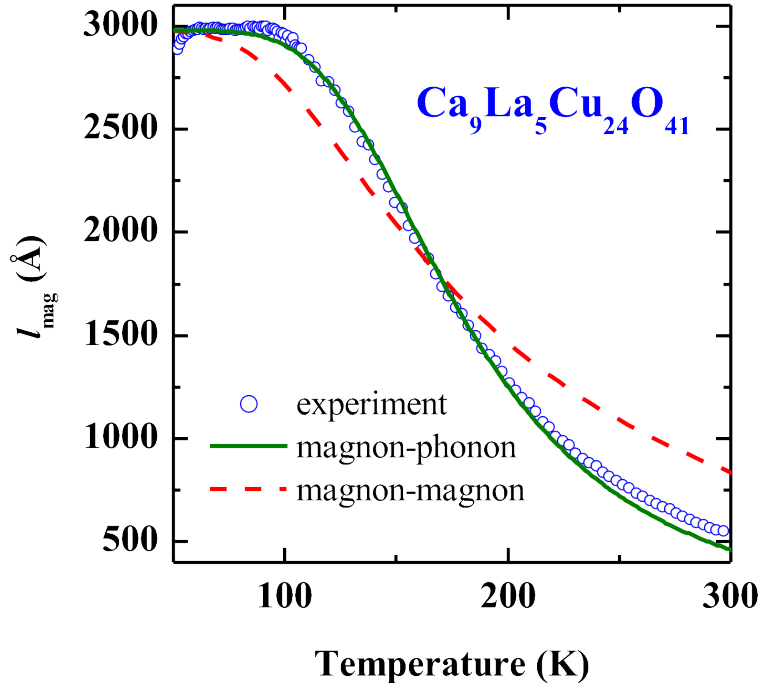


Figure 16: l_{mag} of $\text{Ca}_9\text{La}_5\text{Cu}_{24}\text{O}_{41}$ as a function of temperature T . The solid and broken lines represent fits of l_{mag} accounting for magnon-phonon and magnon-magnon scattering respectively. Adapted from [15, 20, 33].

be extracted by comparing the measured κ_{mag} data with Eq. 10 if the previously extracted values for Δ are plugged into it. Hess et al. have decomposed $l_{\text{mag}}(T)$ into a temperature independent magnon-defect part l_0 and a temperature-dependent part $l_h(T)$ which represents solely the magnon-hole scattering, using Matthiessen's rule:

$$l_{\text{mag}}(T)^{-1} = l_0^{-1} + l_h(T)^{-1}. \quad (11)$$

It could be shown that on the one hand l_h at high temperatures $T > T^*$ is of the same order of magnitude than the mean distance of holes in the ladders. On the other hand, it was found that l_h has a very similar temperature dependence as the electrical resistivity, which further confirms that κ_{mag} depends sensitively on the charge dynamics in the material [19].

Magnon-phonon scattering

It is clear from the above discussion of magnon-hole scattering in $\text{Sr}_{14-x}\text{Ca}_x\text{Cu}_{24}\text{O}_{41}$, that it must be unimportant in $\text{Ca}_9\text{La}_5\text{Cu}_{24}\text{O}_{41}$. In spite of this, the measured κ_{mag} substantially deviates for $T \gtrsim 100$ K from the theoretically calculated κ_{mag} based on a constant mean free path. Formally, this deviation can be captured by a temperature dependent mean free path $l_{\text{mag}}(T)$, where the temperature dependence suggests the presence of a further temperature dependent scattering process. Hess et al. have analyzed this in more detail [15, 20], the results of which have been summarized by [33]:

Apart from magnon-hole scattering, which is unimportant in $\text{Ca}_9\text{La}_5\text{Cu}_{24}\text{O}_{41}$, only magnon-magnon scattering or magnon-phonon scattering are thinkable processes which could cause this temperature dependence of l_{mag} . As has been mentioned above, the T -dependence of l_{mag} in $\text{Ca}_9\text{La}_5\text{Cu}_{24}\text{O}_{41}$ can be calculated from the κ_{mag} data using Eq. 10 by plugging in the previously extracted $\Delta/k_B = 418$ K [15, 20]. The resulting $l_{\text{mag}}(T)$ as shown in Fig. 16 reflects the different T -regimes which govern κ_{mag} . For $T \lesssim 110$ K, l_{mag} is T -independent with a mean value $l_0 = 2980$ Å which reflects the scattering of magnons off static defects. In order to describe the T -dependent l_{mag} at higher T it was assumed (as in the case of magnon-hole scattering, see Eq. 11) that all scattering mechanisms were independent of each other and Matthiessen's

rule applied

$$l_{\text{mag}}^{-1} = l_0^{-1} + \gamma_{\text{ph}} d_{\text{ph}}^{-1} + \gamma_{\text{mag}} d_{\text{mag}}^{-1}. \quad (12)$$

Here, d_{ph} and d_{mag} are the mean 'distances' of phonons and magnons respectively, as calculated from the particle densities with γ_{ph} and γ_{mag} the corresponding scattering probabilities. Since it is unclear as to what extent the separate scattering mechanisms contribute to l_{mag} , its behavior was analyzed based on the assumption that only one mechanism is active in addition to magnon-defect scattering.

The case of dominant magnon-phonon scattering was modeled by three energy-degenerate non-dispersive optical branches along the ladder direction, yielding

$$\frac{1}{d_{\text{ph}}} = \frac{7.6 \cdot 10^9 \text{m}^{-1}}{\exp(\Delta_{\text{opt}}/(k_B T)) - 1} \quad (13)$$

with Δ_{opt} the optical gap (cf. [20] for details). The experimental l_{mag} was then fitted with $l_{\text{mag}}^{-1} = l_0^{-1} + \gamma_{\text{ph}} d_{\text{ph}}^{-1}$ using γ_{ph} and Δ_{opt} as free parameters. The fit (solid line in Fig. 16) describes the data fairly well. Remarkably, the value found for $\Delta_{\text{opt}}/k_B = 795$ K is of the same order of magnitude as the energy of the longitudinal Cu-O bond stretching mode which is involved in the two-magnon-plus-phonon absorption observed in optical spectroscopy [137, 149]. The scattering probability is obtained as $\gamma_{\text{ph}} = 3.2 \cdot 10^{-2}$, i.e. significantly smaller than that of magnon-hole scattering for mobile holes.

For the assumption of dominant magnon-magnon scattering, a less satisfactory agreement was obtained with $l_{\text{mag}}^{-1} = l_0^{-1} + \gamma_{\text{mag}} d_{\text{mag}}^{-1}$, where

$$\frac{1}{d_{\text{mag}}} = \frac{1}{\pi c_L} \int_0^\pi \frac{3}{3 + \exp(\epsilon_k/k_B T)} dk \quad (14)$$

(broken line in Fig. 16). c_L is the lattice constant along the ladders and ϵ_k was taken from Johnston et al. for the case of isotropic ladder coupling [150], with $\epsilon_{k=\pi}/k_B = \Delta/k_B = 418$ K employed. Note that $\gamma_{\text{mag}} = 0.05$ and thus of similar magnitude as γ_{ph} .

The comparison between both fits suggests that scattering off optical phonons is dominant in this compound, since an almost perfect description of l_{mag} is obtained without the necessity to invoke magnon-magnon scattering as additional scattering mechanism. Nevertheless, a contribution from magnon-magnon scattering cannot be excluded on basis of this analysis. Scattering off optical phonons is a plausible scattering mechanism for magnons since the longitudinal Cu-O bond stretching mode directly affects the Cu-O distance and hence the magnetic exchange constant of the ladders J . It is worth mentioning that the scattering off acoustic phonons appears unlikely, since the magnon energies with a $\Delta/k_B \sim 400$ K clearly are higher than that of acoustic phonons, unlike that of optical phonons. One should note, however, that a Debye temperature⁶ $\Theta_D \sim 300$ K in $(\text{Sr, Ca, La})_{14}\text{Cu}_{24}\text{O}_{41}$ is very close to the lower bound of the spread of measured values for the spin gap in two-leg spin ladder materials, see, e.g. [138]. Thus, though optical phonons are a prominent candidate, acoustic phonons and also magnons cannot be excluded to play a role in the dissipation of magnon heat transport in the two-leg spin ladder compounds $(\text{Sr, Ca, La})_{14}\text{Cu}_{24}\text{O}_{41}$.

3.5. Time-dependent measurements

All data discussed so far have been obtained with the use of the so-called steady-state method, see, e.g. [1]. It should be noted, however, that concerning results for the two-leg spin ladders significant fluctuations of the absolute magnitude of the magnetic contribution to kappa of the very same sample have been observed by several groups. Details of this phenomenon are discussed in [152].⁷ There are a few attempts to overcome these experimental difficulties by dynamical heat transport studies focusing on a

⁶For example, one finds $\Theta_D = 296$ K for $\text{Sr}_{14}\text{Cu}_{24}\text{O}_{41}$ [151].

⁷A careful investigation of the impact of these fluctuations yields that all aspects of the aforementioned analysis of κ_{mag} in $(\text{Sr, Ca, La})_{14}\text{Cu}_{24}\text{O}_{41}$ remain valid. For example, for $\text{Sr}_{14}\text{Cu}_{24}\text{O}_{41}$ fluctuations of κ_{mag} leave the extracted value of the spin gap practically unaffected while in the same measurement the fluctuations of the extracted mean free path value amount to not more than about 10% [152].

single material, namely $\text{Ca}_9\text{La}_5\text{Cu}_{24}\text{O}_{41}$. Interestingly, these studies consistently yield a lower value of κ_{\parallel} , which at room temperature amounts to about 60% of the data shown in Fig. 10. This finding is also in reasonable agreement with more recent steady-state studies by Naruse et al. [153].

Apart from this quantitative result, these dynamic studies are however conflicting with respect to the extraction of the magnon-phonon relaxation time. Thus, the results of these studies [35, 36, 154] are just briefly summarized here, while for an in-depth discussion the reader is referred to the original papers.

Otter et al. have exploited the fluorescent microthermal imaging technique which has been mentioned already in the beginning of this section further to extract the time-dependence of the anisotropic heat spread after locally heating the surface of a $\text{Ca}_9\text{La}_5\text{Cu}_{24}\text{O}_{41}$ crystal in the ac -plane (see Fig. 17) [35]. By analyzing the time-dependent anisotropic heat spread with the three-dimensional heat diffusion equation, the obtained data were used to extract the room-temperature heat conductivity along the a - and c -directions, i.e. κ_{\perp} and κ_{\parallel} , respectively. Interestingly, while the extracted value for κ_{\perp} was found to be in good agreement with the steady-state results shown in Fig. 10, the value for κ_{\parallel} amounts, as already mentioned, only about 60% of the steady-state κ_{\parallel} .

Montagnese et al. employed a different but related dynamic method where they measured the time-of-flight of a heat pulse through a $\text{Ca}_9\text{La}_5\text{Cu}_{24}\text{O}_{41}$ sample for various sample thicknesses. This study allowed to extract the phonon-magnon equilibration time, yielding a very large $\tau_{\text{mp}} \approx 400 \mu\text{s}$ as compared to that for the spin chain compound SrCuO_2 where $\tau_{\text{mp}} \approx 10^{-12} \text{ s}$ [36], and for which the mentioned fluctuations in κ_{\parallel} are absent. This finding is, however, in contrast with very recent measurement results using the time-domain thermoreflectance [154] where a six orders of magnitude faster phonon-magnon equilibration time is found. At present, the origin of these strong discrepancies between both these pioneering studies remains unclear and is not discussed further at this point.

4. Spin chains

4.1. Theoretical preliminaries

The thermal conductivity of spin chains appears particularly interesting because unlike the situation in the previously discussed cases of spin planes and spin ladders, rigorous theoretical predictions exist, in particular for the spin-1/2 Heisenberg chain model which is assumed to be relevant for the cuprate spin chains discussed here. The most spectacular one is certainly the prediction of ballistic, i.e. dissipationless, heat transport which would result in a diverging heat conductivity [12], which can be expressed in the form of a delta peak at zero frequency in the real part of the frequency-dependent thermal conductivity, i.e., $\text{Re } \kappa(\omega) = K_{\text{th}}(T)\delta(\omega)$ [156]. Moreover, the temperature dependence of the thermal Drude weight K_{th} has been calculated *exactly* [52]. Thus, in experimental investigations of the heat conductivity of spin-1/2 Heisenberg chain materials, one should expect to find signatures of the extraordinary properties of the model, though external scattering processes should complicate the picture.

At low temperatures $T \lesssim 0.15J/k_B$, i.e., $T \lesssim 300 \text{ K}$ for $J/k_B \sim 2000 \text{ K}$, the thermal Drude weight depends linearly on temperature, where [38, 43, 44, 52]

$$K_{\text{th}} = \frac{(\pi k_B)^2}{3\hbar} vT, \quad (15)$$

with the velocity v of the spinons at long wave lengths. In a real material, one might qualitatively expect that the external scattering processes cause the delta peak to broaden into, e.g., a Lorentzian in frequency space [156] with a width $1/\tau$, i.e. the scattering rate of the heat current (see Fig. 18). Hence, the heat conductivity of a single chain, $\tilde{\kappa}_{\text{mag}}$, is rendered finite and may be approximated by $\tilde{\kappa}_{\text{mag}} = K_{\text{th}} \tau/\pi$ [38]. If one naturally relates the experimental spinon mean free path l_{mag} with the relaxation time τ via $l_{\text{mag}} = v\tau$ and considers the number of spin chains per unit area n_s , one obtains [38]

$$l_{\text{mag}} = \frac{3}{\pi} \frac{\hbar}{k_B^2 n_s} \frac{\kappa_{\text{mag}}}{T}, \quad (16)$$

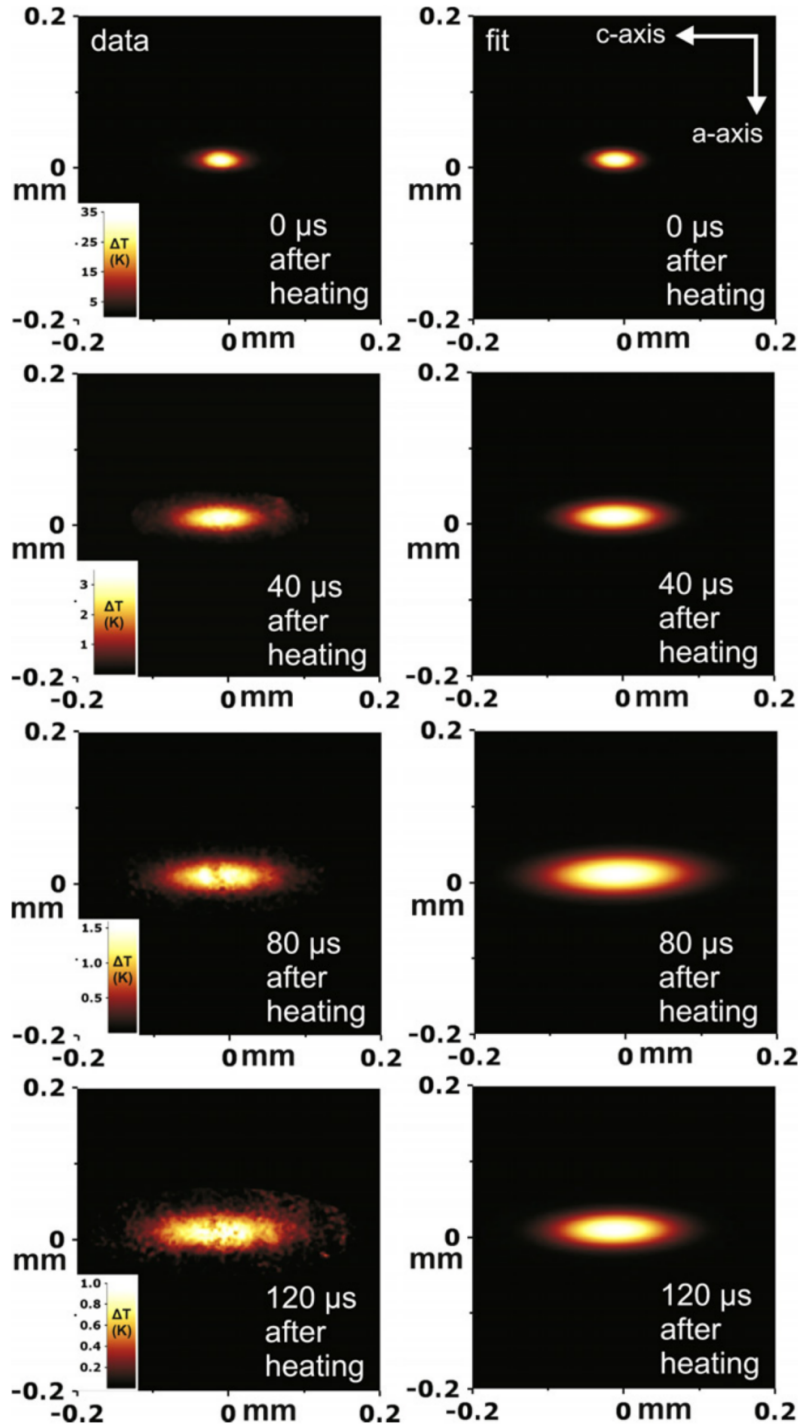


Figure 17: Time evolution of the heat diffusion from a hot spot in the spin ladder compound $\text{Ca}_9\text{La}_5\text{Cu}_{24}\text{O}_{41}$. The left column shows the data, while the right column shows the best Gaussian fit to the data. Heating is done by a laser with a pulse duration of 20 μs . The integration time for the probe UV-pulse is 20 μs . The ladder direction is horizontal. The anisotropy of the diffusion process is clearly seen. Figure taken from [35].

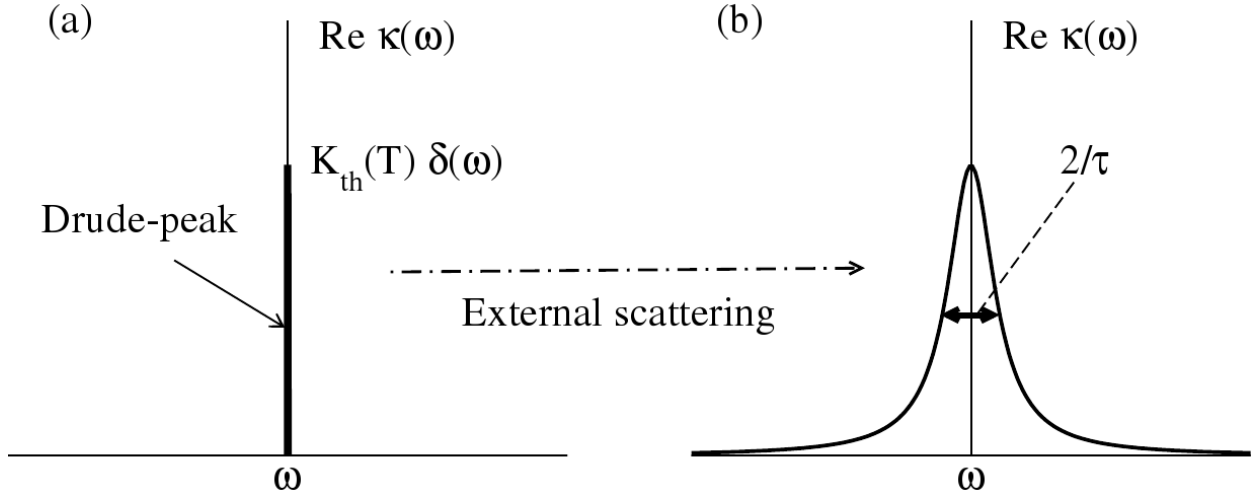


Figure 18: a) Sketch of the real part of the thermal conductivity $\kappa(\omega)$ of the Heisenberg chain as a function of frequency ω . The conductivity is given by $\text{Re } \kappa(\omega) = K_{\text{th}}(T)\delta(\omega)$ due to the exact conservation of the energy-current operator [12, 155]. Thus, the thermal Drude weight K_{th} is nonzero at any finite temperature, and any contribution at finite frequencies vanishes. b) In a real experiment for spin chain materials, one may expect the Drude weight to be broadened into, e.g., a Lorentzian in frequency space by external scattering. τ is the inverse width of such a Lorentzian, and it is related to the life time of the current, or the inverse scattering rate, respectively. Reproduced from [156].

It is interesting and important to note, that the kinetic model in one dimension (Eq. 8), if one uses a Fermi distribution in order to account for the fermionic character of the spinons, yields [22, 33]

$$l_{\text{mag}} = \frac{\pi}{2} \frac{\hbar}{k_B^2 n_s} \frac{\kappa_{\text{mag}}}{T} \left[\int_0^{\frac{J\pi}{2k_B T}} x^2 \frac{\exp(x)}{(\exp(x) + 1)^2} dx \right]^{-1}. \quad (17)$$

The integral in (17) is only weakly temperature dependent and approaches $\pi^2/6$ for $T \rightarrow 0$. Hence, at low temperatures $k_B T \ll J$, which with $J/k_B \sim 2000$ K holds even at room temperature one obtains the same result as in the case of the Drude weight approach, i.e. Eq. 15 and 16 [33, 38].

4.2. Spinon heat transport in 'dirty' spin chains

We start our discussion of the spinon heat conductivity in cuprate spin chain materials with the results for CaCu_2O_3 for which we have already briefly discussed its signatures of magnetic heat conductivity in Section 1.3 (Fig. 2a, see [38] for details on this study). The Cu_2O_3 planes in this material actually form, like in $(\text{Sr, Ca, La})_{14}\text{Cu}_{24}\text{O}_{41}$, a two-leg ladder structure. However, due to strongly bent Cu-O-Cu bonds along the rungs (bonding angle $\sim 123^\circ$) the rung exchange interaction is believed to be strongly reduced ($J_\perp/k_B \sim 100 \dots 300$ K) as compared to the ladder legs ($J_\parallel \sim 2000$ K), and all other exchange interactions present in the compound are expected to be similarly small or even smaller [79, 157, 158]. Thus, it is reasonable to consider this material rather as a chain compound with the chains running along the crystallographic b -axis. Indeed, INS confirms the absence of a spin gap for energies above ~ 3 meV and excitation spectra which are compatible with weakly coupled spin-1/2 Heisenberg spin chains [159]. Concerning its crystal structure, the material is rather disordered due to an inherent significant Ca and oxygen deficiency being balanced by excess Cu [158, 160]. We shall see that this disorder has a substantial impact on both the phononic as well the magnetic heat transport properties.

Fig. 19 shows once more the heat conductivity of CaCu_2O_3 as a function of temperature, for all principal axes of a crystal (see [38], for all details). κ_a and κ_c were measured perpendicular to the chains (thus both are labeled κ_\perp in Fig. 2) and κ_b was measured parallel to the chains. Since the material is electronically insulating, electronic heat conduction is negligible and we, therefore, expect these components to originate

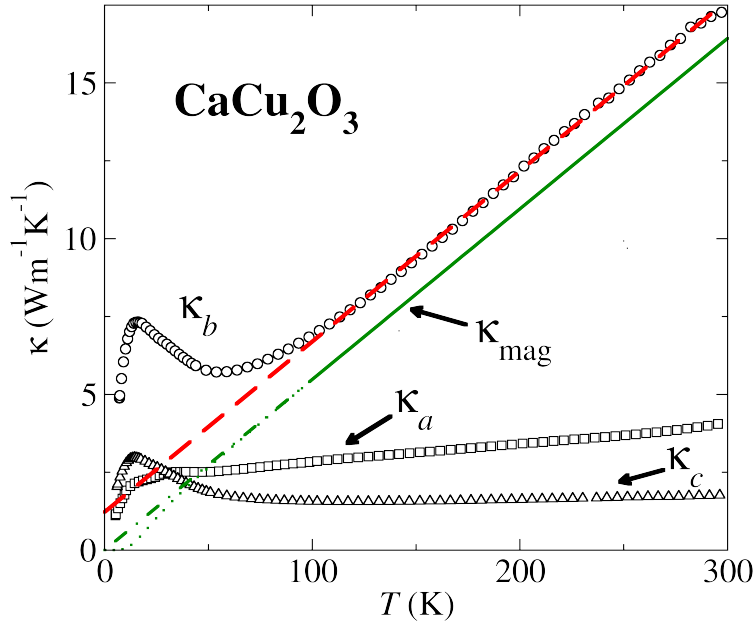


Figure 19: κ_a (\square), κ_b (\circ) and κ_c (\triangle) of CaCu_2O_3 as a function of temperature. The dashed and solid lines represent a linear fit of the experimental data in the range 100...300 K and the estimated κ_{mag} in this range. Extrapolations of κ_{mag} towards low temperatures (assuming a temperature independent magnetic mean free path as extracted for $T > 100$ K) corresponding to a finite ($\Delta = 3$ meV) and a vanishing spin gap are represented by dotted and dashed-dotted lines, respectively. Figure reproduced from [38].

from phononic heat conduction plus a possible magnetic contribution. The thermal conductivity perpendicular to the chain direction is typical for a strongly suppressed phononic thermal conduction with a high phonon scattering rate [1, 161]: κ_a and κ_c exhibits only a weak T -dependence and possess absolute values ($\lesssim 4 \text{ Wm}^{-1}\text{K}^{-1}$) which are much smaller than the phonon heat conductivity κ_{ph} of other chemically undoped chain or ladder cuprates such as SrCuO_2 , Sr_2CuO_3 (see further down), or $\text{Sr}_{14}\text{Cu}_{24}\text{O}_{41}$ (Fig. 2b). The thermal conductivity perpendicular to the chains can, therefore, be considered to be purely phononic and the strong suppression is naturally explained as a direct consequence of the strong off-stoichiometry of CaCu_2O_3 .

The completely different behavior of κ_b , which is measured *parallel* to the chains, in particular, the strong increase at $T \lesssim 50$ K must arise from magnetic heat conduction in the chains. Such a strong increase of κ with rising T cannot be understood in terms of conventional phonon heat conduction by acoustic phonons, and also thinkable contributions from dispersive optical phonons which possibly play a role in the T dependence of κ_a can be excluded [38]. Interestingly, the high-temperature increase of κ_b turns into *linear* in T for $T \gtrsim 100$ K. It is immediately clear that this linearity in temperature not only holds for the total thermal conductivity $\kappa_b = \kappa_{\text{ph}} + \kappa_{\text{mag}}$ but in particular also for the magnetic contribution κ_{mag} because κ_{ph} is only weakly temperature dependent as can be inferred from the phononic κ_a and κ_c . Therefore, the magnetic thermal conductivity of CaCu_2O_3 at $T \gtrsim 100$ K apparently perfectly follows the expected temperature dependence of the thermal Drude weight K_{th} as given in Eq. 15.

Hess et al. have investigated this result further and extracted in a simple procedure the magnetic heat conductivity by presuming that the observed slope in the data is that of κ_{mag} [38]. As can be seen in Fig. 19, a linear fit in the range 100...300 K (dashed line) describes the data almost perfectly and thus yields $\kappa_{\text{ph},b} = 1.2 \text{ Wm}^{-1}\text{K}^{-1}$ and $\kappa_{\text{mag}} = 0.055 \text{ Wm}^{-1}\text{K}^{-2} \times T$ in this temperature regime. The extracted κ_{mag} for $T > 100$ K is plotted in Fig. 19 as a solid line. κ_{mag} at lower T cannot be inferred from the data.

Obviously, the mean free path of such a linear κ_{mag} should be temperature independent in the framework of the model described above. Comparison with Eq. 16 yields $l_{\text{mag}} = 22 \pm 3 \text{ \AA}$ for the entire range

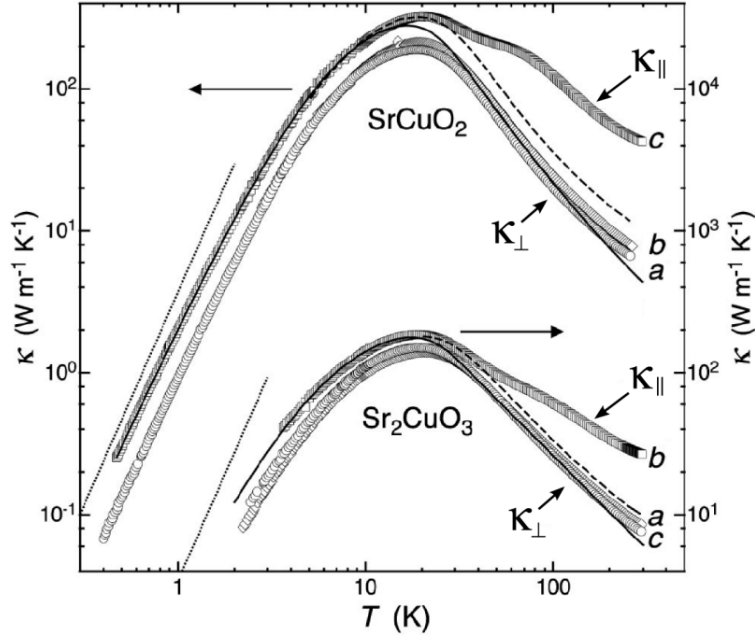


Figure 20: Temperature dependences of the thermal conductivities of SrCuO_2 and Sr_2CuO_3 along the a , b , and c axes. The dotted lines represent estimated limits of the thermal conductivity due to the finite size of the samples. The solid and dashed lines represent different evaluations of the phonon contribution, see [22], where the figure has been adapted from, for details.

100...300 K corresponding to about 6 lattice spacings [38]. Such a mean free path appears to be extremely short, in particular in view of the much larger mean free paths which were obtained on La_2CuO_4 and $(\text{Sr}, \text{Ca}, \text{La})_{14}\text{Cu}_{24}\text{O}_{41}$ (see the previous sections). The large impurity density which is implied by it is however qualitatively consistent with the fact that the material is intrinsically disordered. Furthermore, it is even quantitatively consistent with an independent measurement of the impurity density of the material, which in this special case is possible via the magnetic susceptibility (see [38], for details).

A temperature-independent l_{mag} as is found here seems at first glance surprising. It may indicate, however, that spinon-impurity scattering arising from effective chain cuts through the impurities is dominating over all other scattering processes, in particular, spinon-phonon scattering. In the Boltzmann-type view that has been introduced above one may understand this, provided Matthiessen's rule holds, by assuming

$$l_{\text{mag}}^{-1} = l_0^{-1} + l_{\text{sp}}(T)^{-1} + l_{\text{ss}}(T)^{-1}, \quad (18)$$

where l_{sp} and l_{ss} stand for *a priori* thinkable temperature-dependent spinon-phonon and spinon-spinon scattering lengths, respectively. A constant l_{mag} may then naturally arise if $l_0 \ll l_{\text{sp}}, l_{\text{ss}}$, a situation which seems to be plausible in the situation of a 'dirty' spin chain as obviously is realized in CaCu_2O_3 . In order to experimentally obtain access to these apparently masked scattering processes it seems straightforward to study κ_{mag} of spin chain materials which are chemically cleaner than CaCu_2O_3 and where $l_0 \gg l_{\text{sp}}, l_{\text{ss}}$ can be expected to be realized. In this situation, which shall be discussed in the next section, it should be possible to study the relevance of spinon-phonon and spinon-spinon scattering directly.

4.3. 'Ballistic' spinon heat transport in 'clean' spin chains

The spin chain compounds SrCuO_2 and Sr_2CuO_3 are both considered as being excellent realizations of the spin-1/2 Heisenberg model and are not prone to the stoichiometric problems that arise in CaCu_2O_3 . They are therefore ideal candidates to further studying relevant spinon scattering processes. Sologubenko et al. were the first to study the heat conductivity of these materials already in 2000 and 2001 [21, 22]. Fig. 20 presents their data for the heat conductivity of these materials measured along all crystal directions.

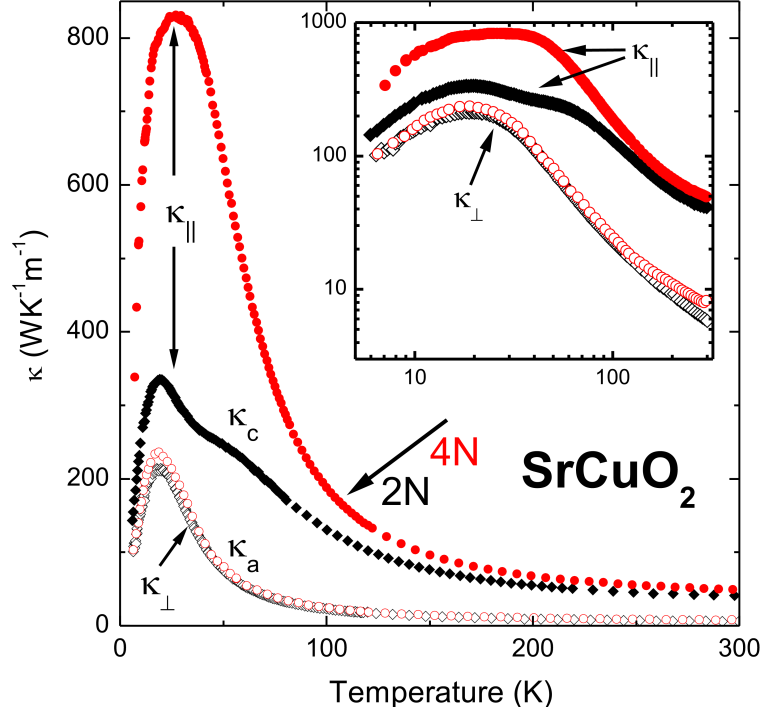


Figure 21: κ_a and κ_c of SrCuO_2 for different purity values. Closed (open) symbols represent c axis (a axis) data, red circles (black diamonds) correspond to '4N' ('2N') purity. Inset: The same data as in the main panel in double-logarithmic representation. Adapted from [39].

As can be seen in the figure, unlike the previously discussed cases, there is no clear double-peak structure or high-temperature increase visible in κ_{\parallel} . Yet, there obviously is an enhancement which develops in κ_{\parallel} at elevated temperature and causes a significant anisotropy between κ_{\parallel} and κ_{\perp} . Sologubenko already at that time concluded the presence of substantial spinon heat conduction in these materials based on these data. The solid and dashed lines in the Figure represent two different approaches to evaluate the phononic contribution to κ_{\parallel} . The detailed evaluation and analysis of the resulting spinon heat conductivity (see [22]) is omitted here because more recent data allow a more precise view on the matter.

These new data emerged recently by two groups who independently from each other discovered that the heat conductivity in SrCuO_2 and Sr_2CuO_3 depends crucially on the chemical purity of sample, where in particular the spinon heat conductivity κ_{mag} turned out to be extremely sensitive to chemical impurities [39, 40, 162, 163].

Ballistic spinon heat transport in SrCuO_2

Hlubek et al. [39] and Kawamata et al. [162] studied independently from each other the effect of chemical purity on the magnetic heat conductivity of double-chain compound SrCuO_2 , with very similar results. Fig. 21 presents the thermal conductivities κ_{\parallel} and κ_{\perp} of SrCuO_2 which were obtained on single crystals with 99% ('2N') and 99.99% ('4N') chemical purity as obtained by Hlubek et al. [39].⁸ Hlubek et al. report for both κ_{\perp} and κ_{\parallel} of the '2N' sample very similar results as previously found by Sologubenko et al. (see Fig. 20). However, they observed a drastically enhanced spinon heat conductivity of the samples with the higher purity ('4N') [39]: The thermal conductivity parallel to the spin chains of the '2N' sample, $\kappa_{\parallel,2N}$, exhibits a low-temperature peak at ~ 20 K and a shoulder at $T \gtrsim 40$ K. This shoulder and the

⁸The chemical purity refers to that of the primary chemicals CuO and SrCO_3 used in for the crystal growth by the traveling solvent floating zone method [39].

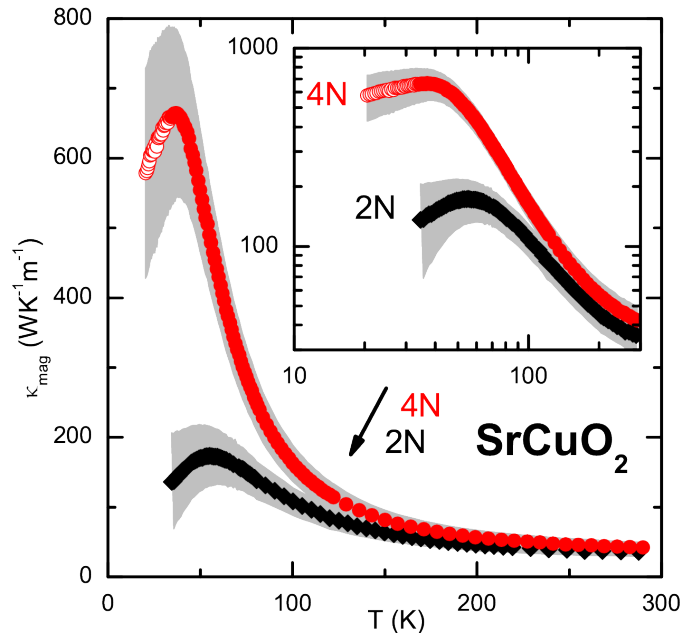


Figure 23: κ_{mag} of SrCuO_2 for different purities. Open symbols represent low- T κ_{mag} which is disregarded in the further analysis. The shaded areas show the uncertainty of the estimation of κ_{mag} due to an assumed relative error of 30% for the phononic background. Inset: The same data as in the main panel in double-logarithmic representation. Adapted from [39].

Again assuming $\kappa_{\parallel} = \kappa_{\text{ph}} + \kappa_{\text{mag}}$, the phonon heat conductivity parallel to the spin chains κ_{ph} may be reasonably approximated from the measured κ_{\perp} , i.e., $\kappa_{\text{ph}} \approx \kappa_{\perp}$ where a certain amount of anisotropy should be taken into account [22, 39]. Thus, κ_{mag} can again be estimated from the measured data by $\kappa_{\text{mag}} = \kappa_{\parallel} - \kappa_{\perp}$. The relatively large anisotropy of the heat conductivity of the '4N' sample implies that any error in κ_{ph} has only very little effect on κ_{mag} , as long as $\kappa_{\text{mag}} \gg \kappa_{\perp}$.

Fig. 23 shows the thus extracted spinon heat conductivity κ_{mag} of both the '2N' and the '4N' samples as a function of temperature T [39]. Both curves exhibit the characteristic peak structure which qualitatively reflects the competition between the increasing occupation of quasiparticle states and the growing importance of temperature dependent scattering processes with rising temperature [1]. In the regime of the low-temperature increase, the latter are unimportant and only temperature independent boundary scattering dominates. The increase then is the result of the growing number of thermally excited spinons. The most reasonable candidate for the temperature dependent scattering is of course, as mentioned above, the spinon-phonon scattering. Within this scenario, the difference between both curves arises naturally from the different purity of both compounds which yields a corresponding different importance of boundary scattering. This corresponds very well with the concept that a single impurity within a chain serves as a boundary in one dimension. Note, that the peak value of $\sim 660 \text{ W m}^{-1} \text{ K}^{-1}$ of the '4N' is to the best of our knowledge a 'record' as it exceeds the largest reported magnetic heat conductivities [15, 22] by more than a factor of 3.

A more direct view on the temperature dependence of spinon scattering processes is provided by the spinon mean free path that can be computed according to Eq. 16. Resulting data are shown in Fig. 24. Both data sets show a strong decrease with increasing temperature, consistent with the above expectation of a growing importance of spinon scattering with increasing temperature. At the same time, the different magnitude of the curves which is most pronounced at lowest temperature signals the different importance of impurity scattering.

Following a conjecture of Sologubenko et al. [22], the data in Fig. 24 have been modeled by Hlubek et

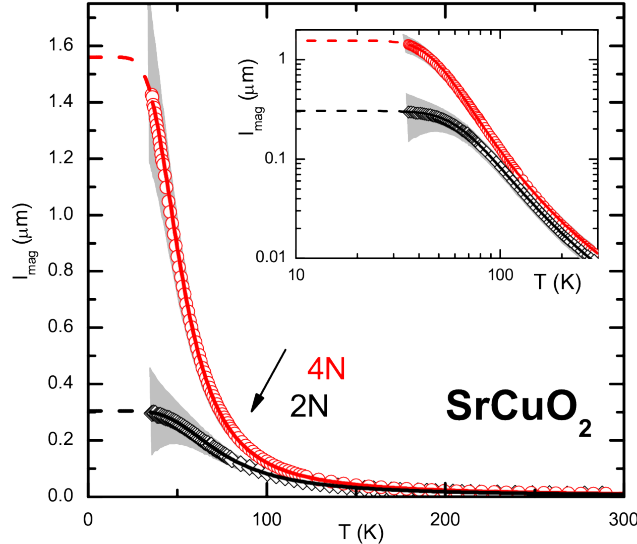


Figure 24: Magnetic mean-free paths of SrCuO₂ for different purities. The solid lines were calculated according to Eq. 19. The shaded area illustrates the uncertainty from the estimation of the phononic background. Adapted from [39].

al. using Matthiessen's rule for the *extrinsic* spinon-defect and spinon-phonon scattering, i.e., employing a reduced version of Eq. 18, where the *intrinsic* spinon-spinon scattering as expressed by l_{ss} has been discarded:

$$l_{\text{mag}}^{-1} = l_0^{-1} + l_{\text{sp}}(T)^{-1}. \quad (19)$$

An empirical expression has been used to model the spinon-phonon scattering, which represents a general umklapp process [22, 39]:

$$l_{\text{sp}}(T) = \frac{\exp(T_u^*/T)}{A_s T}. \quad (20)$$

Here, T_u^* represents the energy scale of the scattering phonons, and A_s a scattering cross section. The solid lines in Fig. 24 represent fits to the data employing Eqs. 19 and 20, where for both purity levels the same T_u^* has been used [39]. This reasonable assumption accounts for the expectation that the relevant energy scale for the scattering is the same for both purity levels. The other parameters $l_{0,2N}$, $l_{0,4N}$, $A_{s,2N}$, $A_{s,4N}$ were employed as free fit parameters. Ideally, the purity should be solely captured by the spinon-defect scattering lengths $l_{0,2N}$, $l_{0,4N}$, since one would expect also $A_{s,2N} \approx A_{s,4N}$, where deviations between these two values (up to 30%) should be allowed for in order to compensate geometrical errors of the individual measurements of the heat conductivity. As can be inferred from the figure, these constraints allow excellent fits. Hlubek et al. report the energy scale $T_u^* \sim 200$ K which is of the same order of magnitude as the Debye temperature of the material, corroborating spinon-phonon scattering as being the dominant temperature dependent process. The analysis yields further the spinon-defect scattering lengths $l_{0,2N} \approx 300$ nm and $l_{0,4N} \approx 1.6$ μm , which correspond to more than 750 and 4100 lattice spacings, respectively [39].

This result is remarkable in two aspects: i) it suggests that indeed only the extrinsic spinon-defect and spinon-phonon scattering are relevant for relaxing the heat current. Thus the findings provide an experimental corroboration of the theoretical prediction of *ballistic* heat transport in the $S = 1/2$ antiferromagnetic Heisenberg chain. ii) in the high-purity sample, an extraordinary scattering length of more than one micrometer is apparently present at low temperature, which apparently is only limited by the impurities in

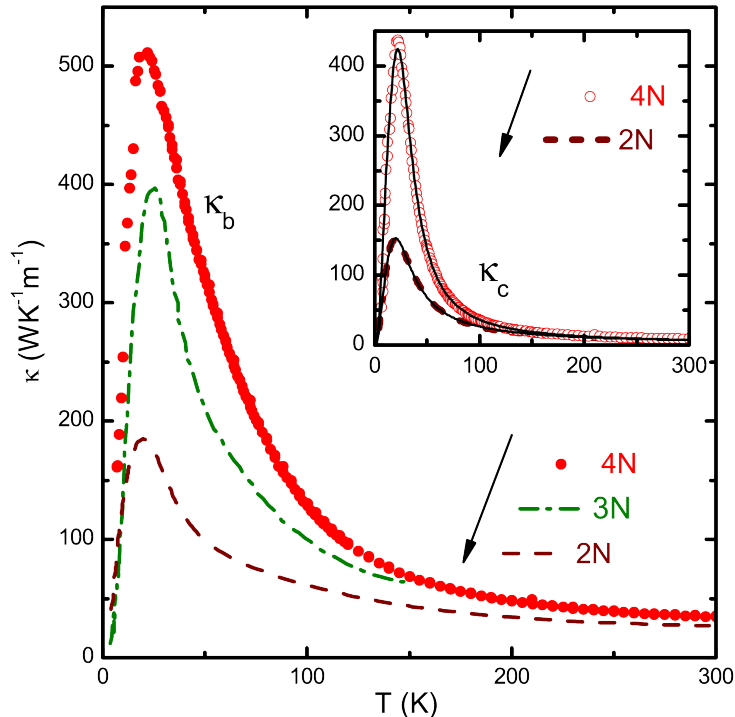


Figure 25: Thermal conductivity of Sr_2CuO_3 parallel to the spin chains (κ_b) for various purities. The dashed lines represent results from Sologubenko et al. with '2N' purity, reproduced from [21]. The dash-dotted line has been obtained by Kawamata et al for '3N' purity and is reproduced from [163]. Inset: thermal conductivity of Sr_2CuO_3 perpendicular to the spin chains (κ_c) for '2N' (also reproduced from [21]) and '4N' purity. The solid lines are fits to the Callaway model [108]. Adapted from [40].

the chains. This suggests that much larger spinon mean free paths could be achievable in perfectly clean crystals of SrCuO_2 .

Ballistic spinon heat transport in Sr_2CuO_3

After the pioneering experiments of Sologubenko et al. on the single chain material Sr_2CuO_3 [21, 22] with 99% purity (labeled '2N' hereafter), the spinon heat transport in this compound has been under scrutiny by two further studies. Kawamata et al. investigated the heat transport of the pure material on a crystal where chemicals with 99.9% purity (labeled '3N' hereafter) had been used for the crystal growth [163]. Hlubek et al. investigated a crystal with even higher purity (99.99% purity of the starting chemicals, labeled '4N' hereafter), and performed a comparative study of the effect of the different purity levels [40].

Fig. 25 depicts the corresponding data for the thermal conductivity parallel to the spin chains (κ_{\parallel} , main panel), and except for the 3N purity, perpendicular to them (κ_{\perp} , inset). κ_{\perp} , like in SrCuO_2 exhibits a temperature dependence that is characteristic for phononic heat conductivity. The height of the characteristic phononic peak at $T \approx 22$ K sensitively depends on the density of impurities in the system, which generate phonon-defect scattering. In fact, the data for both purities can be described well in the framework of a model by Callaway [108], where the difference between both curves is largely captured by different point defect scattering strength (see Reference [40] for details).

Very similarly as described above for SrCuO_2 , the spinon heat conductivity has been obtained via $\kappa_{\text{mag}} = \kappa_{\parallel} - \kappa_{\perp}$ for the '4N' sample, which is shown together with similarly obtained results from References [21, 22, 163] for '3N' and '2N' in Fig. 26. The very similar temperature dependence of κ_{mag} as compared to that of SrCuO_2 , though with somewhat smaller values is evident. Hlubek et al. pointed out that the

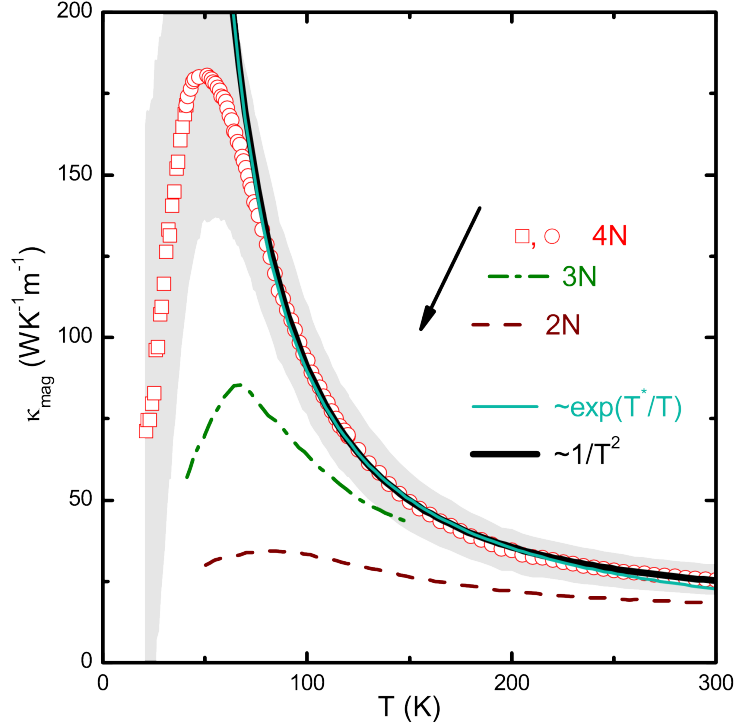


Figure 26: Estimated magnetic thermal conductivity of Sr_2CuO_3 for '4N' (circles, squares), '3N' (dash-dotted line) [163], and '2N' (dashed line) [21] purity. The shaded area illustrates the uncertainty from the estimation of the phononic background. The '4N' results shown in squares instead of circles have a large uncertainty. The thick solid line is a fit for $T > 80$ K with $\kappa_{\text{mag,fit1}} \sim 1/T^2$. The thin solid line is a fit with $\kappa_{\text{mag,fit2}} \sim \exp(T^*/T)$. See Ref. [40] where the figure has been reproduced from for a further discussion.

high-temperature decay of κ_{mag} can be fit well with $\kappa_{\text{mag}} \sim \exp(T^*/T)$, with T^* a characteristic energy scale, which can be related to prevailing umklapp processes [40].

Hlubek et al. extracted from the data in Fig. 26 the spinon mean free path following Eq. 16, and analyzed the temperature dependence according to Eqs. 19 and 20. Remarkably, the analysis work equally well (see Fig. 27) as before for SrCuO_2 with $l_0 = 0.54 \pm 0.05 \mu\text{m}$ (corresponding to approximately 1370 lattice spacings), $T_u^* = 210 \pm 11$ K [40]. It is important to point out that the energy scale for the phonon scattering T_u^* is practically the same for both SrCuO_2 and Sr_2CuO_3 . This is consistent with the fact that in both materials the spin chains are formed by practically the same CuO_2 plaquettes, suggestive of a very similar local spin-phonon coupling. The low-temperature mean free path limit, l_0 , is significantly smaller for Sr_2CuO_3 than that of SrCuO_2 . For a direct quantitative comparison, Fig. 27 shows l_{mag} of both compounds in relation to the number of lattice spacings. Despite the same formal chemical purity, the double chain compound's mean free path is about a factor of three larger, consistent with a relatively higher chemical stability of the compound [40].

Hlubek et al. attempted for the first time a deeper insight into the spin-phonon interaction by calculating l_{sp} directly from a spin-phonon scattering theory for the XY-limit of the Heisenberg model [56] with promising results at high temperature. However at lower temperature, the agreement between the experimental results and the theoretical l_{sp} becomes less satisfactory (see [40] for details). Very recently, Chernyshev and Rozhkov reanalyzed the experimental data of Hlubek et al. for both SrCuO_2 and Sr_2CuO_3 with an alternative theoretical model which specifies l_{sp} including realistic numerical values for the spin-phonon interaction [64]. Also in this case, the analysis relies for both compounds on just two types of scattering processes, viz. spinon-defect and spinon-phonon scattering. Thus the earlier statement for a strong experimental confirmation of ballistic heat transport holds for both materials.

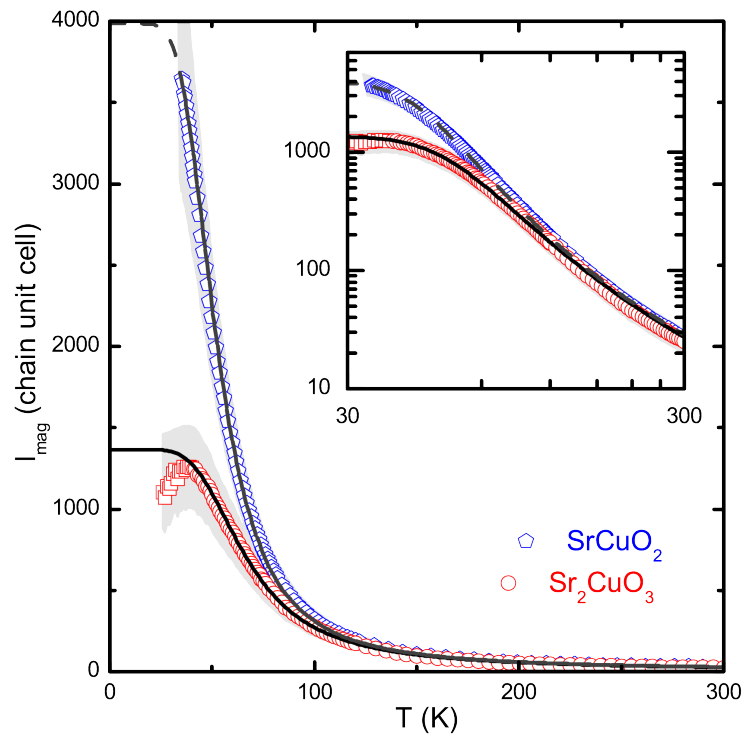


Figure 27: Magnetic mean free paths of SrCuO_2 (pentagon shape) and Sr_2CuO_3 (circles) for 4N purity. The shaded area illustrates the uncertainty from the estimation of the phononic background. The lines are fits to the mean free paths. Figure taken from [40].

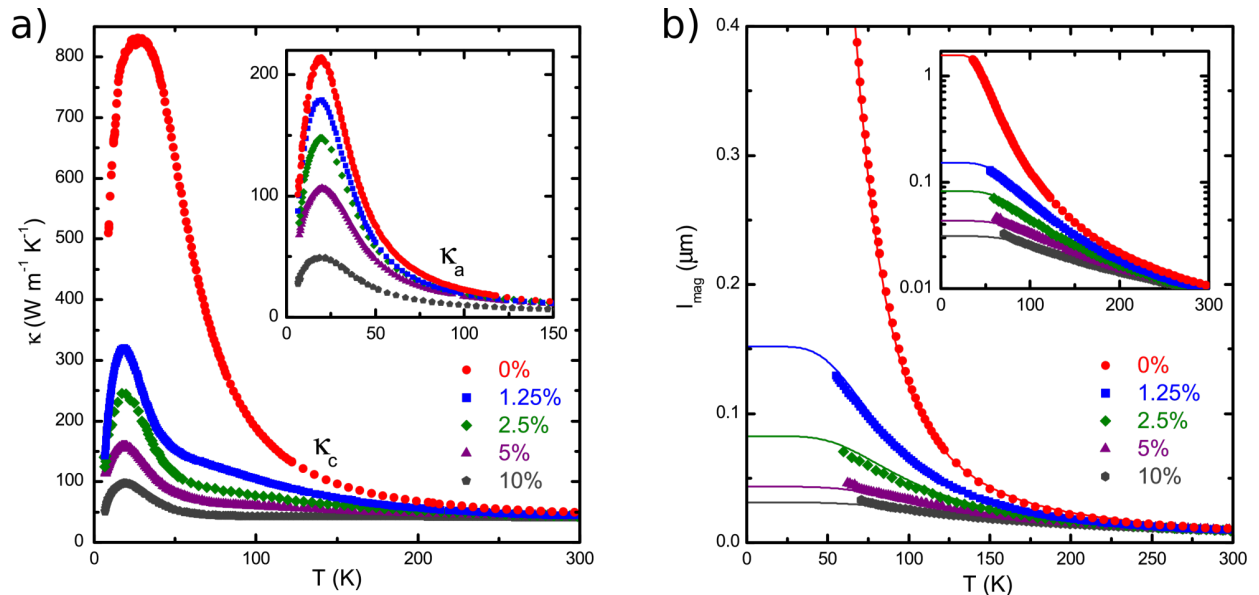


Figure 28: a) Thermal conductivity κ_c parallel to the spin chain (κ_{\parallel}) for $\text{Sr}_{1-x}\text{Ca}_x\text{CuO}_2$ at different doping levels. Inset: Thermal conductivity κ_a for the same doping levels perpendicular to the spin chain (κ_{\perp}). b) l_{mag} of $\text{Sr}_{1-x}\text{Ca}_x\text{CuO}_2$ for different levels of doping. Toward low temperatures, the error in the estimation of κ_{mag} increases due to an increase in the phononic heat conductivity. Thus, the values of l_{mag} are shown only at temperatures above which the error in l_{mag} is reasonably small. The solid lines were calculated according to Eqs. 19, 20. Figures taken from [41].

4.4. Spin chains with doping induced disorder

The ballistic transport in the isotropic Heisenberg chain implies the natural question about the impact of subtle disorder on the transport properties. Such disorder should break the integrability of the spin model and thus a very substantial impact on the spinon heat conductivity is expected. One possibility to approach this problem in SrCuO_2 or Sr_2CuO_3 is to substitute Ca for Sr in small amounts, thus creating bond disorder due to the different ionic radii of Sr^{2+} and Ca^{2+} . It turns out that this disorder type has a strong impact not only on the spinon heat transport but also on the ground state of the spin chains as is evidenced by Nuclear Magnetic Resonance (NMR) measurements [37, 41, 42, 166, 167]. Hammerath et al. performed NMR measurements at the ^{63}Cu nucleus for $\text{Sr}_{1-x}\text{Ca}_x\text{CuO}_2$ at $x = 0, 0.1$ and $\text{Sr}_{1.9}\text{Ca}_{0.1}\text{CuO}_3$ determined the spin-lattice relaxation rate $1/T_1$ as a function of temperature [166, 167]. The data very clearly reveal a doping induced spin gap which according to Hammerath et al. is solely induced by the bond disorder on the intrachain coupling [167]. It should be noted, however, that a priori, it cannot be excluded that a finite amount of the doped Ca, instead of replacing the Sr in the structure, replaces Cu inside the CuO_2 -chain structures. In this case, a more severe site disorder would be the result which cuts the spin chains (which in the clean compounds possess a large average length of several thousand unit cells, according to the spinon mean free path, see Fig. 27). Indeed, a specific investigation of such a site disorder has been addressed by substituting Ni for Cu *inside* the CuO_2 -chain structures of Sr_2CuO_3 as well as SrCuO_2 [168, 169] in NMR measurements and INS measurements. Both approaches led to the conclusion that finite size effects play an important role, i.e. the Ni effectively cuts the chains into finite segments which exhibit a gapped ground state.

Remarkably, the Ca-induced disorder has a dramatic impact on the heat conductivity parallel to the spin chains κ_{\parallel} , while the phononic heat conductivity κ_{\perp} is only moderately affected. This implies a very strong suppression of the spinon heat conductivity κ_{mag} upon increasing the disorder. This is illustrated in Fig. 28a for the Ca-doped double-chain compound, i.e. $\text{Sr}_{1-x}\text{Ca}_x\text{CuO}_2$ [41]. A very similar result is obtained for Ca-doped Sr_2CuO_3 (not shown) [42].

The spinon heat conductivity can be calculated from the heat conductivity data in exactly the same

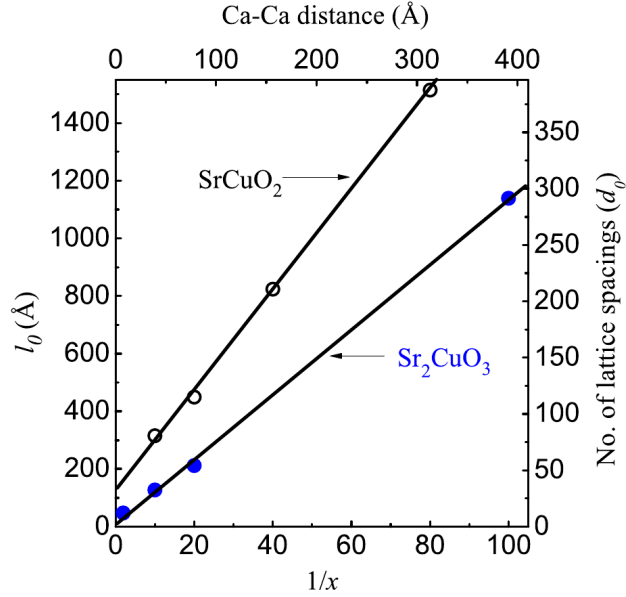


Figure 29: Spinon-defect scattering length l_0 plotted against the inverse of Ca concentration (x) (lower abscissa) and the mean distance between two Ca atoms (upper abscissa) for SrCuO_2 (open symbols) and Sr_2CuO_3 (filled symbols); the solid lines are linear fits to the data. The ordinate on the right expresses the mean free path in terms of the number of lattice spacings between two Cu sites (d_0). Figure taken from [42].

way as it was already explained for the pure compounds above. Similarly, the temperature dependence of the spinon mean free path for various doping levels can be extracted via Eq. 16, resulting in the data shown in Fig. 28b. Note, that a possible impact of the spin pseudogap can be excluded to have a significant impact on the spinon heat conductivity and the mean free path because at the size of the gap is too small ($\Delta/k_B \sim 50$ K [166, 167]) to play a significant role for the spinon heat conductivity which is studied at $T \gtrsim 50$ K only [41, 42].

The data in Fig. 28b, and corresponding data for $(\text{Sr}_{1-x}\text{Ca}_x)_2\text{CuO}_3$ can be analyzed remarkably well as in the case of the clean compounds following Eqs. 19, 20. Thereby, essentially the spinon-defect scattering length l_0 turns out as the crucial parameter which is determined by the doping level whereas the phonon scattering term can be set identical for all doping levels (solid lines in Fig. 28b).

It is very instructive to plot the obtained values of the spinon-defect scattering length l_0 as a function of the mean distance between two Ca atoms and the inverse of Ca concentration as is shown in Fig. 29. For the single-chain material $(\text{Sr}_{1-x}\text{Ca}_x)_2\text{CuO}_3$, l_0 apparently scales perfectly with the inverse of Ca concentration as $l_0 = \frac{2.91 \cdot d_0}{x}$, where $d_0 = 3.91$ Å is the lattice spacing between two Cu sites along the chain [42]. This implies that the Ca-induced disorder can perfectly be captured in terms of effective defects in the chain, where the scattering probability per defect is equally strong at all concentrations.

Interestingly, the situation is somewhat different for $\text{Sr}_{1-x}\text{Ca}_x\text{CuO}_2$ (see Fig. 29) [41]. There, a linear scaling is present, too, however, with an offset: $l_0 = \frac{4.3 \cdot d_0}{x} + l_{\text{lim}}$, with $l_{\text{lim}} \approx 30 \cdot d_0$ with $d_0 = 3.92$ Å. This indicates that already at intermediate concentrations ($x = 0.1$) the effect of Ca saturates and the mean free path of spinons is not reduced any further upon increasing the Ca concentration. The observed offset was originally interpreted to be due to a limit set by the disorder-induced long-distance decay of the spin-spin correlation [41]. However, since the double-chain nature did not enter the latter interpretation, the fact, that the offset is absent in the single-chain material $(\text{Sr}_{1-x}\text{Ca}_x)_2\text{CuO}_3$ implies a different origin of the offset, which however remains open.

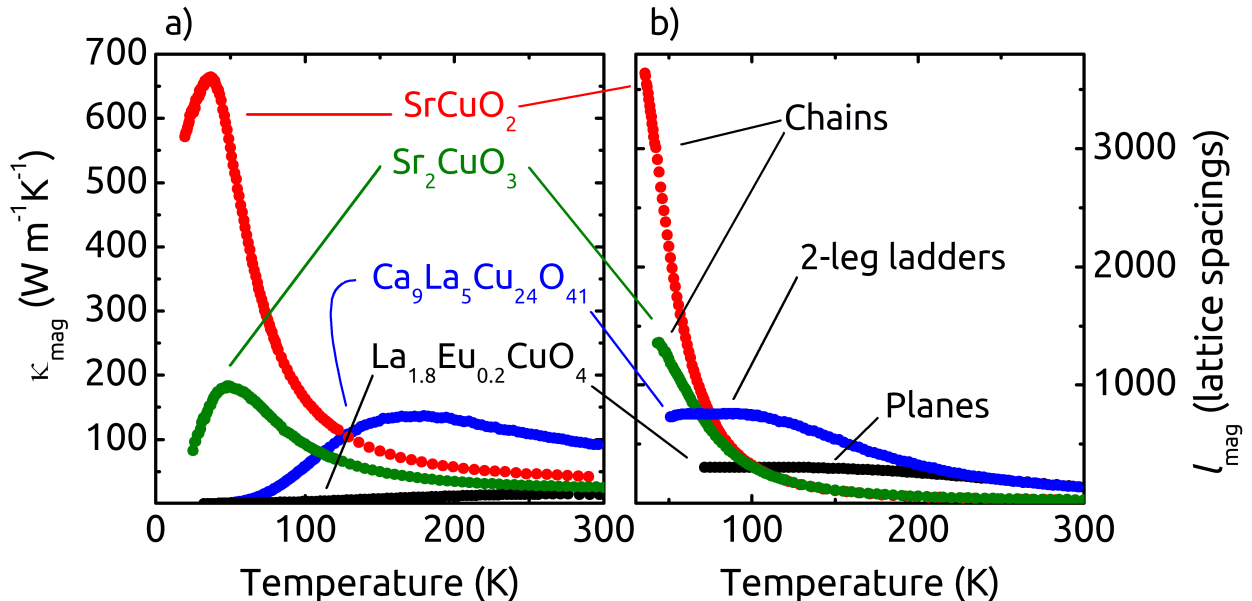


Figure 30: Comparison of the magnetic heat transport of representative low-dimensional spin systems, namely for the spin chain compounds SrCuO_2 and Sr_2CuO_3 [39, 40], the two-leg spin ladder compound $\text{Ca}_9\text{La}_5\text{Cu}_{24}\text{O}_{41}$ [15], and the 2D-HAF material $\text{La}_{1.8}\text{Eu}_{0.2}\text{CuO}_4$ [18]. a) Magnetic heat conductivity as a function of temperature, $\kappa_{\text{mag}}(T)$. b) Magnetic mean free path as a function of temperature, $l_{\text{mag}}(T)$, in units of lattice spacings.

5. Conclusion

We have seen that in the here discussed cuprate materials with large antiferromagnetic exchange interaction which realize low-dimensional $S = 1/2$ Heisenberg systems in the form of chains, two-leg ladders, and planes, a sizeable magnetic heat conductivity arises. The possibility to extract the magnetic heat conductivity in a very clean manner in principle opens up a new approach for sensitively and comprehensively probing magnetic excitations in these systems. Indeed, for each these quantum systems, using the kinetic model, it is possible to formulate a relatively simple way towards rationalizing the observed temperature dependences of κ_{mag} and to draw basic conclusions about the involved scattering processes of the heat-carrying magnetic excitations. So far, these considerations have been done individually for the various systems which are very different in terms of their elementary excitations, namely gapless spinons for the one-dimensional chains, triplon excitations with a large excitation gap for the ladders, and spin wave-like excitations in two-dimensions (with only small anisotropy gaps). Important conclusions could be drawn: Quite importantly, the kinetic model apparently yields realistic length scales of the magnetic mean free path l_{mag} , despite the simplicity of the model. Based on this finding, the discussed data confirmed the ballistic nature of the heat transport of integrable spin chain systems which truly is a fundamental finding. On the other hand, we have seen that in the non-integrable two-leg spin ladders the magnetic heat transport is nevertheless substantial with l_{mag} exceeding the spin-spin correlation length by about three orders of magnitude.

Beyond these findings for the individual systems, it is interesting to directly compare the magnetic heat transport of these systems and to investigate whether the differences in the nature of the spin system also yield different transport and whether, nevertheless, similarities emerge. Fig. 30a shows a collection of data of κ_{mag} of the chain systems SrCuO_2 and Sr_2CuO_3 , of the two-leg ladder material $\text{Ca}_9\text{La}_5\text{Cu}_{24}\text{O}_{41}$, and of the 2D-HAF $\text{La}_{1.8}\text{Eu}_{0.2}\text{CuO}_4$. These data can be considered in so far as being representative as they correspond to clean compounds where the up to present largest mean free paths have been extracted [15, 18, 39, 40]. The data are the same as discussed in the previous sections, but this figure shows them for the first time together on the same scale and indeed reveals remarkable differences. Quite clearly, the chain compound SrCuO_2 exhibits a 'record' value for κ_{mag} of almost $700 \text{ W m}^{-1} \text{K}^{-1}$ which is many times larger than that of

(i) the single chain compound Sr_2CuO_3 and, furthermore, (ii) that of the 2-leg ladder and the 2D-HAF.

The first observation (i) has been recognized earlier [40] and already discussed in the previous section. A closer investigation of the mean free path of these two Heisenberg chain materials as shown in panel (b) of Fig. 30 reveals that l_{mag} apparently can be separated in two regimes. On the one hand, this is at $T \gtrsim 100$ K where there is virtually no difference between both curves. Here, according to the analysis, spinon-phonon scattering is dominant, where the data suggest that this type of scattering has no difference in both compounds. On the other hand, at $T \lesssim 100$ K l_{mag} of Sr_2CuO_3 approaches a much lower low-temperature limit than that of SrCuO_2 . Hence, the difference seems to imply a different inherent perfectness of the chains in the two compounds.

Upon trying to obtain some further understanding of the more interesting observation (ii), it is important to note that the very large value of κ_{mag} of SrCuO_2 occurs at relatively low temperature $T \lesssim 100$ K where κ_{mag} of both the ladder compound $\text{Ca}_9\text{La}_5\text{Cu}_{24}\text{O}_{41}$ and of the 2D-HAF material $\text{La}_{1.8}\text{Eu}_{0.2}\text{CuO}_4$ is very small. In both cases, this comparably small low-temperature value of κ_{mag} can be straightforwardly be understood: for the two-leg ladder material $\text{Ca}_9\text{La}_5\text{Cu}_{24}\text{O}_{41}$, the significant spin excitation gap $\Delta \sim 400$ K prohibits a significant population of triplons below about 100 K. Similarly, for the 2D-HAF, the low-temperature thermal population of magnetic excitations is much 'slower' than that of the one-dimensional Heisenberg chain. One can convince oneself about this fact from considering the temperature dependence of the magnetic specific heat c_{mag} of both systems which is linear in temperature for the chain system whereas the two-dimensional spin plane possesses a quadratic low-temperature increase. Indeed, an estimation of the magnetic specific heat at $T = 100$ K (i.e. $k_B T \ll J$) using the estimate $\kappa_{\text{mag}} \sim c_{\text{mag}} v_0 l_{\text{mag}}$ and the respective kinetic expressions for κ_{mag} in Eqs. 7 and 16 yields an almost two orders of magnitude smaller c_{mag} for the 2D-HAF than that of the Heisenberg chain. Here, the magnetic velocity $v_0 \sim Jd/\hbar$ with d the distance between neighboring spins has been used. Thus, taking further into account the mean free path l_{mag} at about 100 K being of a similar order of magnitude for all compounds (see further below), it is not surprising that the magnetic heat conductivity of the Heisenberg chain is by far the largest at low temperatures.

Fig. 30b compares the temperature dependence of the mean free paths l_{mag} as extracted from the data in panel (a) upon using the kinetic model. Here one finds that l_{mag} of the spin chain compounds additionally exceeds clearly that of the ladder and the plane compounds at $T \lesssim 100$ K. These large low-temperature values of l_{mag} additionally promote the extraordinarily large κ_{mag} of the chains in this regime.

Another interesting finding as revealed by Fig. 30b is the fact that at $T \gtrsim 100$ K the mean free path becomes significantly smaller than that of both the 2-leg ladder and of the plane compounds. Since the temperature-induced reduction of l_{mag} of the spin chain materials has clearly been assigned to spinon-phonon scattering [39, 40, 64], this observation seems to imply that the spinon heat transport of the $S = 1/2$ Heisenberg chain is much more prone to scattering of phonons than the two-leg Heisenberg ladder and the 2D-HAF counterparts. It remains to be clarified to what extent this notion is related to the integrability of the Heisenberg chain model, whose ballistic transport properties potentially could exhibit a particular sensitivity to distortions such as those induced by the phonons. Alternatively, differences in the magnetic and phononic spectrum could play an important role, too. Indeed such seems to be a crucial difference in the spin-phonon scattering of the Heisenberg chains where the gapless spinons can be expected to interact with acoustic phonons and that of the 2-leg spin ladders, where the energy of the acoustic phonons is too small to cause an important interaction with the gapped triplon excitations and instead scattering of optical phonons seems to dominate (see Section 3.4).

Finally, it is to be remarked that little is known from experiments about the temperature evolution of l_{mag} of the 2D-HAF at elevated temperatures since apparently the data shown in Fig. 30b as extracted from Ref. [18] barely touch this regime. An obvious aspect of future research is thus to extend the achievable temperature regime of reliable κ_{mag} -data to much higher temperatures and to verify specific predictions about magnon scattering processes involving phonons and the correlation length [170].

As it has already been mentioned above, all the here discussed analysis is based on the kinetic model (see Section 1.4), the successful applicability of which is surprising in view of the strong quantum nature of the here studied spin models. Another possible direction of future research therefore could address ways to model the magnetic heat transport in the studied systems on a more microscopic level.

It is worth to mention that the large magnetic heat conductivity values of the spin ladder and the chain systems may also open up new technological developments. The exploitation of the resulting anisotropic heat conductivity tensor for thermal management applications already has been investigated (see e.g. [35]). Another, yet unexplored direction would be spin information transport experiments, where electrical pumping and detection of spin currents with the help of the spin-Hall and the inverse spin-Hall effect, as recently successfully used on classical spin systems [171].

Upon concluding, it is important to mention further active research directions which could not be touched in this review. One concerns research on κ_{mag} for systems where the magnetic exchange energy becomes comparable or much smaller than the Debye energy, and how it about evolves when the magnetic systems become less quantum in nature, i.e. when $S > 1/2$. Initial work has already addressed these aspects. Intriguing heat conductivity results for one-dimensional spin systems with relatively small exchange interactions have been obtained for both organic and inorganic materials, see e.g. [32, 172–175] for $S = 1/2$ systems and [28, 30, 55, 176–179] for systems with large spin, see also the reviews [180, 181].

Another dynamic field where magnetic heat transport is being investigated concerns frustrated spin systems, where it promises to become a good probe for accessing possible topological excitations. The class of spin-ice compounds of the type $R_2\text{Ti}_2\text{O}_7$ (R a rare earth element) constitutes a subject on its own where the focus is on magnetic monopole-like excitations [182–191]. Another class concerns highly frustrated layered compounds [192, 193] where very recently $J_{\text{eff}} = 1/2$ -materials with Kitaev interactions came into focus [194–199] since such systems are conjectured as fascinating avenues for exploring the ‘magnetic’ heat transport of topological fractionalized quasiparticles.

Acknowledgments

I am indebted to Neela Sekhar Beesetty, Wolfram Brenig, Bernd Büchner, David Cahill, Sang-Wook Cheong, Alexander Chernyshev, Stefan-Ludwig Drechsler, Hanan ElHaes, Jochen Geck, Ioannis Giapintzakis, Hans-Joachim Grafe, Franziska Hammerath, Fabian Heidrich-Meisner, Nikolai Hlubek, Vladislav Kataev, Rüdiger Klingeler, Andreas Klümper, Gernot Krabbes, Paul van Loosdrecht, Thomas Lorenz, Oleg Mityashkin, Ashwin Mohan, Satoshi Nishimoto, Peter Prelovšek, Pascal Reutler, Alexandre Revcolevschi, Patrick Ribeiro, Georg Roth, Romuald Saint-Martin, Chinnathambi Sekhar, Robin Steinigeweg, Yannic Utz, Anja Waske, Anja Wolter, Babak Zeini, Andrey Zheludev, and Xenophon Zotos for fruitful discussion or collaborations.

Funding: This work was supported by the Deutsche Forschungsgemeinschaft [grant numbers HE3439/7, HE3439/8, HE3439/9, HE3439/12, HE3439/13, SFB 1143 (project C07)]; and the European Commission [grant numbers FP6-032980, PITN-GA-2009-238475].

References

References

- [1] R. Berman, Thermal Conduction in Solids, At the Clarendon Press, Oxford, 1976.
- [2] H. Fröhlich, W. Heitler, Time Effects in the Magnetic Cooling Method II – The Conductivity of Heat, Proc. Roy. Soc. (London) A155 (1936) 640.
- [3] B. Lüthi, Thermal Conductivity of Yttrium Iron Garnet, J. Phys. Chem. Solids 23 (1962) 35.
- [4] R. L. Douglass, Heat Transport by Spin Waves in Yttrium Iron Garnet, Phys. Rev. 129 (1963) 1132–1135.
- [5] J. E. Rives, G. S. Dixon, D. Walton, Effect of Magnons on Thermal Transport in Insulators, J. Appl. Phys. 40 (1969) 1555.
- [6] D. Walton, J. E. Rives, Q. Khalid, Thermal Transport By Coupled Magnons and Phonons in Yttrium Iron Garnet at Low Temperatures, Phys. Rev. B 8 (1973) 1210.
- [7] F. W. Gorter, L. J. Noordermeer, A. R. Kop, A. R. Miedema, Observation of Heat Transport by Magnons, Phys. Lett. 29A (1969) 331.
- [8] H. N. D. Lang, H. van Kempen, P. Wyder, Energy Transport above T_c by Paramagnetic Magnons in Two-Dimensional Ferromagnetic Heisenberg Systems, Phys. Rev. Lett. 39 (1977) 467.
- [9] L. H. M. Coenen, H. N. D. Lang, J. H. M. Stoeling, H. van Kempen, P. Wyder, Two-Dimensional Magnon and Phonon Thermal Conductivity in High Magnetic Fields, Physica B & C 86-88 (1977) 968.

- [10] H. Miike, K. Hirakawa, Evidence of the Diffusive Thermal Conduction in a One-Dimensional Antiferromagnet KCuF_3 above T_N , *J. Phys. Soc. Japan* 38 (1975) 1279.
- [11] M. T. Hutchings, E. J. Samuelsen, G. Shirane, K. Hirakawa, Neutron-Diffraction Determination of the Antiferromagnetic Structure of KCuF_3 , *Phys. Rev.* 188 (1969) 919.
- [12] X. Zotos, F. Naef, P. Prelovšek, Transport and Conservation Laws, *Phys. Rev. B* 55 (1997) 11029.
- [13] K. Kudo, S. Ishikawa, T. Noji, T. Adachi, Y. Koike, K. Maki, S. Tsuji, K. Kumagai, Spin Gap and Hole Pairing of $\text{Sr}_{14-x}\text{A}_x\text{Cu}_{24}\text{O}_{41}$ ($\text{A} = \text{Ca}$ and La) Single Crystals Studied by the Electrical Resistivity and Thermal Conductivity, *Journal of Low Temperature Physics* 117 (1999) 1689–1693.
- [14] A. V. Sologubenko, K. Giannò, H. R. Ott, U. Ammerahl, A. Revcolevschi, Thermal Conductivity of the Hole-Doped Spin Ladder System $\text{Sr}_{14-x}\text{Ca}_x\text{Cu}_{24}\text{O}_{41}$, *Phys. Rev. Lett.* 84 (2000) 2714.
- [15] C. Hess, C. Baumann, U. Ammerahl, B. Büchner, F. Heidrich-Meisner, W. Brenig, A. Revcolevschi, Magnon Heat Transport in $(\text{Sr}, \text{Ca}, \text{La})_{14}\text{Cu}_{24}\text{O}_{41}$, *Phys. Rev. B* 64 (2001) 184305.
- [16] K. Kudo, S. Ishikawa, T. Noji, T. Adachi, Y. Koike, K. Maki, S. Tsuji, K. Kumagai, Spin Gap and Hole Pairing in the Spin-Ladder Cuprate $\text{Sr}_{14-x}\text{A}_x\text{Cu}_{24}\text{O}_{41}$ ($\text{A}=\text{Ca}$ and La) Studied by the Thermal Conductivity, *J. Phys. Soc. Jpn.* 70 (2001) 437.
- [17] C. Hess, U. Ammerahl, C. Baumann, B. Büchner, A. Revcolevschi, Magnon hole scattering in $(\text{Sr}, \text{Ca}, \text{La})_{14}\text{Cu}_{24}\text{O}_{41}$, *Physica B* 312-313 (2002) 612.
- [18] C. Hess, B. Büchner, U. Ammerahl, L. Colonescu, F. Heidrich-Meisner, W. Brenig, A. Revcolevschi, Magnon Heat Transport in Doped La_2CuO_4 , *Phys. Rev. Lett.* 90 (2003) 197002.
- [19] C. Hess, H. ElHaes, B. Büchner, U. Ammerahl, M. Hücker, A. Revcolevschi, Magnon-Hole Scattering and Charge Order in $\text{Sr}_{14-x}\text{Ca}_x\text{Cu}_{24}\text{O}_{41}$, *Phys. Rev. Lett.* 93 (2004) 027005.
- [20] C. Hess, C. Baumann, B. Büchner, Scattering Processes and Magnon Thermal Conductivity in $\text{La}_5\text{Ca}_9\text{Cu}_{24}\text{O}_{41}$, *J. Mag. Mag. Mater.* 290-291 (2005) 322.
- [21] A. V. Sologubenko, E. Felder, K. Giannò, H. R. Ott, A. Vietkine, A. Revcolevschi, Thermal conductivity and specific heat of the linear chain cuprate Sr_2CuO_3 : Evidence for thermal transport via spinons, *Phys. Rev. B* 62 (2000) R6108.
- [22] A. V. Sologubenko, K. Giannò, H. R. Ott, A. Vietkine, A. Revcolevschi, Heat transport by lattice and spin excitations in the spin-chain compounds SrCuO_2 and Sr_2CuO_3 , *Phys. Rev. B* 64 (2001) 054412.
- [23] K. Kudo, T. Noji, Y. Koike, T. Nishizaki, N. Kobayashi, Single-Crystal Growth and Thermal Conductivity of the Four-Leg Spin-Ladder System $\text{La}_2\text{Cu}_2\text{O}_5$, *Journal of the Physical Society of Japan* 72 (2003) 2551–2555.
- [24] Y. Ando, J. Takeya, D. L. Sisson, S. G. Doettinger, I. Tanaka, R. S. Feigelson, A. Kapitulnik, Thermal conductivity of the spin-Peierls compound CuGeO_3 , *Phys. Rev. B* 58 (1998) R2913–R2916.
- [25] A. N. Vasil'ev, V. V. Pryadun, D. I. Khomskii, G. Dhalenne, A. Revcolevschi, M. Isobe, Y. Ueda, Anomalous Thermal Conductivity of NaV_2O_5 as Compared to Conventional Spin-Peierls System CuGeO_3 , *Phys. Rev. Lett.* 81 (1998) 1949–1952.
- [26] M. Hofmann, T. Lorenz, A. Freimuth, G. Uhrig, H. Kageyama, Y. Ueda, G. Dhalenne, A. Revcolevschi, Heat transport in $\text{SrCu}_2(\text{BO}_3)_2$ and CuGeO_3 , *Physica B: Condensed Matter* 312-313 (2002) 597 – 599.
- [27] M. Hofmann, T. Lorenz, K. Berggold, M. Grüniger, A. Freimuth, G. Uhrig, E. Brück, Evidence for a Large Magnetic Heat Current in Insulating Cuprates, *Phys. Rev. B* 67 (2003) 184502.
- [28] A. V. Sologubenko, S. M. Kazakov, H. R. Ott, T. Asano, Y. Ajiro, Diffusive Energy Transport in the $S = 1$ Haldane Chain Compound AgVP_2S_6 , *Phys. Rev. B* 68 (2003) 094432.
- [29] A. V. Sologubenko, H. R. Ott, G. Dhalenne, A. Revcolevschi, Universal Behavior of Spin-Mediated Energy Transport in $S = 1/2$ Chain Cuprates: $\text{BaCu}_2\text{Si}_2\text{O}_7$ as an Example, *Europhys. Lett.* 62 (2003) 540.
- [30] K. Kordonis, A. V. Sologubenko, T. Lorenz, S.-W. Cheong, A. Freimuth, Spin Thermal Conductivity of the Haldane Chain Compound Y_2BaNiO_5 , *Phys. Rev. Lett.* 97 (2006) 115901.
- [31] N. Hlubek, M. Sing, S. Glawion, R. Claessen, S. van Smaalen, P. H. M. van Loosdrecht, B. Büchner, C. Hess, Heat conductivity of the spin-Peierls compounds TiOCl and TiOBr , *Phys. Rev. B* 81 (2010) 144428.
- [32] F. Steckel, A. Matsumoto, T. Takayama, H. Takagi, B. Büchner, C. Hess, Pseudospin transport in the $J_{\text{eff}} = 1/2$ antiferromagnet Sr_2IrO_4 , *EPL (Europhysics Letters)* 114 (2016) 57007.
- [33] C. Hess, Heat conduction in low-dimensional quantum magnets, *The European Physical Journal - Special Topics* 151 (2007) 73–83.
- [34] C. Hess, P. Ribeiro, B. Büchner, H. ElHaes, G. Roth, U. Ammerahl, A. Revcolevschi, Magnon heat conductivity and mean free paths in two-leg spin ladders: A model-independent determination, *Phys. Rev. B* 73 (2006) 104407.
- [35] M. Otter, G. Athanasopoulos, N. Hlubek, M. Montagnese, M. Labois, D. Fishman, F. de Haan, S. Singh, D. Lakehal, J. Giapintzakis, C. Hess, A. Revcolevschi, P. van Loosdrecht, Optical probing of anisotropic heat transport in the quantum spin ladder $\text{Ca}_9\text{La}_5\text{Cu}_{24}\text{O}_{41}$, *International Journal of Heat and Mass Transfer* 55 (2012) 2531 – 2538.
- [36] M. Montagnese, M. Otter, X. Zotos, D. A. Fishman, N. Hlubek, O. Mityashkin, C. Hess, R. Saint-Martin, S. Singh, A. Revcolevschi, P. H. M. van Loosdrecht, Phonon-Magnon Interaction in Low Dimensional Quantum Magnets Observed by Dynamic Heat Transport Measurements, *Phys. Rev. Lett.* 110 (2013) 147206.
- [37] P. Ribeiro, C. Hess, P. Reutler, G. Roth, B. Büchner, Heat Transport in Doped SrCuO_2 , *J. Mag. Mag. Mater.* 290-291 (2005) 334.
- [38] C. Hess, H. ElHaes, A. Waske, B. Büchner, C. Sekar, G. Krabbes, F. Heidrich-Meisner, W. Brenig, Linear Temperature Dependence of the Magnetic Heat Conductivity in CaCu_2O_3 , *Physical Review Letters* 98 (2007) 027201.
- [39] N. Hlubek, P. Ribeiro, R. Saint-Martin, A. Revcolevschi, G. Roth, G. Behr, B. Büchner, C. Hess, Ballistic heat transport of quantum spin excitations as seen in SrCuO_2 , *Phys. Rev. B* 81 (2010) 020405.
- [40] N. Hlubek, X. Zotos, S. Singh, R. Saint-Martin, A. Revcolevschi, B. Büchner, C. Hess, Spinon heat transport and spin-

- phonon interaction in the spin-1/2 Heisenberg chain cuprates Sr_2CuO_3 and SrCuO_2 , *Journal of Statistical Mechanics: Theory and Experiment* 2012 (2012) P03006.
- [41] N. Hlubek, P. Ribeiro, R. Saint-Martin, S. Nishimoto, A. Revcolevschi, S.-L. Drechsler, G. Behr, J. Trinckauf, J. E. Hamann-Borrero, J. Geck, B. Büchner, C. Hess, Bond disorder and breakdown of ballistic heat transport in the spin- $\frac{1}{2}$ antiferromagnetic Heisenberg chain as seen in Ca-doped SrCuO_2 , *Phys. Rev. B* 84 (2011) 214419.
- [42] A. Mohan, N. S. Beesetty, N. Hlubek, R. Saint-Martin, A. Revcolevschi, B. Büchner, C. Hess, Bond disorder and spinon heat transport in the $S = \frac{1}{2}$ Heisenberg spin chain compound Sr_2CuO_3 : From clean to dirty limits, *Phys. Rev. B* 89 (2014) 104302.
- [43] F. Heidrich-Meisner, A. Honecker, D. C. Cabra, W. Brenig, Thermal conductivity of anisotropic and frustrated spin-1/2-chains, *Phys. Rev. B* 66 (2002) R140406.
- [44] F. Heidrich-Meisner, A. Honecker, D. C. Cabra, W. Brenig, Zero-Frequency Transport Properties of One-Dimensional Spin-(1/2) Systems, *Phys. Rev. B* 68 (2003) 134436.
- [45] E. Orignac, R. Chitra, R. Citro, Thermal Transport in One-Dimensional Spin Gap Systems, *Phys. Rev. B* 67 (2003) 134426.
- [46] J. V. Alvarez, C. Gros, Anomalous Thermal Conductivity of Frustrated Heisenberg Spin Chains and Ladders, *Phys. Rev. Lett.* 89 (2002) 156603.
- [47] F. Heidrich-Meisner, A. Honecker, D. C. Cabra, W. Brenig, Comment on “Anomalous Thermal Conductivity of Frustrated Heisenberg Spin Chains and Ladders”, *Phys. Rev. Lett.* 92 (2004) 069703.
- [48] C. Gros, J. V. Alvarez, Gros and Alvarez Reply:, *Phys. Rev. Lett.* 92 (2004) 069704.
- [49] K. Saito, Transport Anomaly in the Low-Energy Regime of Spin Chains, *Phys. Rev. B* 67 (2003) 064410.
- [50] K. Saito, Strong evidence of normal heat conduction in a one-dimensional quantum system, *EPL (Europhysics Letters)* 61 (2003) 34.
- [51] E. Shimshoni, N. Andrei, A. Rosch, Thermal Conductivity of Spin-(1/2) Chains, *Phys. Rev. B* 68 (2003) 104401.
- [52] A. Klümper, K. Sakai, The thermal conductivity of the spin- $\frac{1}{2}$ XXZ chain at arbitrary temperature, *J. Phys. A* 35 (2002) 2173–2182.
- [53] K. Sakai, A. Klümper, Non-dissipative thermal transport in the massive regimes of the XXZ chain, *Journal of Physics A: Mathematical and General* 36 (2003) 11617.
- [54] X. Zotos, High Temperature Thermal Conductivity of 2-Leg Spin-1/2 Ladders, *Phys. Rev. Lett.* 92 (2004) 067202.
- [55] J. Karadamoglou, X. Zotos, Diffusive Transport in Spin-1 Chains at High Temperatures, *Phys. Rev. Lett.* 93 (2004) 177203.
- [56] K. Louis, P. Prelovšek, X. Zotos, Thermal conductivity of one-dimensional spin-1/2 systems coupled to phonons, *Phys. Rev. B* 74 (2006) 235118.
- [57] M.-R. Li, E. Orignac, Heat conduction and Wiedemann-Franz law in disordered Luttinger liquids, *Europhys. Lett.* 60 (2002) 432.
- [58] B. Li, J. Wang, Anomalous Heat Conduction and Anomalous Diffusion in One-Dimensional Systems, *Phys. Rev. Lett.* 91 (2003) 044301.
- [59] A. V. Rozhkov, A. L. Chernyshev, Thermal Conductivity of Quasi-One-Dimensional Antiferromagnetic Spin-Chain Materials, *Phys. Rev. Lett.* 94 (2005) 087201.
- [60] A. L. Chernyshev, A. V. Rozhkov, Thermal transport in antiferromagnetic spin-chain materials, *Phys. Rev. B* 72 (2005) 104423.
- [61] P. Jung, R. Helmes, A. Rosch, Transport in Almost Integrable Models: Perturbed Heisenberg Chains, *Phys. Rev. Lett.* 96 (2006) 067202.
- [62] E. Boulat, P. Mehta, N. Andrei, E. Shimshoni, A. Rosch, Heat transport properties of clean spin ladders coupled to phonons: Umklapp scattering and drag, *Phys. Rev. B* 76 (2007) 214411.
- [63] R. Steinigeweg, J. Herbrych, X. Zotos, W. Brenig, Heat Conductivity of the Heisenberg Spin-1/2 Ladder: From Weak to Strong Breaking of Integrability, *Phys. Rev. Lett.* 116 (2016) 017202.
- [64] A. L. Chernyshev, A. V. Rozhkov, Heat Transport in Spin Chains with Weak Spin-Phonon Coupling, *Phys. Rev. Lett.* 116 (2016) 017204.
- [65] A. Klümper, Thermodynamics of the anisotropic spin-1/2 Heisenberg chain and related quantum chains, *Zeitschrift für Physik B Condensed Matter* 91 (1993) 507–519.
- [66] L. Faddeev, L. Takhtajan, What is the spin of a spin wave?, *Physics Letters A* 85 (1981) 375 – 377.
- [67] E. Dagotto, T. M. Rice, Surprises on the Way from One- to Two-Dimensional Quantum Magnets: The Ladder Materials, *Science* 271 (1996) 618.
- [68] E. Dagotto, Experiments on ladders reveal a complex interplay between a spin-gapped normal state and superconductivity, *Rep. Prog. Phys.* 62 (1999) 1525.
- [69] E. Manousakis, The spin-1/2 Heisenberg antiferromagnet on a square lattice and its application to the cuprous oxides, *Rev. Mod. Phys.* 63 (1991) 1.
- [70] R. Coldea, S. M. Hayden, G. Aeppli, T. G. Perring, C. D. Frost, T. E. Mason, S.-W. Cheong, Z. Fisk, Spin Waves and Electronic Interactions in La_2CuO_4 , *Phys. Rev. Lett.* 86 (2001) 5377.
- [71] A. W. Sandvik, R. R. P. Singh, High-Energy Magnon Dispersion and Multimagnon Continuum in the Two-Dimensional Heisenberg Antiferromagnet, *Phys. Rev. Lett.* 86 (2001) 528–531.
- [72] C.-M. Ho, V. N. Muthukumar, M. Ogata, P. W. Anderson, Nature of Spin Excitations in Two-Dimensional Mott Insulators: Undoped Cuprates and Other Materials, *Phys. Rev. Lett.* 86 (2001) 1626–1629.
- [73] E. Dagotto, J. Riera, D. Scalapino, Superconductivity in ladders and coupled planes, *Phys. Rev. B* 45 (1992) 5744.
- [74] G. Martinez, P. Horsch, Spin polarons in the t-J model, *Phys. Rev. B* 44 (1991) 317–331.

- [75] A. L. Chernyshev, P. W. Leung, Holes in the $t - J_z$ model: A diagrammatic study, *Phys. Rev. B* 60 (1999) 1592–1606.
- [76] P. A. Lee, N. Nagaosa, X.-G. Wen, Doping a Mott insulator: Physics of high-temperature superconductivity, *Rev. Mod. Phys.* 78 (2006) 17–85.
- [77] A. Koitzsch, S. V. Borisenko, J. Geck, V. B. Zabolotnyy, M. Knupfer, J. Fink, P. Ribeiro, B. Buchner, R. Follath, Current spinon-holon description of the one-dimensional charge-transfer insulator SrCuO_2 : Angle-resolved photoemission measurements, *Phys. Rev. B* 73 (2006) 201101.
- [78] T. Vuletić, B. Korin-Hamzić, T. Ivek, S. Tomić, B. Gorshunov, M. Dressel, J. Akimitsu, The spin-ladder and spin-chain system $(\text{La}, \text{Y}, \text{Sr}, \text{Ca})_{14}\text{Cu}_{24}\text{O}_{41}$: Electronic phases, charge and spin dynamics, *Physics Reports* 428 (2006) 169 – 258.
- [79] V. Kiryukhin, Y. J. Kim, K. J. Thomas, F. C. Chou, R. W. Erwin, Q. Huang, M. A. Kastner, R. J. Birgeneau, Magnetic Properties of the $S = 1/2$ Quasi-One-Dimensional Antiferromagnet CaCu_2O_3 , *Phys. Rev. B* 63 (2001) 144418.
- [80] N. Motoyama, H. Eisaki, S. Uchida, Magnetic Susceptibility of Ideal Spin 1 /2 Heisenberg Antiferromagnetic Chain Systems, Sr_2CuO_3 and SrCuO_2 , *Phys. Rev. Lett.* 76 (1996) 3212–.
- [81] C. Hess, B. Büchner, Thermal conductivity of doped La_2CuO_4 as an example for heat transport by optical phonons in complex materials, *Eur. Phys. B* 38 (2004) 37.
- [82] J. M. Ziman, *Electrons and Phonons*, At the Clarendon Press, Oxford, 1960.
- [83] D. T. Morelli, J. Heremans, G. Doll, P. J. Picone, H. P. Jentsen, M. S. Dresselhaus, Thermal properties of single-crystal $\text{La}_2\text{CuO}_{4-\delta}$, *Phys. Rev. B* 39 (1989) 804.
- [84] Y. Nakamura, S. Uchida, T. Kimura, N. Motohira, K. Kishio, K. Kitazawa, T. Arima, Y. Tokura, In-Plane and Out-of-Plane thermal conductivity of $\text{La}_{2-x}\text{Sr}_x\text{CuO}_4$ single crystals, *Physica C* 185-189 (1991) 1409.
- [85] J. L. Cohn, C. K. Lowe-Ma, T. A. Vanderah, Anomalous Phonon Damping and Thermal Conductivity in Insulating Cuprates, *Phys. Rev. B* 52 (1995) 13134.
- [86] X. F. Sun, J. Takeya, S. Komiya, Y. Ando, Thermal conductivity of lightly Sr- and Zn-doped La_2CuO_4 single crystals, *Phys. Rev. B* 67 (2003) 104503.
- [87] X. F. Sun, S. Komiya, Y. Ando, Heat transport of $\text{La}_{2-y}\text{Eu}_y\text{CuO}_4$ and $\text{La}_{1.88-y}\text{Eu}_y\text{Sr}_{0.12}\text{CuO}_4$ single crystals, *Phys. Rev. B* 67 (2003) 184512.
- [88] K. Berggold, T. Lorenz, J. Baier, M. Kriener, D. Senff, H. Roth, A. Severing, H. Hartmann, A. Freimuth, S. Barilo, F. Nakamura, Magnetic heat transport in R_2CuO_4 (R=La, Pr, Nd, Sm, Eu, and Gd), *Phys. Rev. B* 73 (2006) 104430.
- [89] C. Hess, B. Büchner, U. Ammerahl, A. Revcolevschi, Phonon Thermal Conductivity in Doped La_2CuO_4 : Relevant Scattering Mechanisms, *Phys. Rev. B* 68 (2003) 184517.
- [90] C. Hess, B. Büchner, Magnon-hole scattering in $\text{La}_{2-x}\text{Sr}_x\text{CuO}_4$, *Journal of Magnetism and Magnetic Materials* 310 (2007) e412 – e414.
- [91] J.-Q. Yan, J.-S. Zhou, J. B. Goodenough, Thermal conductivity in the stripe-ordered phase of cuprates and nickelates, *Phys. Rev. B* 68 (2003) 104520.
- [92] S. Uchida, T. Ido, H. Takagi, T. Arima, Y. Tokura, S. Tajima, Optical spectra of $\text{La}_{2-x}\text{Sr}_x\text{CuO}_4$: Effect of carrier doping on the electronic structure of the CuO_2 plane, *Phys. Rev. B* 43 (1991) 7942.
- [93] M. Hofmann, T. Lorenz, G. S. Uhrig, H. Kierspel, O. Zabara, A. Freimuth, H. Kageyama, Y. Ueda, Strong Damping of Phononic Heat Current by Magnetic Excitations in $\text{SrCu}_2(\text{BO}_3)_2$, *Phys. Rev. Lett.* 87 (2001) 047202.
- [94] Y. Suemune, Thermal Conductivity of BaTiO_3 and SrTiO_3 from 4.5° to 300°K , *Journal of the Physical Society of Japan* 20 (1965) 174–175.
- [95] E. F. Steigmeier, Field Effect on the Cochran Modes in SrTiO_3 and KTaO_3 , *Phys. Rev.* 168 (1968) 523–530.
- [96] P. Böni, J. D. Axe, G. Shirane, R. J. Birgeneau, D. R. Gabbe, H. P. Jentsen, M. A. Kastner, C. J. Peters, P. J. Picone, T. R. Thurston, Lattice instability and soft phonons in single-crystal $\text{La}_{2-x}\text{Sr}_x\text{CuO}_4$, *Phys. Rev. B* 38 (1988) 185.
- [97] P. Böni, J. D. Axe, G. Shirane, R. Birgeneau, D. Gabbe, H. Jentsen, M. Kastner, P. Picone, T. Thurston, M. Sato, S. Shamoto, Lattice instability in single-crystal $\text{La}_{2-x}\text{Sr}_x\text{CuO}_4$, *Physica B: Condensed Matter* 156-157 (1989) 902 – 905.
- [98] R. J. Birgeneau, C. Y. Chen, D. R. Gabbe, H. P. Jentsen, M. A. Kastner, C. J. Peters, P. J. Picone, T. Thio, T. R. Thurston, H. L. Tuller, Soft-Phonon Behavior and Transport in Single-Crystal La_2CuO_4 , *Phys. Rev. Lett.* 59 (1987) 1329.
- [99] B. Büchner, M. Breuer, A. Freimuth, A. P. Kampf, Critical Buckling for the Disappearance of Superconductivity in Rare-Earth-Doped $\text{La}_{2-x}\text{Sr}_x\text{CuO}_4$, *Phys. Rev. Lett.* 73 (1994) 1841.
- [100] H.-H. Klauss, W. Wagener, M. Hillberg, W. Kopmann, H. Walf, F. J. Litterst, M. Hücker, B. Büchner, From Antiferromagnetic Order to Static Magnetic Stripes: The Phase Diagram of $(\text{La}, \text{Eu})_{2-x}\text{Sr}_x\text{CuO}_4$, *Phys. Rev. Lett.* 85 (2000) 4590.
- [101] B. Keimer, R. J. Birgeneau, A. Cassanho, Y. Endoh, M. Greven, M. A. Kastner, G. Shirane, Soft phonon behavior and magnetism at the low temperature structural phase transition of $\text{La}_{1.65}\text{Nd}_{0.35}\text{CuO}_4$, *Z. Phys. B* 91 (1993) 373.
- [102] J. L. Martínez, M. T. Fernández-Díaz, J. Rodríguez-Carvajal, P. Odier, Lattice instability and low-temperature phase transition in Pr_2NiO_4 , *Phys. Rev. B* 43 (1991) 13766.
- [103] M. Sera, M. Maki, M. Hiroi, N. Kobayashi, Thermal Conductivity of $\text{La}_{2-x-y}\text{Nd}_y\text{Sr}_x\text{CuO}_4$, *J. Phys. Soc. Jpn.* 66 (1997) 765.
- [104] J. Yamada, M. Sera, M. Sato, T. Takayama, M. Takata, M. Sakata, Relationship between Structural Transitions and the Low Temperature Electronic State of $(\text{La}, \text{Nd})_{2-x}\text{M}_x\text{CuO}_4$ (M=Ba, Sr; $x \sim 1/8$), *J. Phys. Soc. Jpn.* 63 (1994) 2314.
- [105] R. Jin, Y. Onose, Y. Tokura, D. Mandrus, P. Dai, B. C. Sales, In-Plane Thermal Conductivity of Nd_2CuO_4 : Evidence for Magnon Heat Transport, *Phys. Rev. Lett.* 91 (2003) 146601.
- [106] M. Braden, W. Paulus, A. Cousson, P. Vigoureux, G. Heger, A. Goukassov, P. Bourges, D. Petitgrand, Structure Analysis of Gd_2CuO_4 : a New Modification of the T' Phase, *EPL (Europhysics Letters)* 25 (1994) 625.

- [107] P. Vigoureux, A. Gukasov, S. Barilo, D. Zhigunov, Neutron scattering study of the structural phase transition in Eu_2CuO_4 , *Physica B: Condensed Matter* 234-236 (1997) 815 – 817.
- [108] J. Callaway, Model for Lattice Thermal Conductivity at Low Temperatures, *Physical Review* 113 (1959) 1046–1051.
- [109] J. Ding Yu, Y. Inaguma, M. Itoh, M. Oguni, T. Kyômen, Effect of oxygen content on the anomalies at successive phase transitions of $\text{La}_2\text{CuO}_{4+\delta}$ single crystal below 320 K, *Phys. Rev. B* 54 (1996) 7455–7461.
- [110] P. Zolliker, D. E. Cox, J. B. Parise, E. M. McCarron III, E. E. Farneth, Neutron and Synchrotron X-Ray Powder-Diffraction Study of $\text{La}_2\text{CuO}_{4+\delta}$, *Phys. Rev. B* 42 (1990) 6332.
- [111] S. M. Hayden, G. Aeppli, R. Osborn, A. D. Taylor, T. G. Perring, S.-W. Cheong, Z. Fisk, High-Energy Spin Waves in La_2CuO_4 , *Phys. Rev. Lett.* 67 (1991) 3622.
- [112] W. Brenig, A. Kampf, Spin Excitations in a Quantum Antiferromagnet with Magnetic Impurities and Vacancies, *Phys. Rev. B* 43 (1991) 12914.
- [113] K. Uchinokura, T. Ino, I. Terasaki, I. Tsukada, Effect of Substitution of Zn^{2+} for Cu^{2+} on the Magnetic Properties of $\text{La}_2\text{Cu}_{1-x}\text{Zn}_x\text{O}_4$ Single Crystals, *Physica B* 205 (1995) 234.
- [114] M. Hücker, V. Kataev, J. Pommer, J. Harraß, A. Hosni, C. Pfitsch, R. Gross, B. Büchner, Mobility of Holes and Suppression of Antiferromagnetic Order in $\text{La}_{2-x}\text{Sr}_x\text{CuO}_4$, *Phys. Rev. B* 59 (1999) 725.
- [115] C. Y. Chen, R. J. Birgeneau, M. A. Kastner, N. W. Preyer, T. Thio, Frequency and magnetic-field dependence of the dielectric constant and conductivity of $\text{La}_2\text{CuO}_{4+y}$, *Phys. Rev. B* 43 (1991) 392–401.
- [116] A. Mohan, O. Mityashkin, S. Singh, B. Büchner, C. Hess, unpublished
- [117] S. Gopalan, T. M. Rice, M. Sgrist, Spin ladders with gaps: A description of a class of cuprates, *Phys. Rev. B* 49 (1994) 8901.
- [118] U. Ammerahl, Einkristallherstellung und physikalische Eigenschaften niedrigdimensionaler Kuprate: Spin-Ketten, - Leitern und -Ebenen, Ph.D. thesis, Universität zu Köln, 2000.
- [119] T. Osafune, N. Motoyama, H. Eisaki, S. Uchida, Optical Study of the $\text{Sr}_{14-x}\text{Ca}_x\text{Cu}_{24}\text{O}_{41}$ System: Evidence for Hole-Doped Cu_2O_3 Ladders, *Phys. Rev. Lett.* 78 (1997) 1980.
- [120] N. Nücker, M. Merz, C. A. Kuntscher, S. Gerhold, S. Schuppler, R. Neudert, M. S. Golden, J. Fink, D. Schild, S. Stadler, V. Chakarian, J. Freeland, Y. U. Idzerda, K. Conder, M. Uehara, T. Nagata, J. Goto, J. Akimitsu, N. Motoyama, H. Eisaki, S. Uchida, U. Ammerahl, A. Revcolevschi, Hole distribution in $(\text{Sr,Ca,La})_{14}\text{Cu}_{24}\text{O}_{41}$ ladder compounds studied by x-ray absorption spectroscopy, *Phys. Rev. B* 62 (2000) 14384.
- [121] U. Ammerahl, B. Büchner, L. Colonescu, R. Gross, A. Revcolevschi, Interplay between magnetism, charge localization, and structure in $\text{Sr}_{14-x}\text{Ca}_x\text{Cu}_{24}\text{O}_{41}$, *Phys. Rev. B* 62 (2000) 8630.
- [122] M. Matsuda, T. Yoshizawa, K. Kakurai, G. Shirane, Quasi-two-dimensional hole ordering and dimerized state in the CuO_2 -chain layers in $\text{Sr}_{14}\text{Cu}_{24}\text{O}_{41}$, *Phys. Rev. B* 59 (1999) 1060.
- [123] L. P. Regnault, J. P. Boucher, H. Moudden, J. E. Lorenzo, A. Hiess, U. Ammerahl, G. Dhalenne, A. Revcolevschi, Spin dynamics in the magnetic chain arrays of $\text{sr}_{14}\text{cu}_{24}\text{o}_{41}$: A neutron inelastic scattering investigation, *Phys. Rev. B* 59 (1999) 1055.
- [124] R. Klingeler, N. Tristan, B. Büchner, M. Hücker, U. Ammerahl, A. Revcolevschi, Magnetization of hole-doped CuO_2 spin chains in $\text{Sr}_{14-x}\text{Ca}_x\text{Cu}_{24}\text{O}_{41}$, *Phys. Rev. B* 72 (2005) 184406.
- [125] R. Klingeler, B. Büchner, K.-Y. Choi, V. Kataev, U. Ammerahl, A. Revcolevschi, J. Schnack, Magnetism of hole-doped CuO_2 spin chains in $\text{Sr}_{14}\text{Cu}_{24}\text{O}_{41}$: Experimental and numerical results, *Phys. Rev. B* 73 (2006) 014426.
- [126] P. Abbamonte, G. Blumberg, A. Rusydi, A. Gozar, P. G. Evans, T. Siegrist, L. Venema, H. Eisaki, E. D. Isaacs, G. A. Sawatzky, Crystallization of charge holes in the spin ladder of $\text{Sr}_{14}\text{Cu}_{24}\text{O}_{41}$, *Nature* 431 (2004) 1078–1081.
- [127] A. Rusydi, P. Abbamonte, H. Eisaki, Y. Fujimaki, G. Blumberg, S. Uchida, G. A. Sawatzky, Quantum Melting of the Hole Crystal in the Spin Ladder of $\text{Sr}_{14-x}\text{Ca}_x\text{Cu}_{24}\text{O}_{41}$, *Phys. Rev. Lett.* 97 (2006) 016403.
- [128] V. Kataev, K.-Y. Choi, M. Grüninger, U. Ammerahl, B. Büchner, A. Freimuth, A. Revcolevschi, Interplay of spin and charge dynamics in $\text{Sr}_{14-x}\text{Ca}_x\text{Cu}_{24}\text{O}_{41}$, *Phys. Rev. B* 64 (2001) 104422.
- [129] M. Uehara, T. Nagata, J. Akimitsu, H. Takahashi, N. Môri, K. Kinoshita, Superconductivity in the Ladder Material $\text{Sr}_{0.4}\text{Ca}_{13.6}\text{Cu}_{24}\text{O}_{41.84}$, *J. Phys. Soc. Jpn.* 65 (1996) 2764.
- [130] M. Isobe, T. Ohta, M. Onoda, F. Izumi, S. Nakano, J. Q. Li, Y. Matsui, E. Takayama-Muromachi, T. Matsumoto, H. Hayakawa, Structural and electrical properties under high pressure for the superconducting spin ladder system $\text{Sr}_{0.4}\text{Ca}_{13.6}\text{Cu}_{24}\text{O}_{41+\delta}$, *Phys. Rev. B* 57 (1998) 613.
- [131] U. Ammerahl, A. Revcolevschi, Crystal growth of the spin-ladder compound $(\text{Ca,La})_{14}\text{Cu}_{24}\text{O}_{41}$ and observation of one-dimensional disorder, *J. Crystal Growth* 197 (1999) 825.
- [132] M. Matsuda, K. Katsumata, T. Yokoo, S. M. Shapiro, G. Shirane, Magnetic ordering in the $s=1/2$ quasi-one-dimensional compound $\text{La}_6\text{Ca}_8\text{Cu}_{24}\text{O}_{41}$, *Phys. Rev. B* 54 (1996) 15626.
- [133] M. Matsuda, K. M. Kojima, Y. J. U. J. L. Zarestky, K. Nakajima, K. Kakurai, T. Yokoo, S. M. Shapiro, G. Shirane, Ordering of oxygen moments in ferromagnetic edge-sharing CuO_4 chains in $\text{La}_{14-x}\text{Ca}_x\text{Cu}_{24}\text{O}_{41}$, *Phys. Rev. B* 57 (1998) 11467.
- [134] M. Matsuda, K. Katsumata, R. S. Eccleston, S. Brehmer, H.-J. Mikeska, Magnetic excitations and exchange interactions in the spin-1/2 two-leg ladder compound $\text{La}_6\text{Ca}_8\text{Cu}_{24}\text{O}_{41}$, *Phys. Rev. B* 62 (2000) 8903.
- [135] K. Kumagai, S. Tsuji, K. Maki, NMR/NQR Studies on Magnetism of Spin Ladder $\text{Sr}_{14-x}\text{A}_x\text{Cu}_{24}\text{O}_{41}$ ($\text{A}=\text{Ca}$ and La), *J. Phys. Soc. Jpn.* 69 (2000) Suppl. B. 39.
- [136] U. Ammerahl, B. Büchner, C. Kerpen, R. Gross, A. Revcolevschi, Ising-like antiferromagnetism in $\text{Ca}_9\text{La}_5\text{Cu}_{24}\text{O}_{41}$, *Phys. Rev. B* 62 (2000) R3592–R3595.
- [137] M. Windt, M. Grüninger, T. Nunner, C. Knetter, K. P. Schmidt, G. S. Uhrig, T. Kopp, A. Freimuth, U. Ammerahl, B. Büchner, A. Revcolevschi, Observation of Two-Magnon Bound States in the Two-Leg Ladders of $(\text{Ca,La})_{14}\text{Cu}_{24}\text{O}_{41}$,

- Phys. Rev. Lett. 87 (2001) 127002.
- [138] S. Notbohm, P. Ribeiro, B. Lake, D. A. Tennant, K. P. Schmidt, G. S. Uhrig, C. Hess, R. Klingeler, G. Behr, B. Büchner, M. Reehuis, R. I. Bewley, C. D. Frost, P. Manuel, R. S. Eccleston, One- and Two-Triplon Spectra of a Cuprate Ladder, Phys. Rev. Lett. 98 (2007) 027403.
- [139] R. S. Eccleston, M. Uehara, J. Akimitsu, H. Eisaki, N. Motoyama, S. I. Uchida, Spin Dynamics of the Spin-Ladder Dimer-Chain Material $\text{Sr}_{14}\text{Cu}_{24}\text{O}_{41}$, Phys. Rev. Lett. 81 (1998) 1702.
- [140] G. Deng, N. Tsyrlin, P. Bourges, D. Lamago, H. Ronnow, M. Kenzelmann, S. Danilkin, E. Pomjakushina, K. Conder, Spin-gap evolution upon Ca doping in the spin-ladder series $\text{Sr}_{14-x}\text{Ca}_x\text{Cu}_{24}\text{O}_{41}$ studied by inelastic neutron scattering, Phys. Rev. B 88 (2013) 014504.
- [141] K. Kumagai, S. Tsuji, M. Kato, Y. Koike, NMR Study of Carrier Doping Effects on Spin Gaps in the Spin Ladder $\text{Sr}_{14-x}\text{A}_x\text{Cu}_{24}\text{O}_{41}$ (A=Ca, Y, and La), Phys. Rev. Lett. 78 (1997) 1992.
- [142] M. Takigawa, N. Motoyama, H. Eisaki, S. Uchida, Spin and charge dynamics in the hole-doped one-dimensional-chain-ladder composite material $\text{Sr}_{14}\text{Cu}_{24}\text{O}_{41}$: Cu NMR/NQR studies, Phys. Rev. B 57 (1998) 1124.
- [143] T. Imai, K. R. Thurber, K. M. Shen, A. W. Hunt, F. C. Chou, ^{17}O and ^{63}Cu NMR in Undoped and Hole Doped Cu_2O_3 Two-Leg Spin Ladder $\text{A}_{14}\text{Cu}_{24}\text{O}_{41}$ ($\text{A}_{14} = \text{La}_6\text{Ca}_8, \text{Sr}_{14}, \text{Sr}_{11}\text{Ca}_3$), Phys. Rev. Lett. 81 (1998) 220.
- [144] K. Magishi, S. Matsumoto, Y. Kitaoka, K. Ishida, K. Asayama, M. Uehara, T. Nagata, J. Akimitsu, Spin gap and dynamics in $\text{Sr}_{14-x}\text{Ca}_x\text{Cu}_{24}\text{O}_{41}$ comprising hole-doped two-leg spin ladders: Cu NMR study on single crystals, Phys. Rev. B 57 (1998) 11533.
- [145] M. Otter, V. Krasnikov, D. Fishman, M. Pshenichnikov, R. Saint-Martin, A. Revcolevschi, P. van Loosdrecht, Heat transport imaging in the spin-ladder compound $\text{Ca}_9\text{La}_5\text{Cu}_{24}\text{O}_{41}$, Journal of Magnetism and Magnetic Materials 321 (2009) 796 – 799.
- [146] X. Zotos, Issues on the Transport of One Dimensional Quantum Systems, Journal of the Physical Society of Japan 74S (2005) 173–180.
- [147] T. Vuletić, T. Ivek, B. Korin-Hamzić, S. S. Tomić, B. Gorshunov, M. Dressel, C. Hess, B. Büchner, J. Akimitsu, Phase diagrams of $(\text{La},\text{Y},\text{Sr},\text{Ca})_{14}\text{Cu}_{24}\text{O}_{41}$: Switching between the ladders and the chains, J. Phys. IV France 131 (2005) 299–304.
- [148] T. Vuletić, B. Korin-Hamzić, S. Tomić, B. Gorshunov, P. Haas, T. Rößm, M. Dressel, J. Akimitsu, T. Sasaki, T. Nagata, Suppression of the Charge-Density-Wave State in $\text{Sr}_{14}\text{Cu}_{24}\text{O}_{41}$ by Calcium Doping, Phys. Rev. Lett. 90 (2003) 257002.
- [149] M. Grüninger, D. van der Marel, A. Damascelli, A. Erb, T. Nunner, T. Kopp, Midinfrared absorption in $\text{YBa}_2\text{Cu}_3\text{O}_6$: Evidence for a failure of spin-wave theory for spin $\frac{1}{2}$ in two dimensions, Phys. Rev. B 62 (2000) 12422–12426.
- [150] D. C. Johnston, M. Troyer, S. Miyahara, D. Lidsky, K. Ueda, M. Azuma, Z. Hiroi, M. Takano, M. Isobe, Y. Ueda, M. A. Korotin, V. I. Anisimov, A. V. Mahajan, L. L. Miller, Magnetic Susceptibilities of Spin-1/2 Antiferromagnetic Heisenberg Ladders and Applications to Ladder Oxide Compounds, arXiv:cond-mat/0001147 (2000).
- [151] M. W. McElfresh, J. M. D. Coey, P. Strobel, S. von Molnar, Electronic properties of $\text{Sr}_{14}\text{Cu}_{24}\text{O}_{41}$, Phys. Rev. B 40 (1989) 825.
- [152] C. Hess, Thermischer Transport in Übergangsmetalloxiden mit niedrigdimensionalen Ladungs- und Spinstrukturen, Mensch- und Buch-Verlag, 2002.
- [153] K. Naruse, T. Kawamata, M. Ohno, Y. Matsuoka, K. Kumagai, Y. Koike, Thermal conductivity due to magnons in high-quality single crystals of the two-leg spin-ladder system $(\text{Ca},\text{Sr},\text{La})_{14}\text{Cu}_{24}\text{O}_{41}$, Solid State Communications 154 (2013) 60 – 63.
- [154] G. T. Hohensee, R. B. Wilson, J. P. Feser, D. G. Cahill, Magnon-phonon coupling in the spin-ladder compound $\text{Ca}_9\text{La}_5\text{Cu}_{24}\text{O}_{41}$ measured by time-domain thermoreflectance, Phys. Rev. B 89 (2014) 024422.
- [155] T. Niemeijer, H. van Vianen, A note on the thermal conductivity of linear magnetic chains, Physics Letters A 34 (1971) 401 – 402.
- [156] F. Heidrich-Meisner, Transport Properties Of Low-Dimensional Quantum Spin Systems, Ph.D. thesis, Technische Universität Carolo-Wilhelmina zu Braunschweig, 2005. URL: <http://www.digibib.tu-bs.de/?docid=00001712>.
- [157] M. Goiran, M. Costes, J. M. Broto, F. C. Chou, R. Klingeler, E. Arushanov, S.-L. Drechsler, B. Bchner, V. Kataev, High-field ESR studies of the quantum spin magnet CaCu_2O_3 , New Journal of Physics 8 (2006) 74.
- [158] T. K. Kim, H. Rosner, S.-L. Drechsler, Z. Hu, C. Sekar, G. Krabbes, J. Málek, M. Knupfer, J. Fink, H. Eschrig, Unusual Electronic Structure of the Pseudoladder Compound CaCu_2O_3 , Phys. Rev. B 67 (2003) 024516.
- [159] B. Lake, A. M. Tsvetik, S. Notbohm, D. Alan Tennant, T. G. Perring, M. Reehuis, C. Sekar, G. Krabbes, B. Büchner, Confinement of fractional quantum number particles in a condensed-matter system, Nat Phys 6 (2010) 50–55.
- [160] K. Ruck, M. Wolf, M. Ruck, D. Eckert, G. Krabbes, K. Müller, CaCu_2O_3 , A Nonstoichiometric Compound: Structural Disorder and Magnetic Properties, Mater. Res. Bull. 36 (2001) 1995.
- [161] R. Berman, P. G. Klemens, F. E. Simon, Effect of Neutron Irradiation on the Thermal Conductivity of a Quartz Crystal at Low Temperature, Nature 166 (1950) 864.
- [162] T. Kawamata, N. Kaneko, M. Uesaka, M. Sato, Y. Koike, Enhancement of thermal conductivity due to spinons in the one-dimensional spin system SrCuO_2 , Journal of Physics: Conference Series 200 (2010) 022023.
- [163] T. Kawamata, N. Takahashi, T. Adachi, T. Noji, K. Kudo, N. Kobayashi, Y. Koike, Evidence for Ballistic Thermal Conduction in the One-Dimensional $S = 1/2$ Heisenberg Antiferromagnetic Spin System Sr_2CuO_3 , Journal of the Physical Society of Japan 77 (2008) 034607.
- [164] N. Hlubek, Magnetic heat transport in one-dimensional quantum antiferromagnets, Ph.D. thesis, Technische Universität Dresden, 2011.
- [165] F. Heidrich-Meisner, A. Honecker, W. Brenig, Thermal Transport of the XXZ Chain in a Magnetic Field, Phys. Rev. B 71 (2005) 184415.

- [166] F. Hammerath, S. Nishimoto, H.-J. Grafe, A. U. B. Wolter, V. Kataev, P. Ribeiro, C. Hess, S.-L. Drechsler, B. Büchner, Spin Gap in the Zigzag Spin-1/2 Chain Cuprate $\text{Sr}_{0.9}\text{Ca}_{0.1}\text{CuO}_2$, *Phys. Rev. Lett.* 107 (2011) 017203.
- [167] F. Hammerath, E. M. Brüning, S. Sanna, Y. Utz, N. S. Beesetty, R. Saint-Martin, A. Revcolevschi, C. Hess, B. Büchner, H.-J. Grafe, Spin gap in the single spin- $\frac{1}{2}$ chain cuprate $\text{Sr}_{1.9}\text{Ca}_{0.1}\text{CuO}_3$, *Phys. Rev. B* 89 (2014) 184410.
- [168] Y. Utz, F. Hammerath, S. Nishimoto, C. Hess, N. S. Beesetty, R. Saint-Martin, A. Revcolevschi, B. Büchner, H.-J. Grafe, Suppression of the impurity-induced local magnetism by the opening of a spin pseudogap in Ni-doped Sr_2CuO_3 , *Phys. Rev. B* 92 (2015) 060405.
- [169] G. Simutis, S. Gvasaliya, M. Månsson, A. L. Chernyshev, A. Mohan, S. Singh, C. Hess, A. T. Savici, A. I. Kolesnikov, A. Piovano, T. Perring, I. Zaliznyak, B. Büchner, A. Zheludev, Spin Pseudogap in Ni-Doped SrCuO_2 , *Phys. Rev. Lett.* 111 (2013) 067204.
- [170] A. L. Chernyshev, W. Brenig, Thermal conductivity in large $-J$ two-dimensional antiferromagnets: Role of phonon scattering, *Phys. Rev. B* 92 (2015) 054409.
- [171] L. J. Cornelissen, J. Liu, R. A. Duine, J. B. Youssef, B. J. van Wees, Long-distance transport of magnon spin information in a magnetic insulator at room temperature, *Nature Physics* 11 (2015) 1022.
- [172] A. V. Sologubenko, K. Berggold, T. Lorenz, A. Rosch, E. Shimshoni, M. D. Phillips, M. M. Turnbull, Magnetothermal Transport in the Spin- $\frac{1}{2}$ Chains of Copper Pyrazine Dinitrate, *Phys. Rev. Lett.* 98 (2007) 107201.
- [173] C. S. Lue, C. N. Kuo, D. S. Tasi, Y. K. Kuo, Z. He, M. Itoh, Magnon-mediated thermal conductivity in the dimerized spin-gap compound $\text{BaCu}_2\text{V}_2\text{O}_8$, *Phys. Rev. B* 78 (2008) 012406.
- [174] A. V. Sologubenko, T. Lorenz, J. A. Mydosh, B. Thielemann, H. M. Rønnow, C. Rüegg, K. W. Krämer, Evidence for spinon localization in the heat transport of the spin- $\frac{1}{2}$ ladder compound $(\text{C}_5\text{H}_{12}\text{N})_2\text{CuBr}_4$, *Phys. Rev. B* 80 (2009) 220411.
- [175] B.-G. Jeon, B. Koteswararao, C. B. Park, G. J. Shu, S. C. Riggs, E. G. Moon, S. B. Chung, F. C. Chou, K. H. Kim, Giant suppression of phononic heat transport in a quantum magnet BiCu_2PO_6 , *Scientific Reports* 6 (2016) 36970.
- [176] A. V. Sologubenko, T. Lorenz, J. A. Mydosh, A. Rosch, K. C. Shortsleeves, M. M. Turnbull, Field-Dependent Thermal Transport in the Haldane Chain Compound NENP, *Phys. Rev. Lett.* 100 (2008) 137202.
- [177] Y. Kohama, A. V. Sologubenko, N. R. Dilley, V. S. Zapf, M. Jaime, J. A. Mydosh, A. Paduan-Filho, K. A. Al-Hassanieh, P. Sengupta, S. Gangadharaiah, A. L. Chernyshev, C. D. Batista, Thermal Transport and Strong Mass Renormalization in $\text{NiCl}_2\text{-}4\text{SC}(\text{NH}_2)_2$, *Phys. Rev. Lett.* 106 (2011) 037203.
- [178] X. F. Sun, X. G. Liu, L. M. Chen, Z. Y. Zhao, X. Zhao, Large magnetic heat transport in a haldane chain material $\text{ni}(\text{c}_3\text{h}_{10}\text{n}_2)_2\text{no}_2\text{clo}_4$, *Journal of Applied Physics* 113 (2013) 17B514.
- [179] A. V. Savin, G. P. Tsironis, X. Zotos, Thermal conductivity of a classical one-dimensional Heisenberg spin model, *Phys. Rev. B* 72 (2005) 140402.
- [180] A. V. Sologubenko, T. Lorenz, H. R. Ott, A. Freimuth, Thermal conductivity via magnetic excitations in spin-chain materials, *Journal of Low Temperature Physics* 147 (2007) 387–403.
- [181] X. Zhao, Z. Zhao, X. Liu, X. Sun, Low-temperature heat transport of spin-gapped quantum magnets, *Science China Physics, Mechanics & Astronomy* 59 (2016) 117501.
- [182] B. Klemke, M. Meissner, P. Strehlow, K. Kiefer, S. A. Grigera, D. A. Tennant, Thermal Relaxation and Heat Transport in the Spin Ice Material $\text{Dy}_2\text{Ti}_2\text{O}_7$, *Journal of Low Temperature Physics* 163 (2011) 345–369.
- [183] G. Kolland, O. Breunig, M. Valldor, M. Hiertz, J. Frielingsdorf, T. Lorenz, Thermal conductivity and specific heat of the spin-ice compound $\text{Dy}_2\text{Ti}_2\text{O}_7$: Experimental evidence for monopole heat transport, *Phys. Rev. B* 86 (2012) 060402.
- [184] W. H. Toews, S. S. Zhang, K. A. Ross, H. A. Dabkowska, B. D. Gaulin, R. W. Hill, Thermal Conductivity of $\text{Ho}_2\text{Ti}_2\text{O}_7$ along the [111] Direction, *Phys. Rev. Lett.* 110 (2013) 217209.
- [185] C. Fan, Z. Y. Zhao, H. D. Zhou, X. M. Wang, Q. J. Li, F. B. Zhang, X. Zhao, X. F. Sun, Irreversible magnetic-field dependence of low-temperature heat transport of spin-ice compound $\text{Dy}_2\text{Ti}_2\text{O}_7$ in a [111] field, *Phys. Rev. B* 87 (2013) 144404.
- [186] G. Kolland, M. Valldor, M. Hiertz, J. Frielingsdorf, T. Lorenz, Anisotropic heat transport via monopoles in the spin-ice compound $\text{Dy}_2\text{Ti}_2\text{O}_7$, *Phys. Rev. B* 88 (2013) 054406.
- [187] S. Scharffe, G. Kolland, M. Valldor, V. Cho, J. Welter, T. Lorenz, Heat transport of the spin-ice materials $\text{Ho}_2\text{Ti}_2\text{O}_7$ and $\text{Dy}_2\text{Ti}_2\text{O}_7$, *Journal of Magnetism and Magnetic Materials* 383 (2015) 83 – 87. Selected papers from the sixth Moscow International Symposium on Magnetism (MISM-2014).
- [188] S. J. Li, Z. Y. Zhao, C. Fan, B. Tong, F. B. Zhang, J. Shi, J. C. Wu, X. G. Liu, H. D. Zhou, X. Zhao, X. F. Sun, Low-temperature thermal conductivity of $\text{Dy}_2\text{Ti}_2\text{O}_7$ and $\text{Yb}_2\text{Ti}_2\text{O}_7$ single crystals, *Phys. Rev. B* 92 (2015) 094408.
- [189] Y. Tokiwa, T. Yamashita, M. Udagawa, S. Kittaka, T. Sakakibara, D. Terazawa, Y. Shimoyama, T. Terashima, Y. Yasui, T. Shibauchi, Y. Matsuda, Possible observation of highly itinerant quantum magnetic monopoles in the frustrated pyrochlore $\text{Yb}_2\text{Ti}_2\text{O}_7$, *Nature Communications* 7 (2016) 10807.
- [190] M. Hirschberger, J. W. Krizan, R. J. Cava, N. P. Ong, Large thermal hall conductivity of neutral spin excitations in a frustrated quantum magnet, *Science* 348 (2015) 106–109.
- [191] W. H. Toews, J. A. Reid, R. B. Nadas, A. Rahemtulla, S. Kycia, T. J. S. Munsie, H. A. Dabkowska, B. D. Gaulin, R. W. Hill, Disorder dependence of monopole dynamics in $\text{Dy}_2\text{Ti}_2\text{O}_7$ probed via thermal transport measurements, *Phys. Rev. B* 98 (2018) 134446.
- [192] M. Yamashita, N. Nakata, Y. Kasahara, T. Sasaki, N. Yoneyama, N. Kobayashi, S. Fujimoto, T. Shibauchi, Y. Matsuda, Thermal-transport measurements in a quantum spin-liquid state of the frustrated triangular magnet $\kappa\text{-(BEDT-TTF)}_2\text{Cu}_2(\text{CN})_3$, *Nature Physics* 5 (2008) 44.
- [193] M. Yamashita, N. Nakata, Y. Senshu, M. Nagata, H. M. Yamamoto, R. Kato, T. Shibauchi, Y. Matsuda, Highly Mobile Gapless Excitations in a Two-Dimensional Candidate Quantum Spin Liquid, *Science* 328 (2010) 1246–1248.

- [194] A. Kitaev, Anyons in an exactly solved model and beyond, *Annals of Physics* 321 (2006) 2–111.
- [195] D. Hirobe, M. Sato, Y. Shiomi, H. Tanaka, E. Saitoh, Magnetic thermal conductivity far above the Néel temperature in the Kitaev-magnet candidate α -RuCl₃, *Phys. Rev. B* 95 (2017) 241112.
- [196] R. Hentrich, A. U. B. Wolter, X. Zotos, W. Brenig, D. Nowak, A. Isaeva, T. Doert, A. Banerjee, P. Lampen-Kelley, D. G. Mandrus, S. E. Nagler, J. Sears, Y.-J. Kim, B. Büchner, C. Hess, Unusual Phonon Heat Transport in α -RuCl₃: Strong Spin-Phonon Scattering and Field-Induced Spin Gap, *Phys. Rev. Lett.* 120 (2018) 117204.
- [197] R. Hentrich, M. Roslova, A. Isaeva, T. Doert, W. Brenig, B. Büchner, C. Hess, Large Thermal Hall Effect in α -RuCl₃: Evidence for Heat Transport by Kitaev-Heisenberg Paramagnons, arXiv:1803.08162 (2018).
- [198] Y. Kasahara, K. Sugii, T. Ohnishi, M. Shimozawa, M. Yamashita, N. Kurita, H. Tanaka, J. Nasu, Y. Motome, T. Shibauchi, Y. Matsuda, Unusual Thermal Hall Effect in a Kitaev Spin Liquid Candidate α -RuCl₃, *Phys. Rev. Lett.* 120 (2018) 217205.
- [199] Y. Kasahara, T. Ohnishi, Y. Mizukami, O. Tanaka, S. Ma, K. Sugii, N. Kurita, H. Tanaka, J. Nasu, Y. Motome, T. Shibauchi, Y. Matsuda, Majorana quantization and half-integer thermal quantum Hall effect in a Kitaev spin liquid, *Nature* 559 (2018) 227–231.